Profiling of Functional Intercellular Interactions in a Model of the Leukemia Microenvironment

Artikel1: Multimodal high-content screening platform to study primary leukemia cells in co-culture with bone marrow stroma

Artikel2: Selective metabolic dependence of acute lymphoblastic leukemia on oxidative stress protection by bone marrow stroma

---

Dissertation

zur

Erlangung der naturwissenschaftlichen Doktorwürde

(Dr. sc. nat.)

vorgelegt der

Mathematisch-naturwissenschaftlichen Fakultät

der

Universität Zürich

von

Jeannette Boutter

aus

Deutschland

Promotionskomitee

Prof. Dr. Jean-Pierre Bourquin (Vorsitz und Leitung der Dissertation)

Prof. Dr. Markus Manz

Prof. Dr. Roland Wenger

Dr. Beat C. Bornhauser

Zürich, 2013

The experimental work presented in this thesis was performed at the Division of Pediatric Oncology at the Children's University Hospital Zurich. This thesis was performed under the supervision of PD Dr. Jean-Pierre Bourquin (University Children's Hospital Zürich), Dr. Beat Bornhauser (University Children's Hospital Zürich), Prof. Dr. Roland Wenger (Institute of Physiology, University of Zürich) and Prof. Dr. Markus Manz (Clinic for Hematology, University Hospital Zürich).

Zurich, January 2013

Jeannette Boutter

Summary

During leukemia development malignant cells occupy hematopoietic stem cell niches suppressing normal hematopoiesis and infiltrate other sanctuary niches such as the central nervous system or the testis. Interactions with the microenvironment are critical for leukemia cell survival, but the mechanisms involved in these processes are largely unknown. A better understanding of the patterns of intercellular dependence between leukemia and its microenvironment will possibly provide new options to improve leukemia treatment.

To identify new pathways that contribute to the leukemia niche function, I established a large scale high-content (automated image-based) screening platform using co-cultures of primary acute lymphoblastic leukemia cells (ALL) on human mesenchymal stromal cells (MSC). Patient samples were expanded by xenotransplantation in immunodeficient mice to generate a renewable source of leukemic cells for systematic functional investigation. The methodology and analytic pipeline was developed in our laboratory in collaboration with the Light Microscopy and Screening Centre of ETH Zurich. We established a robust workflow to discriminate viable ALL and stromal cells using a fluorescent dye. Detailed protocols were optimized to use this platform for *in vitro* drug testing and for functional genomic projects.

Based on gene expression and cell surface proteomic data that we had obtained from both cellular compartments, I generated a customized siRNA library for 110 candidate genes with a potential function in stromal support. Primary ALL cells were seeded on reversely transfected MSC cells, and ALL cell viability was assessed after 6 days using the established high-content screening platform. From a first screen with three cases with highly resistant disease, 20 candidate genes were identified that reproducibly reduced ALL survival in this assay. These were validated in 10 different patient samples. Importantly, specific and distinct contributions of stromal genes for the survival of individual ALL samples were detected. The strongest effects were observed after RNA interference of the vascular endothelial growth factor C (VEGFC) or of Basigin (BSG, alias CD147) in a subset of patient samples. Dependence from stromal VEGFC predicted sensitivity to two different VEGF receptor kinase inhibitors, confirming the patient specific support pattern of stromal VEGFC. Furthermore, the Notch and Wnt pathways were identified to play an important role for the support of ALL cells, extending experimental data obtained in other model systems of the tumour microenvironment or HSC niches. The largest subset of ALL samples was most dependent on the expression of BSG on stromal cells. I could show that this multifunctional cell surface protein was required to provide metabolic support to a subset of ALL in association with the solute carrier family 3 protein, SLC3A2. This protein forms heterodimeric amino acid transporters (HAT) on MSCs indicating that amino acid transport of stromal cells is important for survival of ALL cells. Leukemic cells are deficient to import cystine, and a subset of leukemic cases requires continuous supply of cysteine for *de novo* glutathione synthesis. We could show that the metabolic transport function of amino acids by stromal cells maintains glutathione levels and reduces oxidative stress specifically in ALL cells that were dependent on stromal BSG/SLC3A2. Indeed, addition of cysteine but not cystine rescued the effect of RNA interference with BSG/SLC3A2 in stromal cells.

Taken together, I describe the development of a new platform for systematic investigation of interactions between primary leukemia and stromal cells. The identification of relevant and leukemia-specific pro-survival cues from stromal cells validates this approach. Strong interaction patterns such as the one reported here suggest new possibilities for targeted therapy provided appropriate biomarkers are developed to select patient cohorts efficiently. The platform can also be used for the analysis of anti-leukemic activity of small molecules as single agents and in combinations. This work will also constitute the basis for a more comprehensive functional genomic screen and will stimulate the development of in vivo models.

Zusammenfassung

In Leukämien besetzen maligne Krebszellen hämatopoetische Stammzellnischen und unterdrücken dort die normale Hämatopoese. Zusätzlich werden weitere schützende Nischenumgebungen infiltriert, z.B. im zentralen Nervensystem oder in den Hoden. Die spezifischen Wechselwirkungen mit der Umgebung der Nischen sind für das Überleben der leukämischen Zellen von entscheidender Bedeutung, die zugrundeliegenden Mechanismen sind aber weitestgehend unbekannt. Ein besseres Verständnis der Interaktionen zwischen leukämischen Zellen und dem umgebenden Nischengewebe bildet eine Grundlage, um neue Wege in der Krebstherapie aufzuzeigen.

Um die Mechanismen zu identifizieren, die zur schützenden Funktion der Nischenumgebung beitragen, wurde eine Plattform etabliert, um mit bildgebenden Verfahren Ko-Kulturen von primären leukämischen Zellen mit humanen Stromazellen des Knochenmarks automatisiert zu evaluieren. Das Patientenmaterial wurde durch Xenotransplantation in immundefizienten Mäusen amplifiziert, welches eine erneuerbare Quelle zur systematischen und funktionellen Untersuchungen von Leukämiezellen darstellt. Die Methodologie und die analytische Auswertung wurde in Zusammenarbeit mit dem Mikroskopie- und Screening-Zentrum der ETH Zürich entwickelt. Wir konnten einen robusten Arbeitsablauf etablieren, durch den wir in der Lage sind, lebendige leukämische Zellen und Stromazellen in Ko-Kultur mittels eines Fluoreszenzfarbstoffes zu unterscheiden. Die Plattform wurde weiterhin hinsichtlich eines Einsatzes für *in vitro* Studien von neuen potentiell anti-leukämischen Substanzen sowie funktionelle genomische Analysen optimiert.

Basierend auf Genexpressions- und Zelloberflächenproteom-Daten, die wir von beiden Zelltypen generiert haben, wurde eine maßgeschneiderte siRNA-Bibliothek für 110 Kandidat-Gene erstellt, die für die zellulären Interaktionen zwischen Leukämie- und Stromazellen des Knochemarks von Relevanz sein könnten. Primäre Leukämie-Zellen wurden auf MSC-Zellen ausgesät, in denen diese Gene mit Hilfe der RNA Interferenz inhibiert worden waren, und die Viabilität der Leukämie-Zellen wurde nach 6 Tagen mit der obengenannten Plattform evaluiert. In einer ersten Studie mit drei Fällen von hoch-resistenten Leukämien wurden 20 Kandidat-Gene identifiziert, deren Inhibition reproduzierbar das Überleben der leukämischen Zellen verringerten. Diese Effekte wurden in 10 weiteren unterschiedlichen Patientenproben validiert. Von Bedeutung ist hierbei, dass spezifische und unterschiedliche Wirkungen dieser Stromazell-Gene auf das Überleben der einzelnen Patientenproben nachgewiesen werden konnten. Die stärksten Beeinträchtigungen auf das Überleben der leukämischen Zellen wurden nach RNA-Interferenz des vaskulären endothelialen Wachstumsfaktors C (VEGFC) bzw. Basigin (BSG, Alias CD147) in spezifischen Untergruppen von Patientenproben beobachtet. Der Einfluss von VEGFC aus dem Stroma konnte die Empfindlichkeit gegen zwei verschiedene VEGF-Rezeptor-Kinase-Hemmer voraussagen, was das Patienten-spezifische Unterstüzungsmuster weiterhin bestätigt. Darüber hinaus konnte den Notch- und Wnt-Signalwegen eine wichtige Rolle bei der Unterstützung des Überlebens der leukämischen Zellen zugeschrieben werden. Dies erweitert die experimentellen Daten aus anderen Modellsystemen der Tumor-Umgebung oder hämatopoetischen Stammzellnischen. Ein Grossteil aller getesteten Zellen war im hohen Maße von der Expression von BSG auf

Stromazellen abhängig. Es konnte gezeigt werden, dass dieses multifunktionale Zelloberflächenprotein benötigt wird, um metabolische Interaktionen in Verbindung mit dem *solute carrier family* 3-Protein, SLC3A2, aufrecht zu erhalten. SLC3A2 ist Bestandteil von heterodimeren Aminosäuretransporter (HAT) auf der Oberfläche von MSCs, was darauf schließen lässt, dass Aminosäuretransportfunktionen von Stromazellen für das Überleben leukämischer Zellen essentiell sind. Interessanterweise können Leukämiezellen die Aminosäure Cystin nur unzureichend importieren, und eine Untergruppe von leukämischen Patientenzellen erfordert eine kontinuierliche Zufuhr des Cystin-Metaboliten Cystein für die *de novo*-Synthese von Glutathion, ein wichtiges Antioxidans. Tatsächlich erhält die metabolische Transportfunktion von Aminosäuren der Stromazellen den Glutathionspiegel der leukämischen Zellen aufrecht. Das hat zur Folge, dass der oxidative Stresspegel reduziert wird, und dieser Effekt war spezifisch in genau den leukämischen Patientenzellen detektierbar, die eine Abhängigkeit von stromalen BSG/SLC3A2 aufwiesen. Die Zugabe von Cystein, nicht aber von Cystin kehrte den Effekt der RNA Interferenz von BSG/SLC3A2 in Stromazellen auf das Überleben der leukämischen Zellen um.

Zusammenfassend wird hier die Etablierung einer neuen Plattform für die systematische Untersuchung von Interaktionen zwischen primären Leukämiezellen und Stromazellen des Knochenmarks beschrieben. Dieser Ansatz wurde durch die Identifizierung von relevanten und Leukämie-spezifischen Überlebenssignalen von den Stromazellen validiert. Die hier bestätigten spezifischen Interaktionsmuster zeigen neue Möglichkeiten für eine gezielte, maßgeschneiderte Krebstherapie auf, sofern geeignete Biomarker entwickelt werden, um Patientenkohorten effizient auszuwählen. Die hier beschriebene Plattform kann auch für die Analyse von anti-leukämischen Effekten von neuen Substanzen, einzeln und in Kombinationen, verwendet werden. Diese Arbeit bereitet die Grundlage für umfassende, funktionale genomische, in grossem Rahmen durchführbare Studien und wird die Entwicklung von *in vivo* Modellen vorantreiben.

Table of contents

Introduction

1. Acute Lymphoblastic Leukemia- diagnosis and treatment

Acute leukemia is the most common form of cancer in childhood. Although cure rates of around 80% can be achieved, 20% of patients with acute lymphoblastic leukemias relapse, ranking relapsed leukemia among the top four most common diagnoses in pediatric oncology in Switzerland (Swiss cancer registry). Therefore, the current challenges are: the reduction of a long and toxic therapy whenever possible, the identification of patients at risk for relapse who may profit from therapy intensification and the development of novel treatment modalities for patients not responding well to commonly used drugs.

During hematopoesis, hematopoietic stem cells differentiate in the bone marrow giving rise to all lineages constituting the blood (Figure 1). Lesions occurring in the lymphoid lineage at the progenitor stages of the differentiation lead to a block of differentiation and aberrant proliferation of immature cells. Malignant transformations can occur in early B or T lymphocytes, resulting in B or T-acute lymphoblastic leukemia (ALL). After disease onset, the massive proliferation of leukemic cells outcompete normal hematopoiesis, explaining the relative short time course of disease referred by the word acute. The symptoms present at diagnosis are a result of the impaired hematopoiesis in the bone marrow with infiltration of extramedullary sites such as liver, spleen and lymph nodes. Most commonly, patients suffer from general fatigue, anemia, fever, infections, unusal bruising, pain, enlarged lymph nodes/ liver and spleen.

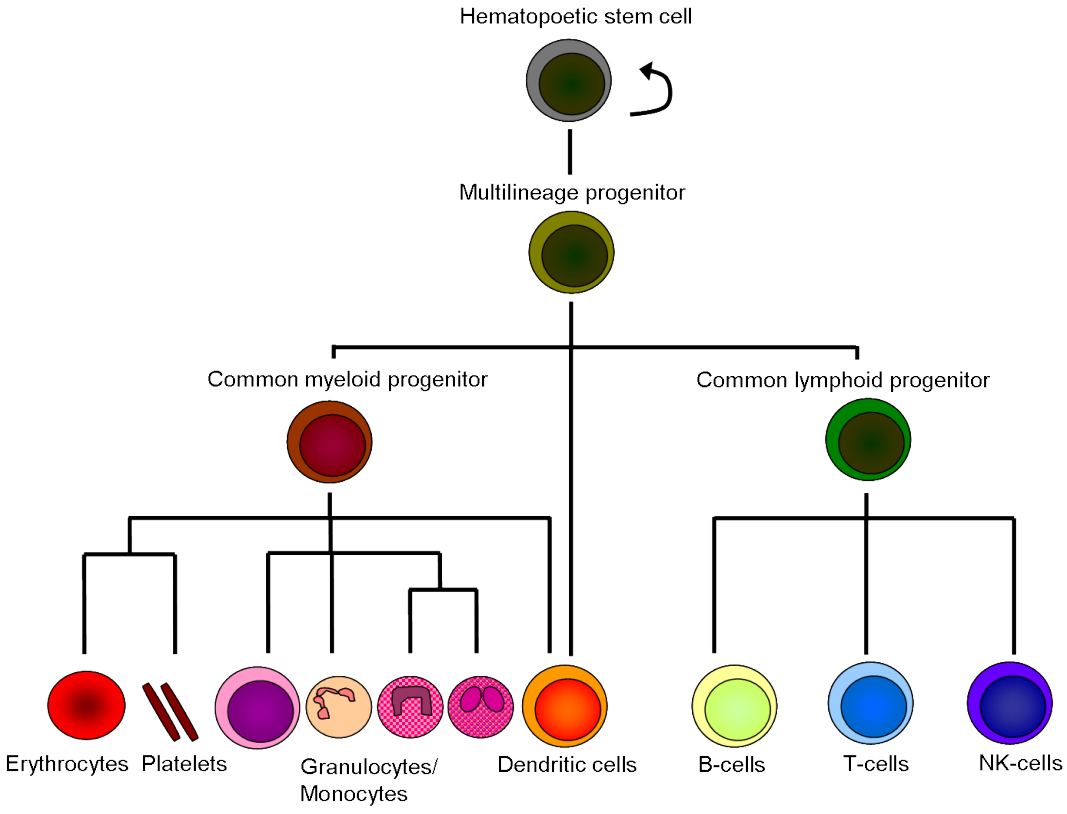

Fig. 1. Scheme of the hematopoietic tree. Differentiation steps are represented leading from the hematopoietic stem cell to the main cells constituting the blood.

For the diagnosis of ALL, a bone marrow biopsy is required to identify the hematopoietic lineage involved in leukemogenesis. Cytogenetics reveal the karyotype of the leukemic populations and can identify present translocations, which are important for risk stratification of patients and ultimately for the treatment given. The Immunophenotyping performed at diagnosis using flow cytometry allows the identification of the lineage and of the maturation stage at which the differentiation is blocked. The lineage and maturation stage can be identified with a combination of cell-surface markers specific for the differentiation status of hematopoietic cells. Leukemic blasts typically have common and aberrant patterns of marker expression compared to the cells they originate from, what allows to follow the malignant cell population by flow cytometry during the treatment. In parallel, Immunoglobulin (Ig) and T cell receptor (TCR) gene rearrangements are assessed. These rearrangements occur during normal lymphoid development and represent a fingerprint for each individual cell and its progeny. Flow cytometry and PCR assess efficacy of the imposed treatment by identification and quantification of residual leukemic cells in the bone marrow during treatment.

Generally, treatment of ALL in Europe is divided in 4 phases [1]. The induction phase aims at reducing leukemia burden and if leukemia cells respond well to therapy a drop of leukemic blasts in the bone marrow is seen within about 4 to 6 weeks. The intensification phase that follows lasts 2 to 4 months with the major aim to maintain remission and to prevent regrowth of leukemic cells especially in the central nervous system (CNS), since around 30% of initial relapses are found in the CNS [2]. A reinduction phase is alternating intensive therapy with therapy pauses and aims at killing the last leukemic cells to avoid future relapses. Finally, the subsequent consolidation therapy lasts until 2 years after diagnosis to ensure full remission. In cases of poor response to induction therapy or if disease is associated with poor prognostic features, hematopoietic stem cell transplantation (HSCT) can be considered. However, the use of HSCT depends on availability of donor cells and prospective studies are currently being conducted to determine the indication of the different HSCT procedures in high-risk or relapse childhood ALL [3-5].

In the last 30 years, ALL therapy was designed as a multiphase treatment process using a combination of cytotoxic drugs that follows risk-directed intensifications. Although treatment tailoring allows to achieve cure rates of around 80% [6], the long and intensive treatment procedures have high toxic effects, which need to be reduced to a minimum for patients responding well to therapy with low risk of relapse. On the other hand, some patients do not respond to current treatment modalities and relapses occur frequently in around 20% of the cases including all risk groups. The risk-based stratification of patients proved to be the right direction to go and needs further understanding and innovation to ensure the amelioration of treatment in ALL. Importantly, future research needs to concentrate on understanding why some patients relapse and on finding methods to identify them in early phases to adapt therapy modalities.

2. Prognostic factors in acute lymphoblastic leukemia

A few significant risk factors have been described in childhood ALL, including leukocyte count at diagnosis, immunophenotype, age, chromosomal abnormalities and response to initial therapy (Table 1) [7, 8]. These risk factors contribute to the stratification of patients and are used to optimize their individual treatment. More intensive chemotherapy is given to patients with unfavorable factors, whereas favourable factors account for less or modified versions of the intensive therapy.

Table 1. Factors used for risk stratification in childhood ALL.

Factor	Favorable	Unfavorable
Age	1-9	<1 or >10
Leukocyte count (x10^9/L)	<5	>50
Immunophenotype	B-cell	T-cell
Genotype	Hyperdiploidy (>50 chrom.), ETV6-RUNX1	Hypodiploidy (<44 chrom.), BCR-ABL1, MLL-X
MRD after induction	<0.01%	>1%

Chrom.= chromosomes. Adapted from [9].

2.1. Genetic aberrations in ALL

Leukemia is a complex genetic disease. Lesions leading to the malignant transformation of progenitor cells include aberrant expression of proto-oncogenes, aneuploidy and chromosomal translocations. Cytogenetic analyses identify the ploidy status of leukemic cells and can reveal some translocations. Only a few genetic lesions have strong prognostic value for risk stratification of the patients (Figure 2). Hyperdiploidy as well as the detection of the *ETV6-RUNX1* translocation product are seen as favourable prognostic factors [10, 11]. In the hyperdiploid patients, around 5% of patients carry the t(1;19) rearrangement, leading to the fusion product *E2A-PBX1* which is also associated with better prognosis [12]. On the other hand, *BCR-ABL1* positive leukemias resulting from the translocation t(9;22), also called Philadelphia chromosome, *E2A-HLF* positive leukemias bearing the translocation t(17;19) and leukemias with MLL rearrangements account for unfavourable outcome with higher risk of relapse [13, 14].

In the last years, knowledge about mutational diversity has increased due to deep-sequencing analysis of the genome of individual patients and profiling strategies. Mutations were observed in transcription factors regulating lymphoid development such as *PAX5*, *EBF* and *IKZF1* [16], in proteins regulating cell cycle such as *CDKN2A* and *CDKN2B* [17], in tumor suppressor genes (*PTEN* and *RB1*) [16] and in regulators of apoptosis (*BTG1*) [16]. A candidate gene sequencing approach comparing diagnostic and relapse ALL identified alterations in the transcription co-activators *CREBBP* and *NCOR1*, as well as in transcription factors *ERG, SPI1, TCF4* and *TCF7L2* [18], that were associated with relapse.

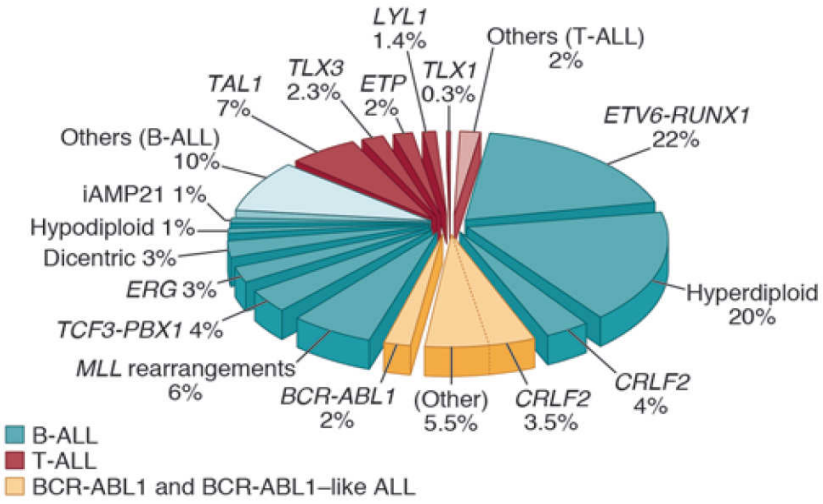

Figure 2. Frequency of cytogenetic subtypes of pediatric ALL. Adapted from [15]. The pie chart includes all major B- and T-lineage subtypes of ALL, to illustrate the relative frequency of each. The recently described *BCR-ABL1*–like subtype and BCR-ABL1 positive ALL are shown in yellow to illustrate the high frequency of childhood B-ALL cases with genetic alterations activating tyrosine kinase and cytokine receptor signaling that may be amenable to targeted therapy.

Recently, a subgroup referred to as *BCR-ABL1*-like ALL was identified [16, 19, 20]. These leukemias are not bearing the translocation leading to the *BCR-ABL1* fusion product but show similar gene expression profiles and have an unfavourable outcome. They have alterations in the transcription factor IKAROS encoded by the *IKZF1* gene. This gene is found to be mutated in 76.2% of childhood *BCR-ABL1* positive ALL and in 90.9% of adult *BCR-ABL1* ALL cases [21]. Additional to mutations in *IKZF1*, mutations in the *CRLF2* gene were found in 40% of *BCR-ABL1*-like ALL cases. Normally, CRLF2 dimerizes with IL7RA to form a receptor triggering JAK/STAT signalling upon TSLP (thymic stromal-derived lymphopoetin) binding. However, mutations in *CRLF2* can lead to aberrantly activated kinase signalling, as was shown in down syndrome ALL where overexpression of *CRLF2* was found in association with activating mutations in the receptor itself or with mutations in JAK2 resulting in a constitutively active JAK/STAT pathway [22].

The mechanism of cooperation of different lesions and the consequences of mutation patterns for each patient are still unclear. In particular, associations of mutational patterns and treatment response remain to be determined. Next generation sequencing of primary leukemias that are currently underway will help us to understand mutational networks, which mutations are driving, cooperating and mutually exclusive. This knowledge will need to be completed with a biological understanding of the functional relevance of the mutations, which could ultimately lead to the identification of potential drug targets enabling a personalized treatment scheme.

2.2. Risk stratification of patients based on response to treatment

Despite tremendous efforts to identify genetic alterations and attempts to correlate these with the outcome of the patients, the best method for risk stratification is the analysis of *in vivo* response to initial chemotherapy. The kinetics showing a reduction in the number of malignant cells detected in the bone marrow during the induction phase of treatment allows stratifying the patients. The assessment of remaining leukemic cells in the bone marrow by

flow cytometry and PCR is called MRD (minimal residual disease) assessment. Several studies have independently confirmed the predictive value of this strategy [23-25].

In the AEIOP-BFM-ALL 2000 study, patients are stratified as high risk when more than 1 leukemic cell per 1000 normal cells was detected (HR; MRD level ≥10^{-3}) at day 78 of treatment. HR patients have a 5-year event free survival (EFS) rate of 50.1% compared to 92.3% in the standard risk group (SR; negative MRD at day 33 with a sensitivity of at least 10^{-4}) (Figure 3). One additional MRD assessment time point at week 22 allows the identification of a subgroup of HR patients with exceedingly high risk for relapse, called very high risk patients (VHR). These patients remain resistant to intensive chemotherapy and represent a patient group for which better treatment alternatives are needed.

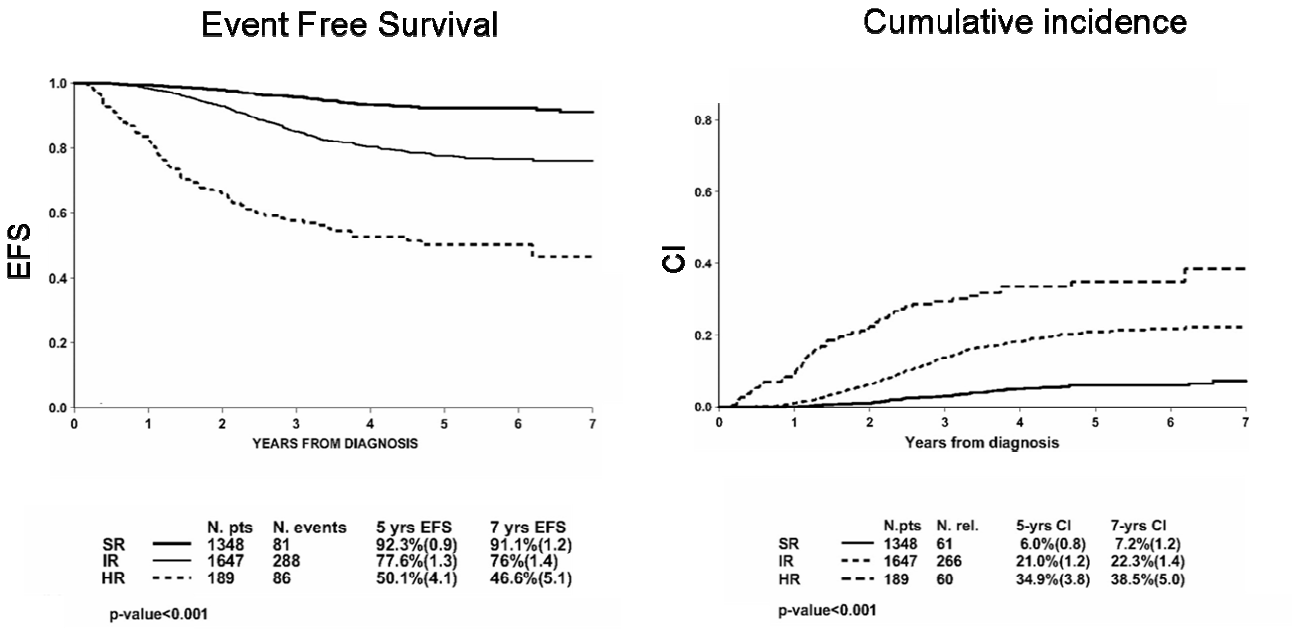

Figure 3. Event-free survival and cumulative incidence of relapse according to PCR-MRD classification in 3184 pB-ALL patients. Adapted from [24].

The outcome of patients with relapse in ALL has remained static over the past two decades [26] requiring the establishment of the best standard treatment strategies and investigating innovative therapies. Therefore, a multi-centre study for children with relapsed acute lymphoblastic leukaemia was initiated in 2010, called IntReALL 2010. The consortium was build between 20 national study groups to recruit enough patients for studying treatment strategies within childhood relapsed ALL. The ALL-REZ BFM Study group is taking part, as well as the COPRALL Study Group, the NOPHO Study Group, the UKALL Relapse Study Group and the AIEOP group.

Obviously, MRD assessment is helping to stratify patients but the molecular mechanisms of persistence remain unclear. Cell intrinsic mechanisms like genetic alterations can render cells more resistant but as well cell extrinsic factors can play a role. We focus here on the question of the influence of the microenvironment in the support of B-ALL.

3. Role of the bone marrow microenvironment in ALL

3.1. Importance of the tumor microenvironment and MSCs

The importance of the microenvironment for a tumor was stated first in 1889 by Stephen Paget in his “seed and soil” theory for metastatic dissemination. In the last years, important insights into the role of the microenvironment became more and more important, not only for metastatic disease but also in primary tumors. In 2011, the tumor microenvironment is stated as one the “hallmarks of cancer” stated by Douglas Hanahan and Robert Weinberg [27]. Indeed, stromal cells are generally recruited to primary tumor sites to form tumor-associated stroma. Some of the stromal stem and progenitor cells seen in different mouse models of various carcinomas are recruited from the bone marrow [28, 29]. The bone marrow comprises mesenchymal stem cells representing an extremely rare cell type comprising 0.01% to 0.001% of all mononuclear cells in the bone marrow, compared to 1% for the hematopoietic stem cell (HSC) population [30]. Unfortunately, plastic adherent cells isolated from the bone marrow are often called mesenchymal stem cells and a controversy arose from the extensive use of such cell fractions in the clinical setting without sufficient and clear biological characterization of these cells. Only cells with a colony-forming efficiency of 100% comprising cells that are uniformly multipotent and self-renewing, as assessed by *in vivo* transplantations, could be called mesenchymal stem cells [31]. Along the same line, it was proposed to name this rare stem cell population, skeletal stem cells. A skeletal stem cell represents a single cell capable of generating a complete heterotopic bone or bone marrow organ (ossicle) *in vivo* [32]. Bone-marrow derived mesenchymal stem cells should be negative for the hematopoietic linage markers CD34 and CD45 [33] and positive for STRO-1, CD146, CD105, ALP, CD49a and CD271, among others [31]. Different markers are used for the characterization of these stem cells as a consensus, but no marker is known so far to be specific uniquely for them.
Because of the ambiguity related to the name of MSC, I will call mesenchymal stem cells, skeletal stem cells and use the acronym MSC for mesenchymal stromal cells.
The functions of bone-marrow derived mesenchymal cells within tumors are not fully understood. *In vivo* models suggest the migration and engraftment of MSCs at injury sites and in neoplasia when inflammation occur [34]. The reported effects of MSC on the progression of primary tumors can be pro- as well as anti-tumorigenic and vary widely depending on the source of MSCs or the tumor model used [35]. However, MSCs seem to be actively recruited to primary tumor sites increasing the complexity of the tumor mass. This property is leading to new therapy approaches based on injecting modified MSCs with anti-tumorigenic properties [36].

3.2. HSCs and their niches

Stem cells need protected and regulated surroundings to maintain their self-renewal capacity. The idea of a specific microenvironment for hematopoietic stem cells arose in the 1970s with an original concept of Ray Schofield saying that functional cell types provide the necessary goods to maintain HSC potency throughout life [37]. This specific

microenvironment, called niche, is a place where cells “not only reside but are regulated, nurtured and protected” [38]. It is thought that HSC are kept quiescent to prevent damage, however the kinetics of the HSC cycling in humans are currently not known [39]. At the same time, the bone marrow is permissive enough for stress signals to allow activation of HSCs upon hematopoietic challenge and replenishment of hematopoietic cells [40]. Up to now, a unique and specific HSC niche in the bone marrow could not yet be characterized [41]. This could be due to the fact that different functional niches exist for different HSC subpopulations, as even highly purified HSC show heterogeneity [41]. Different subtypes of bone marrow stromals cells were described to be able to modulate HSC activity, including osteoblasts [42], Cxcl12-abundant reticular cells [43] and nestin-positive mesenchymal stem cells [44].

The establishment and maintenance of hematopoiesis during life is intimately connected with the circulation of HSC between tissues [45]. A unique trait of HSCs is that they periodically leave the bone marrow niche and enter blood circulation. Later, they re-enter the bone marrow space, a process which is called homing [46, 47]. Mobilization of HSCs can be affected by circadian rhythms [48] and bone remodelling [49]. The circulation of HSCs is thought to be important for homeostasis of hematopoietic cells. Hematopoiesis can occur directly in distant tissues and the turn-over in the HSC niches guarantees transient periods of niche vacancies [46].

The most prominent axis for homing of HSCs is the CXCR4-SDF-1 axis [43, 50]. The cytokine SDF-1 is secreted by cells of the niche in the bone marrow generating a gradient. HSC cells due to expression of the chemokine receptor CXCR4 are attracted to home back to the bone marrow when being in circulation. In the niche itself, adhesion interactions involving integrins and VCAM-1 take place and allow retention of HSCs in the niche [51, 52]. Signals involving calcium are thought to be important for the correct localisation next to the endosteum [53]. Moreover, maintenance and quiescence, as well as self-renewal and expansion of HSCs are regulated by cross-talks with cells within the niche. Secreted stem cell factor (SCF), thrombopoietin (TPO) as well as angiopoetin1 (ANGTP1) are thought to play a role in maintenance and *in vivo* quiescence of HSCs through interactions with their respective receptors KIT, MPL and Tie2 tyrosine kinase (TEK) [54-56]. More recently, angiopoetin-like 3 (ANGPTL3) was shown to help controlling HSC quiescence [57].

The Wnt as well as Notch signaling pathway have been implicated in HSC regulation. Due to the complexity of those pathways, full understanding of their function in HSC expansion remains challenging [41]. For the Wnt pathway, 19 WNT ligands are known to interact with secreted and membrane-associated proteins including at least ten transmembrane Frizzled (FZD) receptors, two low-density lipoprotein receptor-related proteins (LRP5 and LRP6) and an undefined number of extracellular proteins such as Kremlin, Dickkopf (DKK), Wnt-inhibitory factor (WIF), secreted FZDs (sFRP) and Norrin [58]. Depending on the cell type and on the ligand-receptor interactions occuring, the canonical or two different non-canonical Wnt pathways can be activated. The canonical pathway results in the activation of beta-catenin, which translocates to the nucleus and acts as co-activator of transcription factors such as TCF and LEF [58]. WNT3a, WNT5a (mostly non-canonical pathway) or activation of beta-catenin were shown to influence HSC expansion *in vitro* and *in vivo* [59-61]. Moreover, the Wnt pathway regulates expression of VCAM-1 in stromal cells [62]. In the Notch pathway,

NOTCH1 and NOTCH2 activation influence HSC function over ligand interactions mostly via JAG1 [63, 64].

Interactions of HSC with their niche are summarized in Figure 4.

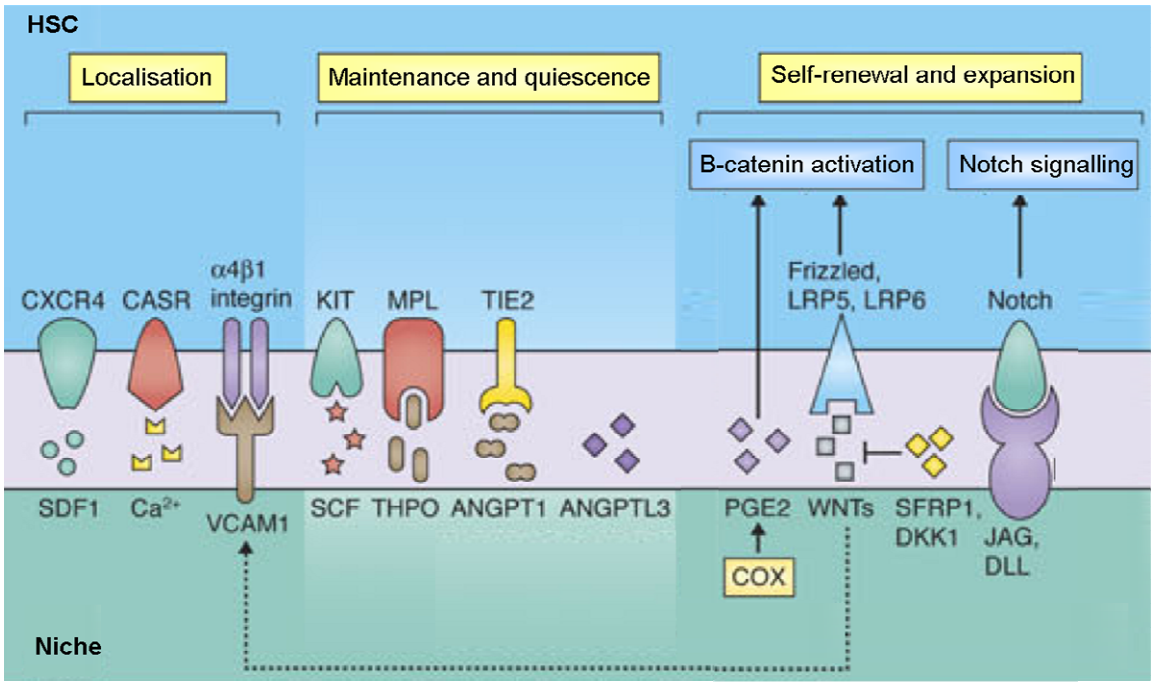

Figure 4. Crosstalk between HSCs and their niche. Adapted from [41].

3.3. Known interactions of B-ALL with the microenvironment

The interactions of B-ALL cells with the microenvironment show similar mechanisms to HSCs. The bone marrow acting as a protective microenvironment will have consequences in leukemia treatment strategies. Thus the identification of protective signals could lead to the development of new anti-leukemic compounds.

Pre-B ALL cells can displace normal HSC upon engraftment in mice [65], indicating that leukemia cells are able to hijack the HSC niche. Indeed, B-ALL cells express the CXCR4 receptor like HSCs, and the SDF-1/CXCR4-axis also plays an important role for homing to the bone marrow of ALL cells [66, 67]. SDF-1 can be expressed by epithelial cells of different organs including lymph nodes, spleen, liver and brain [68, 69]. Furthermore, the expression of CXCR4 on ALL cells correlates with the infiltration in extramedullary sites [70] and the activation of the CXCR4 receptor correlates with a poor outcome in B-ALL [71]. Addition of SDF-1 enhances survival of B-ALL cultures with stromal cells *in vitro* [72]. Inhibitors of the CXCR4 receptor like AMD3100 were shown to reduce proliferation of B-ALL cells *in vitro* [73] and *in vivo* [74]. Moreover, administration of AMD3100 sensitized ALL cells to clinically used drugs in mice [75]. Although this study stated that leukemic cells are more susceptible to AMD3100 than HSC to enter circulation, clinical studies need to assess the effect of those treatment strategies on HSC. Until now, clinical trials for AMD3100 are in phase 1/ 2 for treatment of AML and show promising results [76].

In addition to SDF-1, other cytokines secreted by the microenvironment affect B-ALL cells. IGF-1, VEGF, PDGF, IL-3 and IL-7 [77, 78] [72] were reported to help to sustain B-ALL cells. A mechanism that can induce cytokine release in the bone marrow stroma is hypoxia that upregulates HIF-1α, an oxygen-regulated protein. In bone marrow from patients with ALL, overexpression of HIF-1α was observed [79]. VEGF is a target gene of HIF-1α, which stimulates angiogenesis [80, 81]. Increased angiogenesis was observed in ALL [82] and expression of VEGFR on leukemic cells upon activation by different VEGF ligands promotes proliferation [72].

Besides the role of soluble factors, contact dependent mechanisms play a role in B-ALL support. Similar to HSCs, where intergins ensure retention in the niche via interactions with VCAM-1, pre-B-ALL cells express α4β1 integrin (also referred to as very-late-antigen 4, VLA4) which via interactions with VCAM1 on niche cells influences the homing and engraftment of leukemic cells in mice [83-85]. High expression levels of VLA4 on relapsed ALL cells predict adverse outcome and highlights the biological role of direct cell-to-cell interactions of leukemic cells with the microenvironment during treatment [86].

As in HSCs, the Wnt and Notch pathway are thought to play a role in survival of B-ALL cells. Evidences for the activated Wnt pathway were first found in *E2A-PBX1*-positive leukemias, where the fusion protein activates transcription of WNT16 [87]. However, understanding of the possible functions of the Wnt pathway in B-ALL cells seems as difficult as in HSCs. The activation of proliferation due to WNT3a [88] stands in contradiction to the inhibition of proliferation reported by others [89]. Nevertheless, dysregulation of WNT expression in leukemia cells [90] and the overexpression of LEF1, a key mediator in Wnt signaling associated with unfavourable outcome [91] confirm an important role for Wnt signaling in ALL. Moreover, comparison of diagnostic and relapse cases suggests an involvement of the Wnt pathway in relapse [92].

NOTCH1 is a key regulator of differentiation of T and B lineage during lymphopoesis. PAX5 promotes B cell development by repressing NOTCH1, and pan-hematopoietic PAX5 expression blocks T lymphopoesis [93]. On the other hand, NOTCH1 activation leads to differentiation to the T-lineage and blocks early B cell lymphopoiesis [94]. The Notch pathway arose as a major pathway involved in T-ALL with *NOTCH1* activating mutations found in over 50% of T-ALL [95]. The role of NOTCH in B-cell malignancies is still controversial but gains importance especially in malignancies involving more mature B cells like chronic lymphoblastic leukemia [96]. In B-ALL, induction of Notch pathway via Hes-1 was shown to promote apoptosis [97]. However, expression of NOTCH3 and NOTCH4 from stromal cells *in vitro* proved to have pro-survival effects in B-ALL cells [98]. A better understanding of the Notch pathway itself is required and will help to clarify the functions of different NOTCH receptors and NOTCH ligands.

3.4. Protective effects of the microenvironment on B-ALL cells during treatment

The microenvironmental signals activate pro-survival signaling in leukemia protecting leukemic cells from chemotherapeutic agents. The understanding of these interactions is critical to develop novel treatment approaches.
As briefly introduced, inhibition of CXCR4 on leukemic cells enhanced the cytotoxic and antiproliferative effects of vincristine and dexamethasone *in vitro* [73]. SDF-1 could be shown to act on kinase pathways, like the Akt and MAPK pathways, by enhancing phosphorylation of ERK1/ 2, p38MAPK and Akt [78]. The PI3K/AKT/mTOR pathway is an essential intracellular pathway regulating growth and survival of cells and is often found to be mutated in cancer [99]. Clinical trials using mTOR inhibitors like sirolimus or temsirolimus are currently investigated in pediatric ALL [100]. The MAPK pathway regulates gene expression and cell survival among others [101]. The MAPK pathway involves many kinases regrouped in 3 main branches namely the ERK pathway, p38MAPK and JNK kinases [101]. p38MAPK inhibitors were stated to reduce ALL cells survival *in vitro* [72]. The JAK/STAT pathway playing an important role in ALL, is connected to the AKT and to the MAPK pathways [100], leading to a complex intertwined network of intracellular kinase signalling in ALL.
Moreover, stromal VCAM-1 enhanced resistance of ALL cells to cytarabine and etoposide *in vitro* [102], probably through activation of integrin linked kinases in leukemia cells [103, 104].
The induction of anti-apoptotic proteins upon interaction with the microenvironment may contribute to achieve resistant phenotypes upon treatment. VEGF was shown to inhibit induced apoptosis in B leukemic cells through phosphorylation of BCL-2, a member of the anti-apoptotic family [105]. Moreover, stromal cells were shown to reduce Caspase 3 activity of B-ALL cells leading to a reduction in apoptosis after treatment with cytarabine and etoposide *in vitro* [106]. An overview over the cellular pathways currently targeted as potential therapeutic approaches in pediatric ALL (B and T-ALL) is depicted in Figure 5. Probably CXCR4 and VEGF only represent a small number of the cytokines affecting B-ALL support. More contact dependent mechanisms than VCAM-1 need to exist and the protective effect of the microenvironment can not be limited to the upregulation of the anti-apoptotic pathway. The knowledge of microenvironmental protection of B-ALL cells is still very limited and requests further investigation.

The complexity of aberrant signalling pathways is further increased by aberrant metabolism occurring in cancer cells. Indeed, an important hallmark of cancer cells is their differential metabolic activity compared to normal cells [107]. The preferential nonoxidative use of glucose via glycolysis in cancer cells was stated by Otto Warburg in 1956 and could be confirmed in AML cells [108]. The understanding of metabolic reprogramming of cancer cells gained importance in the last years. The metabolic alterations found in cancer cells get linked to oncogenic signaling and are dependent on the tissue type in which oncogenesis occurs [109]. KRAS influences the activity of the oxidative pentose phosphate pathway in a pancreatic cancer model [110]. The oncogene MYC influences glutaminolysis and renders cancer cells addicted to glutamine [111]. Thus, MYC overexpressing cells, like some neuroblastoma subtypes, are sensitive to glutamine deprivation [112]. Oncogenic mutations were found to occur in metabolic enzymes and the idea of oncometabolites arose. IDH1 and IDH2 mutations found in glioblastoma and AML, lead to increased levels of 2-

hydroxyglutarate, which modifies the epigenetic regulation of the cells by DNA methylation [113, 114]. In chronic lymphoblastic leukemia, the deficiency of cystine import was overcome by continuous supply of cysteine by stromal cells. [115]. Cysteine is needed for the synthesis of the anti-oxidant glutathione, which is critical to control oxidative stress in leukemic cells.
Again, for ALL cells there was only one important study reporting microenvironmental help to maintain their elevated metabolic rate. ALL cells have low asparagine synthetase (ASNS) expression levels with low asparagine biosynthesis and are therefore exquisitely sensitive to asparagine depletion when treated with asparaginase. However, ALL cells are protected in the presence of bone marrow stromal cells, which have high ASNS expression levels and compensate asparagine biosynthesis even upon depletion with asparaginase [116].

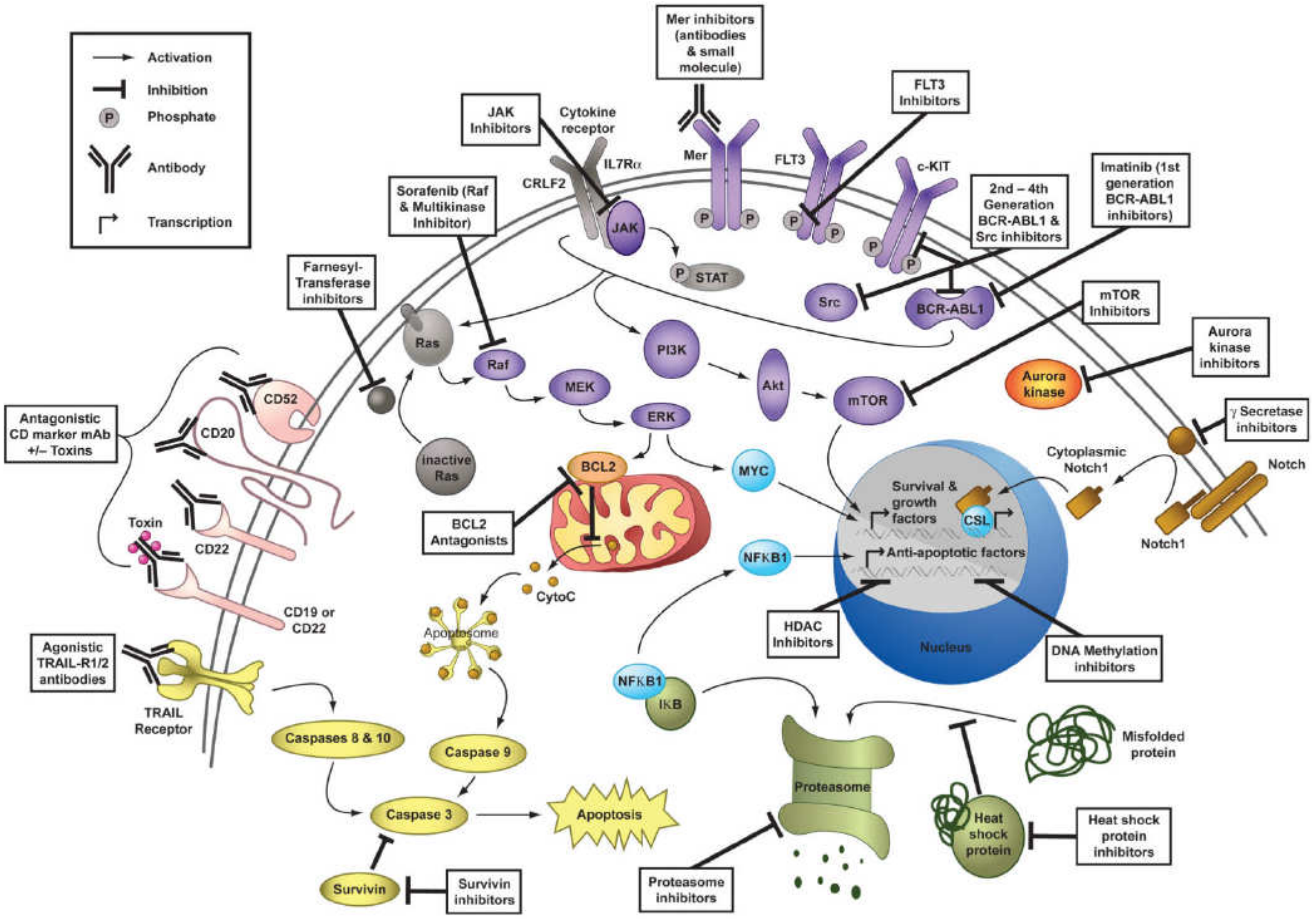

Figure 5. Cellular pathways under investigation as potential therapeutic targets in pediatric ALL. Adapted from [100]. With the exception of Aurora Kinase, which is required for mitotic spindle assembly, all other kinases included here are purple and activate the PI3K-Akt and/or Ras-MAPK prosurvival pathways. Cluster of differentiation (CD) surface marker proteins are pink. Proteins of the apoptotic pathway are yellow. Molecules involved in protein degradation are green. Transcription factors are blue. Compounds in development as targeted therapeutics are described in black boxes.

Most studies investigating microenvironmental interactions were conducted for HSCs. Some pathways were found to play a role in the interactions B-ALL cells undergo with their microenvironment and of these only a few were linked to protective effects against chemotherapy. Furthermore, the maintenance of elevated metabolic rates in cancer cells gained importance in the last years but mostly did not investigate B-ALL. Further studies are required to characterize the microenvironmental interactions specifically in B-ALL.

4. Models of leukemia and leukemic microenvironment

4.1. Maintenance of B-ALL cells *in vitro*

The first B-ALL cell line, REH, was established in 1974 from leukemic cells of a girl with relapsed ALL [117]. Many lines are derived from resistant disease or relapse cases mostly harbouring t(1;19) or t(9;22) translocations [118]. In our laboratory, only the establishment of cell lines from cases positive for the t(17;19) translocation proved to be successful. In general, the establishment of childhood B-ALL cell lines is difficult with success rates of about 10% The acquisition of stromal independence is difficult to achieve and seems to be associated with different translocations. Moreover, additional cytogenetic aberrations can occur *in vitro* [117] and the maintenance of clonal heterogeneity in cell lines is not clear. Thus, cell lines do not represent well the diversity that is characteristic for ALL.

Primary ALL cells rapidly die in suspension cultures *in vitro* and the maintenance of primary leukemic cells *in vitro* only by addition of cytokines was only possible in few cases. Some reports show that B-ALL cells can be supported by addition of IL-3, IL-7 and SCF *in vitro* [119]. However, other groups, including ours, could not reproduce these data [120]. The only efficient way of supporting B-ALL cells *in vitro* is to co-culture the leukemic cells with stromal cells, a methodology used since 30 years [121]. Stromal cells provide the required multitude of survival cues like adhesion molecules and secreted cytokines. Moreover, human leukemic cells are supported on murine-derived stroma, indicating that important microenvironmental interactions are maintained from mouse to human [122]. Only in stromal co-cultures, addition of cytokines (IL-3, IL-7, SDF-1, VEGFs or PDGF) can further enhance short-term survival of leukemic cells [72, 78].

Stromal cells can be isolated from different tissues like the placenta [123], the aorta wall, the thymus, the spleen or the bone marrow [124]. Bone marrow derived MSC form healthy donors can be expanded on a regular basis. However, experimental variability can result form differential culture and expansion conditions and differential genetic backgrounds. Ideally, MSC should be derived from each patient to study matched leukemia and microenvironment interactions. However, the availability of primary MSC is restricted and the establishment of MSC cell lines of each patient with validation of MSC characteristics is challenging. Therefore, several different cell lines derived from primary bone marrow cells are routinely used for experimental set-ups *in vitro.* The OP-9 cell line was derived from the calvaria of a newborn mouse [125] and was shown to be useful in ensuring mouse embryonic stem cells to differentiate into HSCs [126]. The MS-5 cell line was established from adherent cells in long term bone marrow cultures of mice after irradiation and proved to support growth of HSC for longer than 2 months *in vitro* [127]. The HS-5 cell line is derived from human bone marrow and was immortalized by transduction with the human papilloma virus E6/E7 genes [128]. HS-5 cells could support the proliferation of hematopoietic progenitor cells when co-cultured in serum-deprived media with no exogenous factors and expressed high levels of VCAM1 [128]. The MSC cell line is derived from human bone marrow and was immortalized by enforced expression of telomerase [129]. This cell line has the same growth properties than primary MSCs. They show the same doubling time, they are

not forming tumors in immunodeficient mice and have the potential to differentate to osteoblasts and chondrocytes [129]. Moreover, they are supporting normal and leukemic hematopoiesis [129]. Co-cultures of MSCs with primary B-ALL cells proved to sustain viability of leukemic cells in a majority of cases [130, 131]. Long-term support could result in an amplification of cells in some cases, but extensive short-term proliferation of B-ALL cells in the co-culture system was not reported [130, 131]. Moreover, the survival analyses of leukemia cells co-cultured with MSC cells could predict treatment outcome in patients [132]. We preferentially worked with the cell lines of human bone marrow origin. There, we preferentially used the MSC cell line showing a normal karyotype. The HS-5 cell line displayed numerical and structural abnormalities (data not shown).

4.2. Models of B-ALL cells *in vivo*

Animal models are required for studying cancer *in vivo.* Especially for treatment modalities the *in vivo* proof of efficacy is indispensable. For B-ALL, transplantation of HSC transduced with leukemia specific fusion genes like *BCR-ABL1* or *MLL* fusion genes are used and can be useful to look at additional genetic lesions arising *in vivo* [133, 134]. However, these models using fusion genes address very specific subgroups and do not recapitulate the complexity of B-ALL. Xenotransplantions of primary patient material in immunodeficient NSG mice proved to recapitulate genetic complexity and phenotype of the patients [135, 136]. After transplantation, the proportion of human cells is assessed in the peripheral blood of mice to follow engraftment and expansion of leukemic cells (see Figure 6). Intravenous or infemoral injections of human cells into mice lead to development of human leukemias after few weeks with a dissemination pattern similar to the ones observed in humans. Clones present after xenotransplantation could in the majority of the cases be backtracked to clones present at diagnosis [136]. Most importantly, the numbers of cells recovered range from few millions in the bone marrow up to a billion of cells in the spleen. Thus, transplantation in mice leads to an impressive amplification of leukemic material. It constitutes in theory a renewable source of primary B-ALL cells for systemic functional experiments of cases where extensive clinical and diagnostic data are available.

It is of note that leukemia progression and evolution of ALL subclones analyzed in xenograft models are depending on the model used [137]. Although mircroenvironmental cues from mouse and humans are conserved to some extend and cross-species experiments *in vitro* and *in vivo* are possible, the study of microenvironmental interactions of leukemic cells with their corresponding human niche *in vivo* remains challenging.

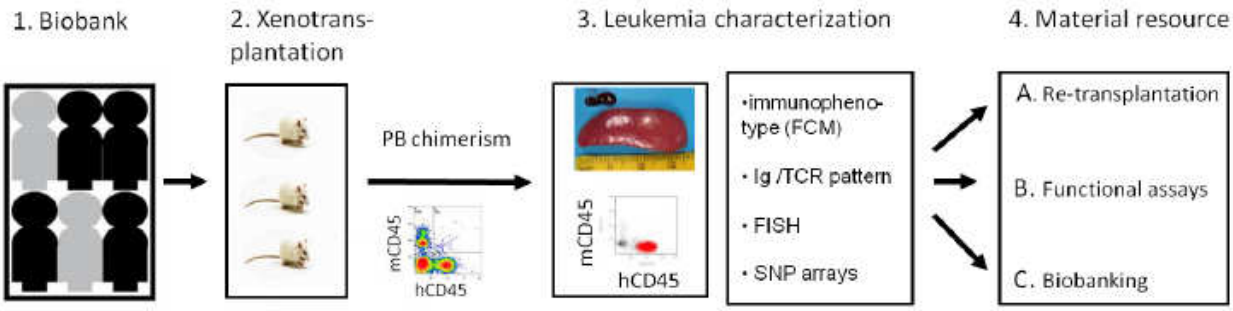

Figure 6. Establishment of leukemia xenograft mouse model. Adapted from [138]. Cells derived from fresh or biobanked human bone marrow aspirates (1) are transplanted into immunodeficient mouse recipient (2) and leukemia development and progression is monitored in peripheral blood by means of flow cytometry. Leukemia developed in mice morphologically, phenotypically and genetically resembles original human disease (3). Leukemia xenograft model serves as renewable source of material for further experiments (4).

4.3. Models of the microenvironment *in vivo*

Knockout mice are one possible tool to study relevant mechanisms *in vivo* by comparing wild type and knockout mice of the same strains for specific questions. Engineering of knockout mice can be long and ineffective but innovative techniques in the last years promise fast and cost-effective results [139]. Especially in studies that investigate the microenvironment of HSCs, knockout mice gave some unexpected results when looking at complex pathways such as the Wnt or the Notch pathway [140-142]. Ultimately, knockout mice can only provide satisfactory answers asking simple questions in known settings where no redundant proteins can rescue the investigated phenotype. Furthermore, translation into humans always needs to be further proven.

The reconstitution of a humanized niche in immunodeficient animals and further manipulation of this reconstituted humanized niche would constitute a model to study niche functions *in vivo*. Currently, the repopulation of human MSCs injected in mice is not efficient due to low-survival rates and poor long-term engraftment rates [143]. Pre-conditioning of MSC with SDF-1 or hypoxia could enhance survival rates after transplantation [144, 145]. The up-regulation of CXCR4 on MSCs enhanced the engraftment rates in the bone marrow of NSG mice [56] and ectopic expression of integrin α4 could increase retention of MSC in the bone of mice [146]. But further improvements are required to model the microenvironment *in vivo* with injected human MSCs.

One possibility in creating human niches *in vivo* is the use of so called humanized mice, which carry functioning human genes, cells, tissues and/or organs. The formation of ectopic, extramedullary bone in mice is one of the approaches in modelling human bone marrow-like microenvironment in an *in vivo* setting [147, 148]. MSCs on polyurethane scaffold could mimic a human bone marrow stromal network with presence of adipocytes, osteoblasts and blood vessels and enabled the growth and maintenance of inoculated human AML cells [148]. Another model illustrated in Figure 7, uses endothelial colony-forming cells (ECFCs), which are blood- or vasculature-derived endothelial progenitor cells (EPCs), mixed with MSCs and Matrigel [147]. 8 weeks after injection in NSG mice, well-vascularized bone like structures developed. HSC and an AML cell line proved to be able to engraft in this

extramedullary bone structures. This model further provides the basis to alter the extramedullary micronvironment by genetic modifications of the MSCs used. Indeed down-regulation of HIF-1α in the MSC compartment lead to 50% decrease of engrafted leukemic cells in the ectopic bone environment [147].

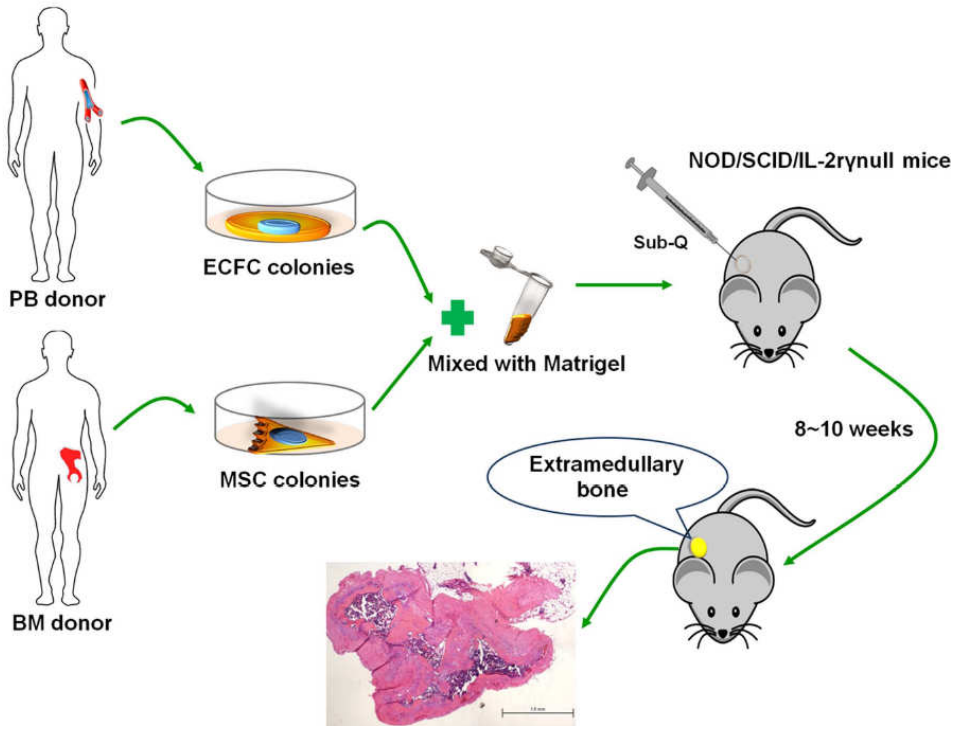

Figure 7. Schema of extramedullary bone/marrow generation. Adapted from [147]. MSCs and ECFCs were isolated from heparinized human BM or peripheral blood through an initial adhesion step and subsequently allowed to proliferate in specific media. Cells mixed with Matrigel were subcutaneously injected into the flanks of NSG mice, and these developed into bone-like tissues with high osteoblastic activity in 8 weeks.

The further development of humanized mice will lead to *in vivo* models resembling more the human settings. Although the NSG mouse model allows robust lymphopoesis upon engraftment of HSC, few human myeloid cells and no human erythrocytes or platelets are generated [149]. This is partially explained by the fact that recipient mice have compromised lymphoid compartments but normal myelopoesis with generation of erythrocytes, platelets and other myeloid cells. On the other hand, mouse cytokines do not support myelopoesis the same way as human cytokines do. The expression of human IL3, SCF and GM-CSF in NSG mice proved to enhance engraftment efficiency in AML models [150] and expression of human IL-3 and GM-CSF supports human macrophage development [151]. Furthermore, human *TPO* increases the levels of human engraftment in the bone marrow of mice, improving the multilineage differentiation of hematopoietic cells, with an increased ratio of myelomonocytic versus lymphoid lineage cells [152]. Moreover, the engineering of more similar human immunity in mice will be of importance when looking at cancer as the immune system is involved in cancer progression [149].

5. In vitro screening systems

Personalized therapy based on “the characteristics of leukemic cells and hosts” identified by innovative screenings systems are required to further improve treatment outcome as stated in the latest review of Ching-Hon Pui [153]. *In vitro* screenings are getting more comprehensive, and whole genome siRNA studies [154] or compound studies involving few hundred thousands of compounds [155, 156] are reality. The ultimate consequence of high throughput screenings is the down-scaling of individual conditions. This down-scaling implies analyses of few cells in 384 well-plate [157] or 1536 well-plate format [156]. Even smaller scales are possible with the spotting of siRNAs and cells on chips giving rise to cell microarrays with 30 to 500 cells per spot [158-160].

5.1. Co-culture systems for screens within a microenvironmental context

In leukemia, *in vitro* studies need to be conducted assessing leukemia cell responses within their microenvironmental context. Therefore, 2-layer systems have been established to screen for drugs killing leukemia cell lines using a stromal layer and leukemic cells plated on top [161]. Due to the amount of cells needed to conduct high-throughput screens, usually first cell lines are used and hits are verified in a second step in primary cells [162, 163]. Recently, a high-throughput compounds screening methodology was reported using primary mouse AML cells [164]. In the case of AML, a smaller scale kinome screening study with primary cells was reported identifying known, activating mutations in *JAK2* and *K-RAS*, as well as a previously undescribed, somatic, activating mutation in the thrombopoietin receptor [165]. Screening studies using primary cells were performed for other cancer types like ovarian carcinoma testing 3 patient samples for 3000 compounds [166]. The development of screening studies goes more and more in the direction of 3D models of different tumor microenvironments [167, 168] and ultimately *in vivo* screenings can be performed [169]. Momentarily, large scale *in vivo* screenings seem to be restricted to RNA interference systems. Gene sets using shRNA pools are downregulated in leukemic cells, which are then transplanted into mice and populations with a growth advantages are identified by sequencing. However, compound screenings in large scale *in vivo* settings are technically not feasible.

5.2. Advantages of image-based screenings

For the establishment of an *in vitro* high-throughput screening technology, the assay development depends on the platform and read-out used to perform the screen. Automated imaging using automated microscopes and automated analysis of images made it possible to conduct high throughput screenings based on visual phenotypes of individual cells [170].
The key steps of the development of an image-based screening are depicted in Figure 8.

The requirements for new *in vitro* screening technologies are high. The methods developed should be fast, cost-effective, user friendly, reliable and applicable to different experimental questions [160, 170]. The assay we developed has the aim to assess reliably viable cell

numbers of both cell types in a co-culture set-up in a 384 well-plate format. In the end, the addition of one solution to the plate was enough to perform automated microscopy and upon image analysis to identify living ALL cells and MSCs.

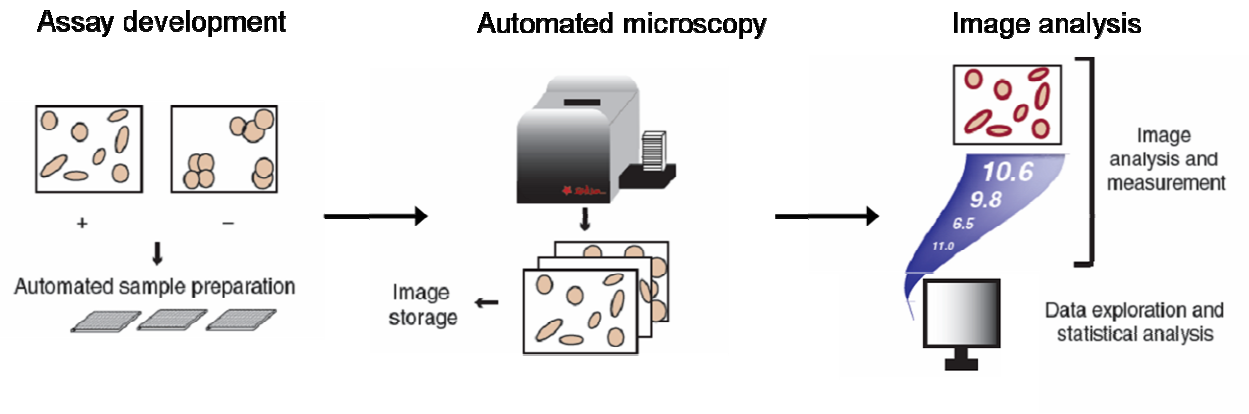

Figure 8. Key steps for establishing an image-based high-throughput screening method. Adapted from [170].

The assay I developed requires the use of an automated microscope and the analysis of the co-cultures images acquired. The image analysis protocol involves a machine learning step, where teaching of the software by the human eye and criteria of scientists can correct and implement complex cellular phenotypes in the computational process. These protocols can be downloaded for free and are thus made accessible to any laboratory and convey to requirements made by the high-throughput screening community [171].

Image-based analysis is not only used to determine cell proliferation or death but can find many applications: identification of cell death induced [154], intracellular localisation of proteins, morphology of organelles, kinetics of divisions [172], morphology of cells [154] or more complex phenotypes like angiogenesis [173] and whole organisms like the zebrafish [174] can be looked at. Ultimately, the image based approach can provide further insights in the interactions taking place between leukemic and stromal cells beyond the question of viability. Further development of the method has a great potential in answering relevant biological questions, also in regard to the protection of leukemic cells by the microenvironment.

Subject of Investigation

Microenvironmental interactions of B-ALL cells remain poorly investigated. Functional investigations of the microenvironment in human ALL are limited by the difficulty to conduct large scale *in vitro* studies. The amount of primary cells needed to conduct such studies became available by xenotransplantation of human leukemia cells in immunodeficient mice providing a powerful tool to model disease and amplify cells.

The major aims of my PhD Thesis were to:

- Establish a methodology using the co-culture system of primary leukemic cells with stromal cells to conduct large scale *in vitro* studies (manuscript 1)

- Investigate functional interactions of the microenvironment and childhood precursor B-ALL cells using RNA interference of stromal genes to identify new mechanisms of support (manuscript 2).

Manuscript 1: Multimodal high-content screening platform to study primary leukemia cells in co-culture with bone marrow stroma (first author).

In this manuscript, a detailed protocol is provided for the developed screening platform on how to conduct RNA interference or compound screening studies. Especially the set-up and different optimization steps of the platform are described.

Manuscript 2: Selective metabolic dependence of acute lymphoblastic leukemia on oxidative stress protection by bone marrow stroma (first author).

In this manuscript, I aimed for the identification of protective cues from MSCs that promote survival of primary B-ALL cells using RNA interference. The downregulation of Basigin (BSG) proved to decrease ALL cell survival in a large subset of B-ALL cases. Among BSG interacting proteins, I identified a member of the solute carrier family 3 (SLC3A2) that displayed the same phenotypic effect. SLC3A2 proteins play an important role in importing and exporting amino acids, including cystine. A subset of patient samples proved to be sensitive to cystine depletion and required continuous supply of cysteine by stromal cells. Cysteine enabled B-ALL cells to synthesize glutathione and to cope with their elevated ROS levels. The role of stromal cells in this important pro-survival mechanism was not previously acknowledged for primary B-ALL cells.

This manuscript includes the main part of the biological findings of my work and thus will be the essential part in the discussion section.

Manuscript 1

Multimodal high-content screening platform to study primary leukemia cells in co-culture with bone marrow stroma

Jeannette Boutter [1,4,5], Anna Rinaldi [1,4,5], Viktoras Frismantas [1,4,5], Andreas Vonderheit [2], Beat Bornhauser [1,5], Jean-Pierre Bourquin [1,5] and Peter Horvath [3]

1. Department of Oncology, University Children's Hospital Zurich, Switzerland
2. Institute of Molecular Biology (IMB), Mainz, Germany
3. Light Microscopy and Screening Centre, ETH Zurich, Switzerland
4. PhD program of the Life Science Zurich Graduate School Zurich, Switzerland
5. Children's Research Center (CRC), University Children's Hospital, Zurich, Switzerland

Submission to Nature Protocols after acceptance of manuscript 2

ABSTRACT

We describe here a simple and robust protocol to conduct high-content screens with primary leukemic cells in co-culture with bone marrow stromal cells in a 384 well-plate format. The addition of a single fluorescence dye to the co-cultures is sufficient to identify living acute lymphoblastic leukemia (ALL) cells and mesenchymal stromal cells (MSCs) using automated microscopy and a specifically developed image analysis pipeline. This open source platform enables identification of both cell compartments at the same time. It can be used for RNA interference studies, or to generate activity profiles of small molecules as single compounds and in combinations, and can be adapted to other cell types. The image acquisition and analysis pipeline takes 5 to 9 hours per plate and enables a rapid evaluation of leukemia cell viability after any perturbation.

INTRODUCTION

Innovative *in vitro* high-content screening methods are demanded for rapid and efficient translation of new anti-leukemic strategies into preclinical models [1]. The bone marrow microenvironment represents a candidate site for leukemic cells to escape chemotherapy, by promoting resistance of leukemic cells to chemotherapeutic agents due to numerous interactions affecting intracellular signalling [2-4]. Compounds to which leukemia cell lines were sensitive proved to be less effective in presence of stromal cells [5, 6]. The microenvironment may counteract treatment strategies and *in vitro* studies need to be conducted within a microenvironmental context to avoid unnecessary failures in further validation steps. Moreover, primary leukemia cells only survive *in vitro* using a co-culture system with mesenchymal stromal cells indicating that stromal cells provide survival cues for primary ALL cells [7, 8]. We therefore sought to establish a co-culture system for high-content screens with primary leukemia cells co-cultured on mesenchymal stromal cells. Due to the amount of cells needed to conduct such high-throughput screens, cell lines rather than primary cells were used so far [6], and hits were verified in a second step with primary cells or *in vivo* [9-11]. Based on the possibility to expand primary ALL cells *in vivo* in xenograft models, sufficient primary leukemic cells for high-throughput functional studies can be

generated. Xenotransplanted leukemia cells recapitulated the original disease reliably, indicating their usefulness for disease modeling [12-14]. We used the protocol described here to assess supportive signals that originate from mesenchymal stromal cells and sustain leukemia cell survival using RNA interference of candidate genes at stromal level (Boutter et al, 2013). Moreover, the assay is used in our laboratory to generate drug response profiles in precursor B-ALL and T-ALL and can be adjusted to other cell types than acute lymphoblastic leukemia cells (see Fig. 9 for an overview).

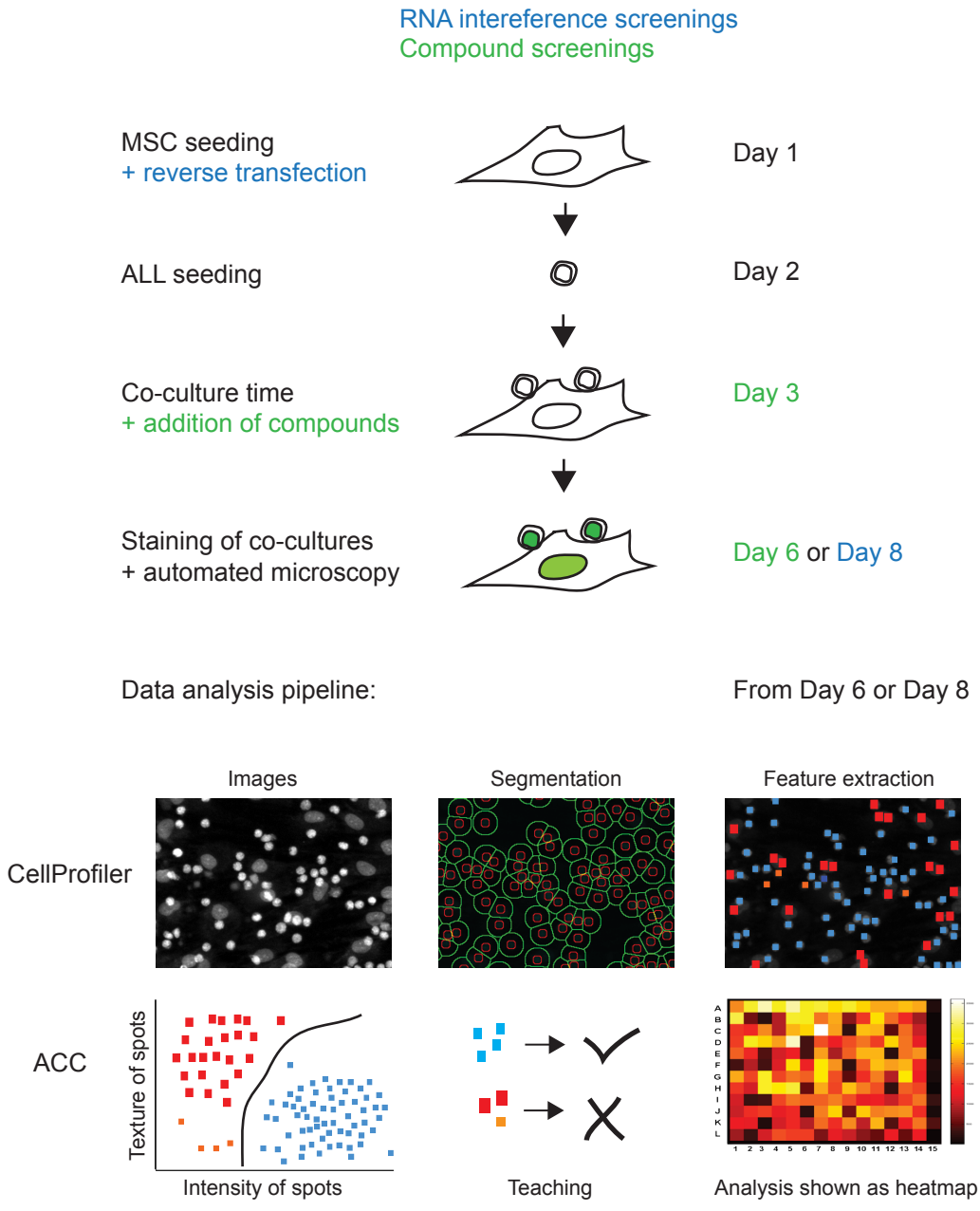

Fig.9. Overview of the high-content screening platform to study primary leukemia cells in co-culture with bone marrow stroma. The steps required only for RNA interference studies are depicted in blue. The steps required specifically for compound screens are shown in green. During image analysis, images are segmented (spots detected are marked by an inner and an outer ring). 52 intensity and texture features are assigned for the inner and outer ring of each spot. The Advanced Cell Classifier (ACC) is assigning the spots that represent living ALL cells (based on the extracted features and on teaching) and analyzes the whole plate. The number of viable ALL cells for each well on a 384 well-plate can be plotted as a heatmap.

The generation of drug response profile could be implemented in a preclinical setting with the aim to identify potential candidate compounds or combinations for the development of alternative treatment regimens that subsequently can be tested in experimental models *in vivo.* Our platform is versatile, and provides the possibility for combination of different dyes to investigate several cellular phenotypes.

The image-based approach we use to assess live and dead cells allows separation of both cellular compartments. Alternative methods such as spectrophotometry based protocols cannot differentiate between the two cellular compartments, and flow cytometry based approaches are not amenable for high throughput procedures. In viability analyses using MTT measurements that rely on detection of mitochondrial activity, the signals in MSCs were between 10 to 100 fold higher than in leukemic cells, rendering detection of differences in leukemia cells difficult. One particular advantage of this protocol is the fact that any effects on both cellular compartments can be verified in a second step by re-analysis of the original images. Especially in conditions where a high decrease in leukemia cell viability is observed, effects on stromal cells have to be considered.

The method presented here allows performing staining and microscopy in a nested manner. While for the first plate images are acquired, a second plate can already be processed for microscopy. The maximal amount of plates run for a day depends on the speed of the automated microscope and the staining protocol used. With our live cell imaging protocol we reach a maximum of 12 plates per day for compound screens with an automated microscope (image acquisition is one hour per plate). The image analysis pipeline and software are freely available under www.highcontentanalysis.org. We focus in this description on the reliable detection of living ALL cells. The main challenges for the analysis were to distinguish living ALL cells from dead cells and from sub-cellular compartments of the MSCs (eg. MSC nucleoli have similar size and intensity than the ALL cells). On the other hand, the method should be robust against different imaging conditions and pitfalls, such as vignetting effect, noise, or changes of illumination. To meet these demands, a two step approach was established. First, we used an ‘a trous’ wavelet transform-based spot detection algorithm to reliably detect ALL cells [15]. This method amplifies spots of a given size and suppresses non-corresponding spots (Fig. 10). The algorithm was implemented in the MatLab software and was built into the CellProfiler framework [16].

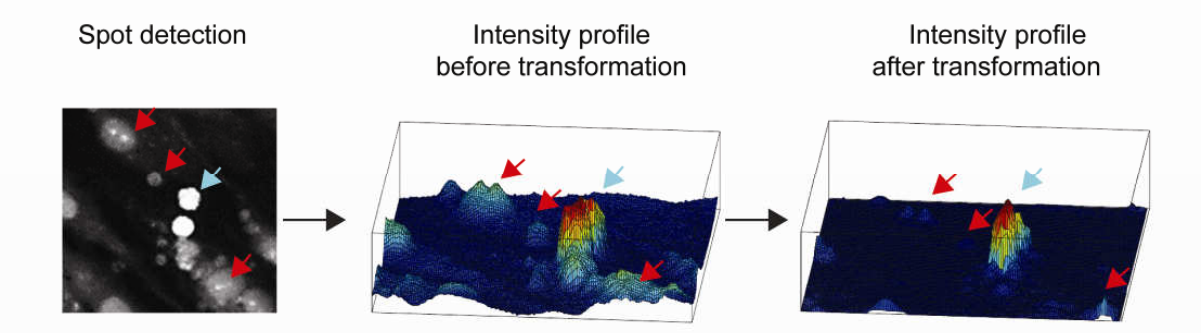

Fig.10. The CellProfiler software assesses the spots on an image. An ‘a trous’ wavelet transform-based algorithm was implemented in the CellProfiler software to improve the spot recognition. After spot detection, the ‘a trous’ wavelet transform-based algorithm transforms the images by amplifying spotsof a given size and suppresses non-corresponding ones. After this transformation, images are segmented and intensity and texture features are assigned for each detected spot.

For each detected spot on an image, over 50 intensity and texture-based features are extracted. The intensity features of detected spots consist for example of minimum, maximum, mean or standard deviation of the underlying pixels. The texture-based features are used to describe the homogeneity of staining pattern seen for each detected spot. None of the extracted features was per se able to reliably separate living ALL cells from misdetections. Therefore in a second step, we decided to use a multi-parametric approach automatically combining features. We used the Advanced Cell Classifier program [17], which is a supervised machine learning tool for high-content analysis (Fig. 11A). The Random forest classification method proved to be the most powerful classification method to detect ALL cells out of six methods tested [18] (see Fig.11B). The ACC relies mostly on intensity-based features to assign living ALL cells (see Fig.11C).

The assay we describe is performed with a live cell staining procedure and remained stable for up to 3 hours after staining (see Figure 12). We could not identify a dye that allowed maintenance of a reliable live and dead cell staining pattern after fixation of the co-cultures. The use of a live cell dye system restricts the amount of plates that can be screened for one given time point of analysis considering the speed of the automated microscope used. As a consequence, analyses like whole genome RNA interference screens with few hundreds of plates or compound screens assessing few hundred thousand of compounds are not feasible using live cell imaging, and will need development of live cell dyes amenable for fixation.
The protocol we present is suited for smaller scale screens such as whole kinome siRNA screens or screens using customized libraries (RNAi or small molecules) to study functionally primary leukemic cells in co-cultures.

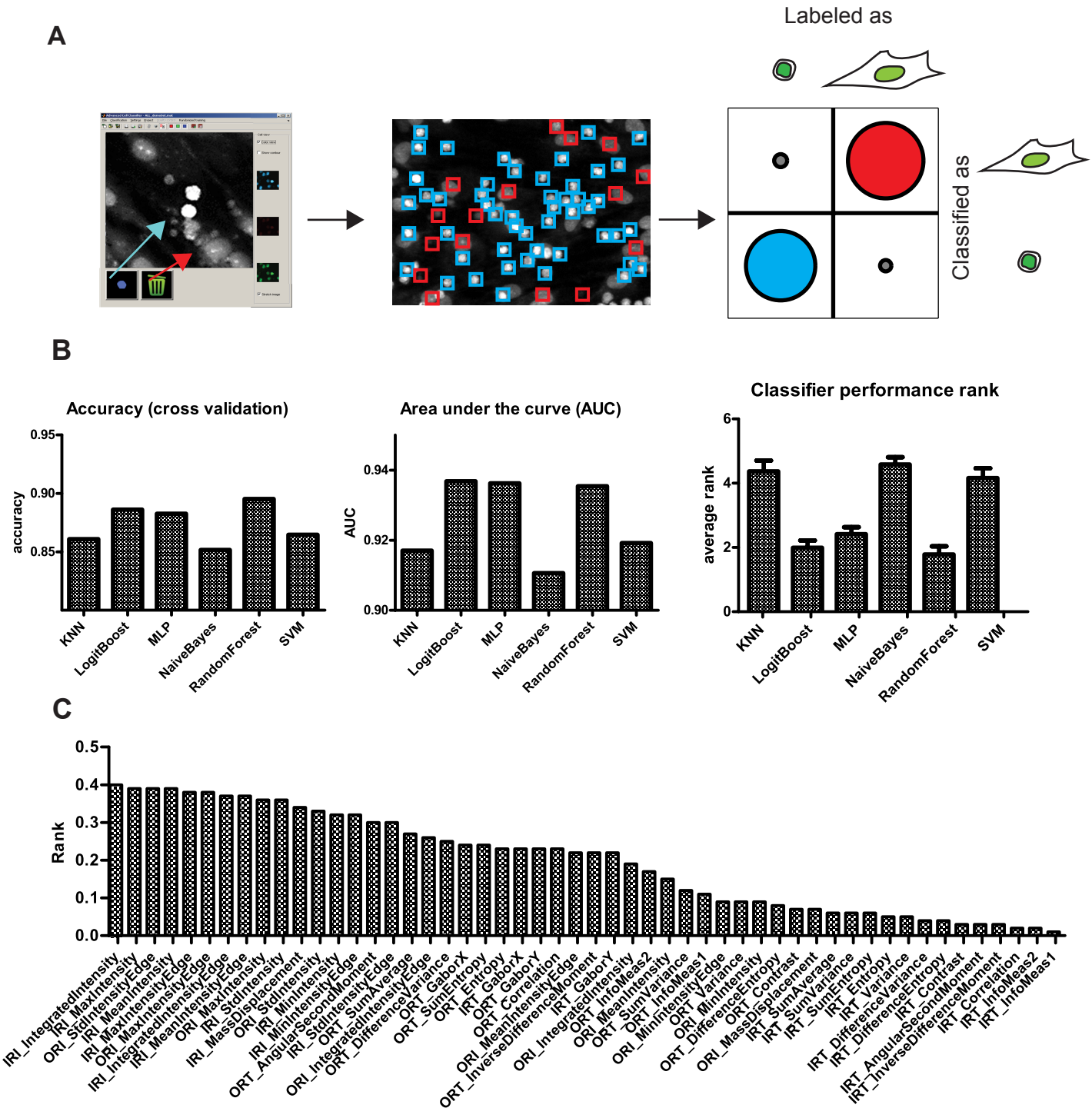

Fig.11. The Advanced Cell Classifier software identifies living ALL cells in the co-cultures with high accuracy. (A) Teaching the ACC manually the difference between living ALL cells (blue arrow) and MSCs or dead ALL cells (red arrow) enables the algorithm to assign all spots on each image that fulfil the criteria of living ALL cells and MSCs (blue boxes versus red boxes). The ACC shows a high correlation between the teaching and the assignement (classification) of cell phenotypes. Low false detection rates are important. (B) The correct classification depends on the classification method used. We assessed six different classification metrics (KNN=K nearest neighbor; LogitBoost=logistic regression with boosting; MLP=multilayer perceptron; Naïve Bayes; Random forest; SVM=support vector machine). Random forest classification reaches the highest accuracy across validations using 5-fold cross validation and the best values for the Area Under the Curve (AUC of ROC curve, which is an analysis tool to select optimal models and to discard suboptimal ones) and thus reaches the lowest average rank. 13 independent datasets from different days and patient samples in co-culture were used for these measurements. (C) The 52 extracted features used for spot recognition are shown ranked by their performance. Intensity features of the inner and outer ring are more important than texture-based features as reflected in their relative importance rank. IRI = inner ring intensity, ORI = outer ring intensity; IRT= inner ring texture, ORT = outer ring texture

Experimental design

Testing of the co-culture

Among different stromal cell lines tested, only cell lines retaining growth inhibition by cell-to-cell contact were appropriate for this microscopic read-out. For RNA interference of genes at stromal level, peptide based transfection reagents proved to subsequently affect ALL cell viability much less than lipid-based transfection reagents. We further assessed different ratios of cells for the co-cultures and found the ratio of ALL cells to MScs of 10:1 to result in stable survival of ALL cells, and down-scaled the conditions to the 384 well-plate format with reproducible results using 2500 MSCs with 25 000 ALL cells. The adaption to the 384 well-plate format represents an important step in down-scaling the co-culture system as 75% of cells are spared compared to 96 well-plates, and the throughput can be considerably increased. The reduction to a 1536 well-plate format could even provide further reduction of cell numbers required, with an additional increase in the speed of the analysis, however care needs to be taken with respect to the stability of the system. The density of leukemic cells *in vitro* proved to be crucial due to paracrine factors [19] and the variability between wells could become critical and may require automated pipetting using robotics.

Optimize the staining procedure

We took advantage of the CyQUANT® Direct Cell Proliferation Assay and changed the protocol for adaptation to microscopy based read-outs. Compound A of this assay stains the nuclei of all cells, both dead and living, and compound B quenches the fluorescence of compound A in dead cells and in the medium resulting in low background levels. The staining procedure can be adapted to different cell types used. Generally, for more cells more compound A is needed. To ensure good distinction between living and dead cells the ratio of compound A to compound B for a given cell number is critical. Equilibrium between compound A and B, which lasts for a few hours, must be reached before imaging. After a few hours, diffusion of compound A from living cells occurs and compound B looses its quenching functions leading to an overlap of dead and living cell staining intensity (see Fig.12A). The time until equilibrium is reached and its duration can be assessed by performing time course experiments with repetitive analyses (see Fig.12B). Depending on how the automated microscope proceeds through the plate (left to right for example), control wells over the whole plate should be included. Only in equilibrium conditions, the staining remains stable over time, which results in control wells with the same viable cell numbers independently of their positions on the plate. Moreover, we advise to validate the microscopy method by performing experiments in parallel with an alternative method (e.g. flow cytometry). We further optimized the staining procedure by replacing the 2 step addition of staining solutions described for RNA interference studies by the usage of a single addition step used in the protocol described for compound screens

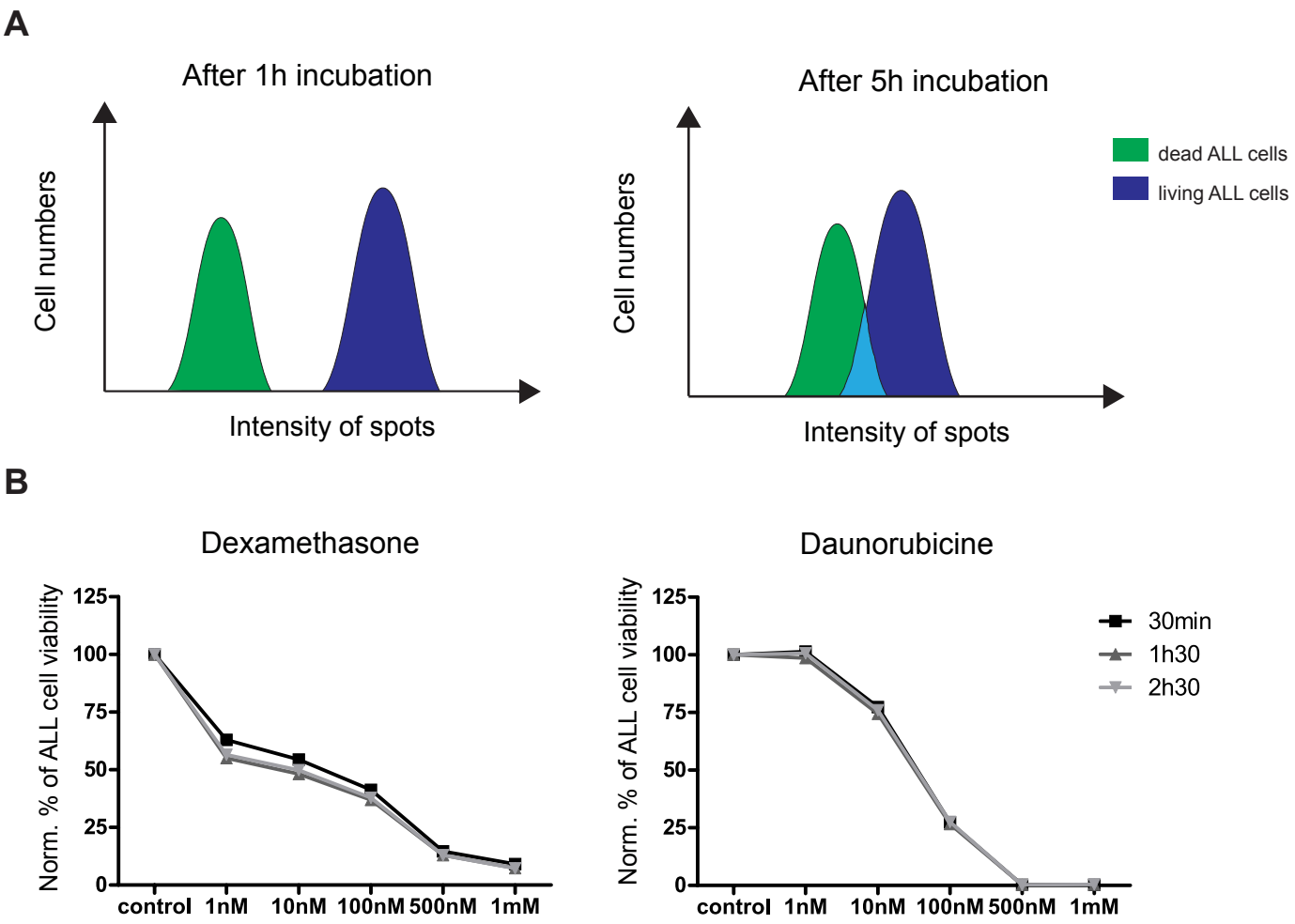

Fig.12. The staining of the co-cultures is stable for 3 consecutive hours. (A) Clear intensity differences are seen for living and dead ALL cells one hour after incubation with the staining solution. After 5 hours of incubation, the differences of intensities gets smaller and no clear distinction is possible between living and dead ALL cells. (B) Two plates with co-cultures of ALL and MSCs treated with Dexamethasone or Daunorubicine were assessed reliably until 3 hours post-staining.

Proceed with quality control experiments

In the 384 well-plates, positive and negative controls should be present in adequate numbers and preferentially following random patterns. We also included one control row covering the whole length of the plate. For RNA interference, we used negative control siRNAs and siRNAs affecting the MSCs resulting in loss of leukemia cell viability. The siRNA library can be diluted in daughter plates where positive and negative controls are present. The volume of siRNA solution in the daughter plates can be adapted to the number of plates and replicates to be performed per screening round. For drug screens, DMSO control wells and drugs that proved to kill leukemia cells in most of the cases tested are used. We used 5 concentrations 1nM, 10nM, 100nM, 1µM and 10µM, to calculate accurate IC50 values. The compound library with a concentration of 10mM is used to do serial dilution to achieve desired concentrations in daughter plates. Pipetting schemes and dilutions can be adapted freely to the desired conditions. Importantly, we did not see any changes in the standard deviations of cell numbers if the seeding of the cells and/or the staining procedure was performed manually or with a pipetting robot (data not shown). We recommend the use of pipetting robots to respect complex pipetting schemes, if required.

MATERIALS

REAGENTS

- MSC cell line (Applied Biological Materials Inc., cat. no. T0523)
- ALL cells: primary human cells isolated from the spleen after transplantation in NSG mice
- CyQUANT® Direct Cell Proliferation Assay with compound A and B (Life Technologies, cat. no. C35011 or C35012)
- RPMI-1640 medium (e.g., Life technologies, cat. no. 21875091)
- Penicillin-Streptomycin, liquid (e.g., Life technologies, cat. no.15140148)
- Heat inactivated FBS (e.g., Life technologies, cat. no.10082147)
- Hydrocortisone (Sigma-Aldrich, cat. no. H0888)
- Trypsin/EDTA (e.g., Life technologies, cat. no. 25200-056)
- Compound libraries (e.g., Tocris Bioscience, cat. no. 2884)
- DMSO (Sigma-Aldrich, cat. no. D8418)
- AIM-V medium (Life technologies, cat. no.12055091)
- siRNA oligonucleotide libraries (e.g., Thermo Scientific)
- INTERFERin transfection reagent (Polyplus transfection, cat. no. 409-10)
- Nulcease free water (Qiagen, cat. no. 129114)
- Positive control siRNAs (Qiagen, cat. no 1027281)
- Negative control siRNAs (Qiagen, cat. no 1027299 and Thermo Scientific cat. no. D-001810-01-05)

EQUIPMENT

- 384 well-plates for microscopy, black with clear bottom (Thermo Scientific, cat. no. 4332)
- 384 deep well-plates for diltutions (Greiner bio-one, cat. no. 781280)
- Aluminium sealing Films (Axygen, cat. no. PCR-AS-200)
- Multichannel pipette with 12 channels (e.g., Eppendorf, cat. no. 4861000139)
- Reservoirs (Nalge Nunc International, cat. no.370905)
- Automated liquid handling robot (e.g., Eppendorf, cat. no. 5070 000.719) with recommended tips
- Automated fluorescence microscope with environmental control and 10x objective (e.g., Molecular Devices, ImageXpress Micro microscope)
- Computer with MatLab software
- Hard drives/ server for storage of images

REAGENT SETUP

MSC Medium RPMI-1640 is supplemented with 0.5% (v/v) penicillin-streptomycin, 1µM hydrocortisone and 10% (v/v) heat inactivated FBS
Growth medium RPMI-1640 is supplemented with 0.5% (v/v) penicillin-streptomycin and 10% (v/v) heat inactivated FBS
Medium for transfection RPMI-1640 is supplemented with 0.5% (v/v) penicillin-streptomycin

EQUIPMENT SETUP

For experiments with RNA interference libraries or compound libraries, the use of an automated liquid handling robot is recommended. Complex pipetting schemes can be pre-programmed and used for each experiment.

PROCEDURE

MSC seeding

1. Prepare MSC for RNA interference studies (option A) or for compound screenings (option B).

A) RNA interference studies

(i) Dilute the siRNA library with nuclease free water and prepare daughter plates using the 384 deep well-plates including positive and negative siRNA controls in a randomized pattern with a final concentration of 240 nM. Store the mother and daughter plates sealed at -80℃.

(ii) Trypsinize MSC cells and resuspend the pellet in growth medium having 50'000 cells/ ml.

(iii) Pipette 10µl of siRNA from the daughter plates (240 nM) into the 384 well-plates for microscopy.

(iv) Prepare the transfection reagent mix with per well 0.5 µl of INTERFERin and 19.5 µl medium for transfection and add 20 µl of transfection reagent mix to each well containing siRNAs.

(v) Vortex gently the plate and incubate for 10 minutes at room temperature.
CRITICAL STEP The same batch of the transfection reagent should be used for the whole experiment. Therefore, we recommend testing different batch numbers of the transfection reagent and then using only one batch for all screening procedures.

(vi) Add 50 µl of MSC cells in growth medium (2500 cells) to each well (manual or robot pipetting) and place the plates in the incubator for 24 hours.

B) Compound screening

(i) Trypsinize MSC cells and resuspend the pellet in growth medium having 50'000 cells/ml.

(ii) Add 50 µl of MSC cells in growth medium (2500 cells) to 384 well-plates for microscopy (manual or robot pipetting) and place the plates in the incubator for 24 hours.

CRITICAL STEP MSC cells are slowly proliferating and should always have a density between 40 and 80% with regular passaging to avoid dedifferentiation. Low-number passage should be used. Hydrocortisone is toxic for leukemia cells and should not be added when plating MSCs for co-cultures.

ALL seeding

2. Prepare ALL cells for RNA interference studies (option A) or for compound screenings (option B).

A) RNA interference studies

(i) Thaw the frozen ALL cell aliquots using growth medium and spin down the cells. Resuspend the pellet in AIM-V medium with a final dilution of 500'000 cells/ ml.

(ii) Remove medium from transfected MSC cells and add 50 µl of ALL cells (25'000cells) in AIM-V medium (manual or robot pipetting). Place the plates in the incubator for 6 days.

B) Compound screening

(i) Dilute the compound library with DMSO to a final concentration of 10mM and prepare daughter plates using the 384 deep well-plates. Store the mother and daughter plates sealed at -80℃.

(ii) Thaw the frozen ALL cell aliquots using the medium and spin down the cells. Resuspend the pellet in growth medium so that 25'000ALL cells are in 57,5µl.

(iii) Remove medium from MSC cells and add 57.5 µl of ALL cells in growth medium to each well (manual or robot pipetting). Place the plates in the incubator for 24 hours.

(iv) After 24 hours, add 5ul of the compound library daughterplates to the co-culture plates using a pipetting roboter. Follow the deployed pipetting scheme to obtain on the same plate the desired concentrations for each drug.

Staining of co-cultures

3. Stain co-cultures for RNA interference studies (option A) or for compound screenings (option B).

A) RNA interference studies

(i) Prepare Cyquant staining solution in AIM-V medium to add 25µl per well reaching a final dilution of component A of 1:375 and of component B of 1:75.

(iii) Add 25µl of staining solution to each co-culture well (manual pipetting) and place the plates in the incubator for 45 minutes.

(iv) Remove staining solution carefully.

(v) Add 30µl of AIM-V medium with compound B diluted 1:100 and incubate the plate for 1 hour at 37℃, 5%CO_2.

B) Compound screening

(i) Prepare Cyquant staining solution in growth medium to add 20µl per well reaching a final dilution of component A of 1:1240 and of component B of 1:80.

(ii) Add 20µl of staining solution to each co-culture well (manual pipetting) and place the plates in the incubator for 1 hour.

TROUBLESHOOTING

Automated microscopy

4. Put the plates into the automated microscope with powered environmental control (37℃, 5%CO_2)

5. Load your settings (plate type, objective type, fluorescence settings of the green channel and focus settings) and check that the plate is in the focus and the illumination time is adequate. CRITICAL STEP Used plates need to be configured in the automated microscope as the focus settings and plate sizes are highly dependent on the plate types used. Illumination time needs to be adapted to be in the optimal range of pixel intensity. Wells with the highest cell number (usually negative control wells) should be unsaturated allowing a maximal range of intensity changes in images for the analysis.

6. Start the imaging. PAUSE POINT

Image analysis

7. Image segmentation and feature extraction

(i) Go to the folder where the images from the automated microscope are stored and create 3 new folders named ‘anal1’, ‘anal2’ and ‘anal3’. Layout of the folders should be a Project folder containing a Plate folder containing the 3 anal folders with the tif files from the automated microscope.

(ii) Rename the images if necessary using the Plate folder name, followed by the well and the number of the image (if more than one image per well was taken).

(iii) Start MatLab and open CellProfiler.

(iv) Load the analysis pipeline “ALL_10x_pipe” into the CellProfiler

(v) Load the images from the automated microscope by inserting the address of the Plate folder into the CellProfiler windows “Default Image Folder” and “Default Output Folder”

(vi) Click on Analyze images. PAUSE POINT

8. Machine learning

(i) Open Matlab and load the Advanced Cell Classifier (ACC) script.

(ii) Open a new project and select the Project folder containing all files.

(iii) Select 384 well-plate in “plate type”

(iv) Start selecting living ALL cells and mark them as positive examples.

(v) Select dead ALL cells, debris and nucleoli of MSC cells and mark them as negative examples.

(vi) Click on “train classifier” and choose the classifier SimpleLogistic.weka and click on Train.

(vii) Go to your positive and negative controls and check that only living ALL cells are recognized. CRITICAL STEP Recognition should be easy and few positive and negative examples (n=20) are sufficient for the ACC to accurately recognize the cells.

(viii) If the training gives satisfactory results, click on “Predict selected plates”. The analysis will be stored in the folder anal2 as excel file named *name_cumul_1_v_1_2* and contain the numbers of living ALL cells per well.
PAUSE POINT
TROUBLESHOOTING.

9. Quality control

Once the staining is performed, the plate can be imaged for consecutive 3 hours (see Fig.12). The standard deviations for the same conditions achieve maximally 20% (see Fig. 13). Viability decrease of ALL cells in biological replicates was reproducible with low standard deviations. For technical replicates, the variability can increase especially in compound screens, where the IC50 depends on a curve fitting process taking place on a logarithmic scale (see Fig.13). Therefore we recommend using 2 parameters to assess the effect of a compound on ALL cell viability, i.e. IC50 and area under the curve (AUC).

TIMING

Step 1: 1 to 4 hours for transfection studies (optionally automated)
Step 2: 2 to 10 hours for compound addition to plates (automatically)
Step 3: 1 to 2 hours
Step 4 to 6: up to an hour, depending on the speed of the microscope and numbers of images taken
Step 7: 2 to 4 hours
Step 8: 1 to 2 hours
Step 9: typically done before screening procedure during optimization steps, per screen around 15 min are needed.

TROUBLESHOOTING

Step 3.

- If the cell numbers for the same conditions on a plate are not equal (e.g., show a gradient from left to right) the staining equilibrium was not reached.
- If the staining is too faint, more compound A is needed.
- If no clear distinction can be made between living and dead cells based on the staining intensity (positive and negative control wells have the same staining pattern), not enough compound B was used.

Step 8.

- As different patient samples can have different cell staining phenotypes, it is recommended to use one primary cell type per teaching in the ACC step.
- If living cells were detected in the positive control wells but a clear distinction between positive and negative control wells is possible, re-perform the machine learning process in step 8, using more examples for living and dead cells.
- During teaching, it is best to use clear examples of living ALL cells and examples of recognized spots which are clearly not living ALL cells. The Advanced Cell Classifier software will implement the information of these clear examples and extract features living cells should have. Even in difficult images, the ACC will be able to recognize

the correct classification. One should not try to classify the cells where no clear phenotype is recognizable, as this would weaken the decision-making process of the algorithm.

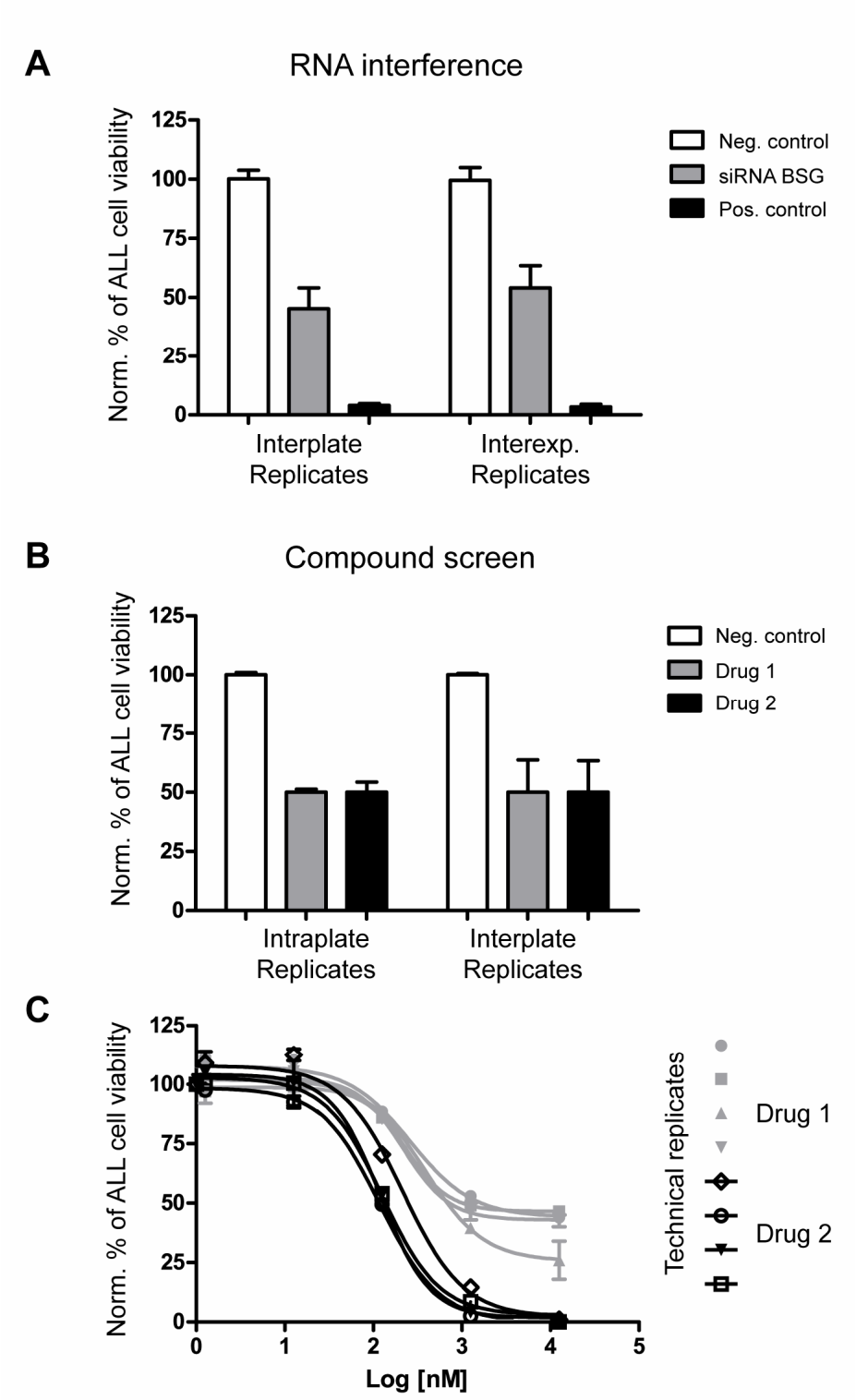

Fig.13. High reproducibility of replicates is achieved for RNA interference and compound screen studies. (A) Results of treatment of MSC with positive control, siRNA for BSG or negative controls are shown with SEM for interplate and interexperiment replicates for one patient sample. (B) Negative control and 2 IC50 values for two different drugs are shown for intraplate and interplate replicates. (C) The dose response curves used to assess SEM of biological replicates in (B) are shown.

ANTICIPATED RESULTS

The co-cultures display patient specific characteristics requiring a machine learning step. With this approach a reliable assessment of primary living ALL cells from different cases in co-cultures is possible. Examples of images from different patient samples in co-culture with clear ALL cell viability decreases achieved by RNA interference or with small molecules compared to the negative controls, are shown in Fig.5 A. Images with suboptimal staining conditions are shown in Fig. 5 B. The conditions where not enough compound B is used are most difficult to recognize, as dead cells will appear stained. However, all wells in the plate will look the same and show the same cell number after analysis. Moreover, dead cells don't show a co-culture pattern seen in Fig. 5A, but are typically equally distributed over the well. Moreover, examples of images with normal and affected MSC layer are shown in Fig.5B. Even in difficult images, the ACC is usually able to recognize the requested phenotypes, and gives correct ratios for the investigated effects. However, we recommend optimizing staining and experimental conditions to ensure a good reproducibility of obtained results.

Authorship Contributions:

J.B., A.R. and V.F. performed experiments and analyzed data; A.V. helped in setting up the platform; P.H. established the image analysis pipeline; B.B. and J.-P.B. designed research and all authors wrote the manuscript.

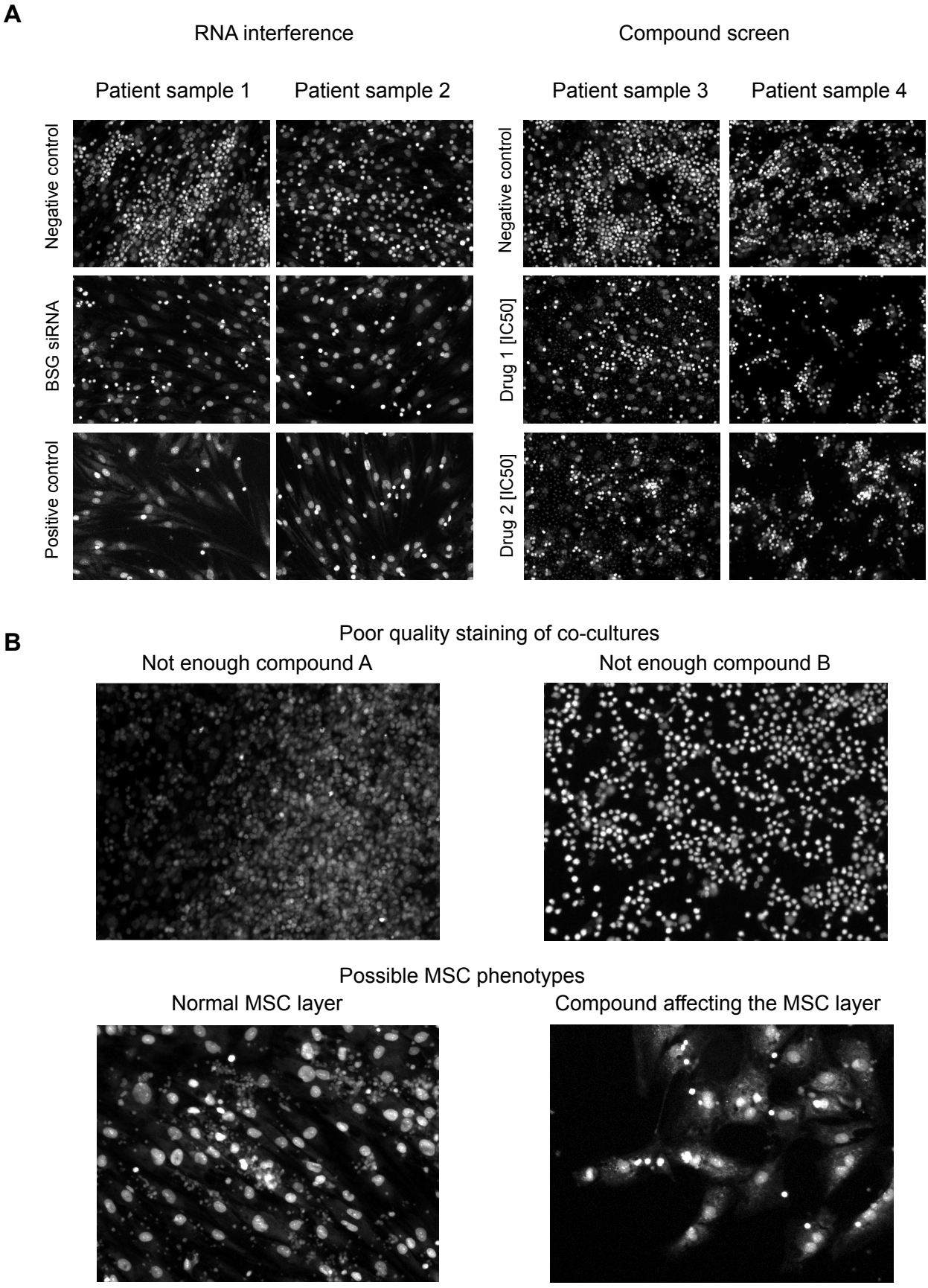

Fig.14. Microscopy images of co-cultures of different patient samples. (A) In the negative control images, patient-specific patterns in the co-cultures are seen, e.g. some ALL cells cluster more than others. Less viable ALL cells are seen after RNA interference of BSG in stroma, the positive control and for 2 drugs used at ≈IC50. (B) Images with suboptimal staining conditions are shown. In conditions with insufficient compound A, ALL cells are not brightly stained. In conditions with insufficient compound B, dead ALL cells appear stained. (C) Effects on MSCs are detected reliably. A comparison with a normal phenotype of the MSC layer (left) and with affected MSC layer (right) is given.

REFERENCES

1. Pui, C.H., et al., *Pediatric acute lymphoblastic leukemia: where are we going and how do we get there?* Blood, 2012. **120**(6): p. 1165-74.
2. Bailey, L.C., et al., *Bone-marrow relapse in paediatric acute lymphoblastic leukaemia.* Lancet Oncol, 2008. **9**(9): p. 873-83.
3. Dias, S., et al., *VEGF(165) promotes survival of leukemic cells by Hsp90-mediated induction of Bcl-2 expression and apoptosis inhibition.* Blood, 2002. **99**(7): p. 2532-40.
4. Mudry, R.E., et al., *Stromal cells regulate survival of B-lineage leukemic cells during chemotherapy.* Blood, 2000. **96**(5): p. 1926-32.
5. Iwamoto, S., et al., *Mesenchymal cells regulate the response of acute lymphoblastic leukemia cells to asparaginase.* J Clin Invest, 2007. **117**(4): p. 1049-57.
6. McMillin, D.W., et al., *Tumor cell-specific bioluminescence platform to identify stroma-induced changes to anticancer drug activity.* Nat Med, 2010. **16**(4): p. 483-9.
7. Gluck, U., et al., *Long-term proliferation of human leukemia cells induced by mouse stroma.* Exp Hematol, 1989. **17**(5): p. 398-404.
8. Whitlock, C.A. and O.N. Witte, *Long-term culture of B lymphocytes and their precursors from murine bone marrow.* Proc Natl Acad Sci U S A, 1982. **79**(11): p. 3608-12.
9. Tibes, R., et al., *RNAi screening of the kinome with cytarabine in leukemias.* Blood. **119**(12): p. 2863-72.
10. Nijmeijer, B.A., et al., *Monitoring of engraftment and progression of acute lymphoblastic leukemia in individual NOD/SCID mice.* Experimental Hematology, 2001. **29**(3): p. 322-9.
11. McDermott, S.P., et al., *A small molecule screening strategy with validation on human leukemia stem cells uncovers the therapeutic efficacy of kinetin riboside.* Blood. **119**(5): p. 1200-7.
12. Clappier, E., et al., *Clonal selection in xenografted human T cell acute lymphoblastic leukemia recapitulates gain of malignancy at relapse.* J Exp Med, 2011. **208**(4): p. 653-61.
13. Notta, F., et al., *Evolution of human BCR-ABL1 lymphoblastic leukaemia-initiating cells.* Nature, 2011. **469**(7330): p. 362-7.
14. Schmitz, M., et al., *Xenografts of highly resistant leukemia recapitulate the clonal composition of the leukemogenic compartment.* Blood, 2011.
15. Olivo-Marin, J.-C., *Extraction of spots in biological images using multiscale products.* Pattern Recognition, 2002. **35**(9): p. 1989-1996.
16. Carpenter, A.E., et al., *CellProfiler: image analysis software for identifying and quantifying cell phenotypes.* Genome Biol, 2006. **7**(10): p. R100.
17. Horvath, P., et al., *Machine learning improves the precision and robustness of high-content screens: using nonlinear multiparametric methods to analyze screening results.* J Biomol Screen, 2011. **16**(9): p. 1059-67.
18. Duda R, H.P., Stork D, *Pattern Classification (2nd edition).* Wiley-Interscience, 2000.
19. Freedman, M.H., et al., *Autocrine and paracrine growth control by granulocyte-monocyte colony-stimulating factor of acute lymphoblastic leukemia cells.* Blood, 1993. **81**(11): p. 3068-75

Manuscript 2

Selective metabolic dependence of acute lymphoblastic leukemia on oxidative stress protection by bone marrow stroma

Jeannette Boutter [1, 7, 8], Yun Huang [1], Andreas Vonderheit [2], Michael A. Grotzer [1], Cornelia Eckert [3], Gunnar Cario [4], Bernd Wollscheid [5], Peter Horvath [6], Beat C. Bornhauser [1, *] and Jean-Pierre Bourquin [1, *, #]

1. Department of Pediatric Oncology, University Children's Hospital Zurich, Switzerland
2. Institute of Molecular Biology (IMB), Mainz, Germany
3. Department of Pediatric Oncology/Haematology, Charité Universitätsmedizin Berlin, Germany
4. Department of Pediatrics, University Medical Centre Schleswig-Holstein, Kiel, Germany
5. Department of Biology, Institute of Molecular Systems Biology, ETH Zurich, Switzerland
6. Light Microscopy and Screening Centre, ETH Zurich, Switzerland
7. PhD program of the Life Science Zurich Graduate School Zurich, Switzerland
8. Children's Research Center (CRC), University Children's Hospital Zurich, Switzerland

* contributed equally to this study
# corresponding author

Manuscript submitted to Journal of Experimental Medicine

ABSTRACT

Interactions with the bone marrow microenvironment are essential for leukemia cell survival. We developed an image-based RNA interference platform to identify protective cues from bone marrow derived mesenchymal stromal cells (MSCs) that promote survival of primary acute lymphoblastic leukemia (ALL) cells. Using a candidate gene approach, we detected specific and distinct contributions of stromal genes to survival of individual ALL samples. The strongest effects were observed after downregulation of the vascular endothelial growth factor C (VEGFC) or of Basigin (BSG, alias CD147). Dependence from stromal VEGFC predicted sensitivity to VEGF receptor kinase inhibitors. BSG expression was required to provide metabolic support to a subset of ALL via SLC3A2, which forms heterodimeric amino acid transporters (HAT) on MSC. Cystine import by stromal HATs provides the limiting substrate to generate cysteine for ALL cells. This metabolic interaction maintains glutathione levels and reduces oxidative stress specifically in ALL cases that were dependent on stromal BSG/SLC3A2. Thus, functional evaluation of intercellular interactions between leukemia cells and their niche with such a platform will provide a new layer of personalized information for the development of rationale treatment combinations.

INTRODUCTION

Leukemia cells subvert normal hematopoietic stem cell niches and can infiltrate sanctuary sites such as the central nervous system to escape therapy [65]. Microenvironmental interactions are important for leukemia cell survival, and maintenance of primary leukemic cells *in vitro* is achieved by co-culture with stromal cells [121, 122]. The intercellular crosstalk between leukemia cells and their microenvironment is strongly influencing their cellular states and their responsiveness to chemotherapy [102, 161]. The identification of leukemia-specific patterns of intercellular dependence will possibly provide new options to refine treatment.

Mesenchymal stromal cells (MSC) that are derived from human bone marrows support leukemia survival in cocultures. [129, 131] and reconstitute functional hematopoietic niches *in vivo* [147, 184]. Explanted MSC include multipotent skeletal progenitors that can form heterotopic bone in transplantation models. Evidence from mouse models indicate that the hematopoiesis-supporting niche is derived from mesenchymal stem cells [41, 44]. These cells, which can regenerate bone tissue with osteoblasts and stroma *in vivo*, were localized to the perivascular space [31]. The pathways and molecular interaction that determine the hematopoietic stem and progenitor cell niche are explored using different experimental models [185]. Only a few mechanisms have been described that support leukemia propagating cells in precursor B acute lymphoblastic leukemia (BCP-ALL). Factors that contribute to the localisation of leukemia cells in the niche such as the chemokine receptor CXCR4 [67, 186] or the α4β1integrin, VLA-4, have been implicated [85, 86]. Growth factors such as SDF-1 and VEGF were critical to maintain certain BCP-ALL samples in stromal co-cultures [72]. Given the metabolic deregulation with increased dependence on glycolysis observed in myeloid leukemia cells [108], dependence on metabolic support from stroma could be essential for leukemia survival.

Here we have developed an image-based platform for functional genomic interrogation of the intercellular crosstalk between leukemia and bone marrow derived MSCs. Our recently established xenograft model of ALL [136, 187] enabled systematic functional evaluation of patient derived primary leukemia samples. Using a candidate gene approach, we identified reproducible patient specific dependence patterns on stromal gene expression, involving different pathways. The most detrimental effect on leukemia survival was achieved by down-regulation of Basigin (CD147, BSG) on stroma, which we show to be critical for the function of an amino acid transporter including the subunit SLC3A2. A subset of ALL samples was critically dependent on metabolic support from stroma cells to protect them from oxidative stress, suggesting important underlying differences between individual leukemias with respect to metabolic deregulation. As recently shown in a model of chronic lymphocytic leukemia, we could confirm that the protective mechanism involved production of cysteine to maintain gluthathione levels in leukemia cells, resulting in protection from oxidative stress [115].

RESULTS

Bone marrow derived mesenchymal stromal cells provide different pro-survival cues to support B-cell precursor ALL

Bone marrow derived, immortalized MSCs have been established to support leukemia cell survival in a model of the leukemia microenvironment [129]. With the aim to use this system for the functional investigation of critical intercellular interactions between leukemia and stromal cells, we determined the kinetics of 24 primary BCP ALL samples on human MSC in the 384 well-plate format (Fig. 15 and suppl. Table 1). These samples included cases from different prognostic groups based on clinical criteria [24] (Suppl. Table 1). In single cell suspension cultures, the viability dramatically decreased within one week (Figure 15A and B and data not shown). In contrast, 21 out of 24 ALL samples were maintained alive on stroma in serum-free culture conditions (Fig. 15B). As reported previously [131], such cultures could be maintained over weeks by serial replating on MSCs (not shown). Out of the three cases that showed proliferation, a sample with a translocation t(17;19) could be established as a cell line under serum-containing conditions (VHR-23). Only 3 samples could not be maintained in MSC co-cultures, suggesting important differences in the dependence from microenvironmental factors among different ALL samples. Neither supplementation of the culture medium with FCS nor a change of the medium formulation influenced the results significantly (data not shown). We next used the transwell system to physically separate the two compartments, in order to understand to which extent direct cell-to-cell contact was required for survival support for 7 selected cases (Fig. 15C). While a majority of the samples clearly depended on contact-mediated support, 2 cases that carried the translocations t(17;19) and t(1;19), respectively, were maintained by soluble factors only. Collectively, these results suggest important underlying differences among ALL samples with respect to the dependence from the microenvironment. Given the marked difference in survival observed within one week of culture with or without MSC support, we hypothesized that this model would reflect important interactions and could serve as a platform for functional investigations.

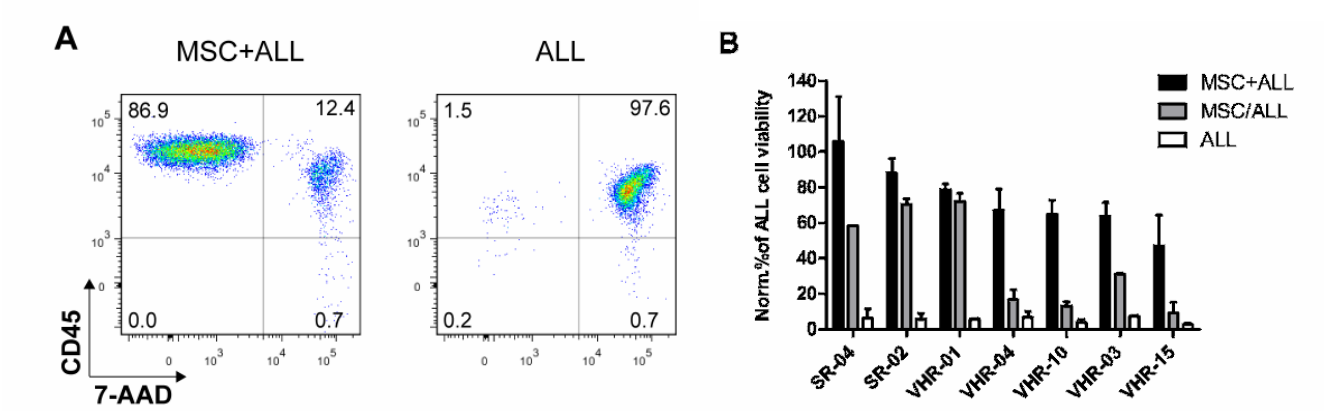

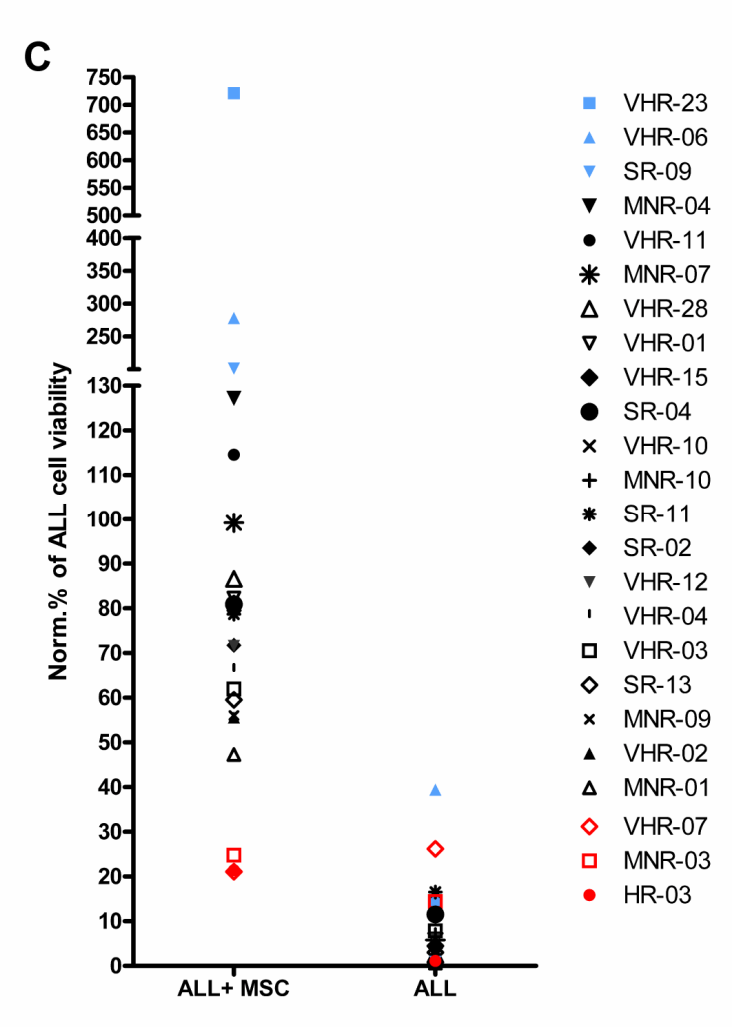

Fig. 15. Bone marrow derived mesenchymal stromal cells (MSC) provide different pro-survival cues to support B-cell precursor ALL. (A) Comparison of viability of ALL cells in suspension or in co-culture with MSCs for 6 days was assessed by flow cytometry using CD45 and 7-AAD staining. (B) 24 BCP-ALL cases were tested for their survival on MSCs after 6 days of co-culture. Viable cell numbers at days 6 were compared to the viable cell numbers of primary ALL cells assessed at day 1. SR: standard risk group. HR: high risk group. VHR: very high risk group. MNR: morphological non responder, relapse cases. (C) Comparison of ALL cell viability in co-culture with MSCs (MSC+ALL), separated via a Transwell (MSC/ALL) or in suspension culture alone (ALL) after 3 days. SR-02 is carrying a t(1;19) and VHR-01 a t(17;19) translocation. Viability was assessed by FACS and performed at least in duplicates and normalized to the viable cell numbers of primary ALL cells assessed at day 1.

Automated live cell imaging facilitates large-scale cell viability analysis of leukemia co-cultures on MSCs

To analyse adherent co-cultures of two cell types without disrupting their interactions, we developed a microscopy-based screening platform in a 384 well format that is suitable for assays at large scale (Fig. 16). Optimal cell culture conditions were met with 25’000 leukemia cells per well in a 10:1 ratio on MSCs, which is relevant given the limited availability of primary patient material. Use of a live cell permeable fluorescent dye resulted in the best contrast between living ALL cells and MSCs, enabling the discrimination of ALL and MSC nuclear structures using the same fluorescence channel by microscopy (Fig. 16A). Image acquisition was set to cover more than half of the well’s surface area. For image analysis, an ‘a trous’ wavelet transform-based spot detection algorithm was implemented using the

CellProfiler software to identify ALL cells [179, 180]. To further avoid misdetections, ALL cells were classified using a machine-learning program called Advanced Cell Classifier (ACC) [181]. A good correlation of the cell viability data that was obtained by automated microscopy and 7-AAD staining analyzed by flow cytometry of the same experiments was reproducibly achieved, an example is provided in Fig. 15B. This constitutes the basis of a platform for small molecule and RNA interference screening.

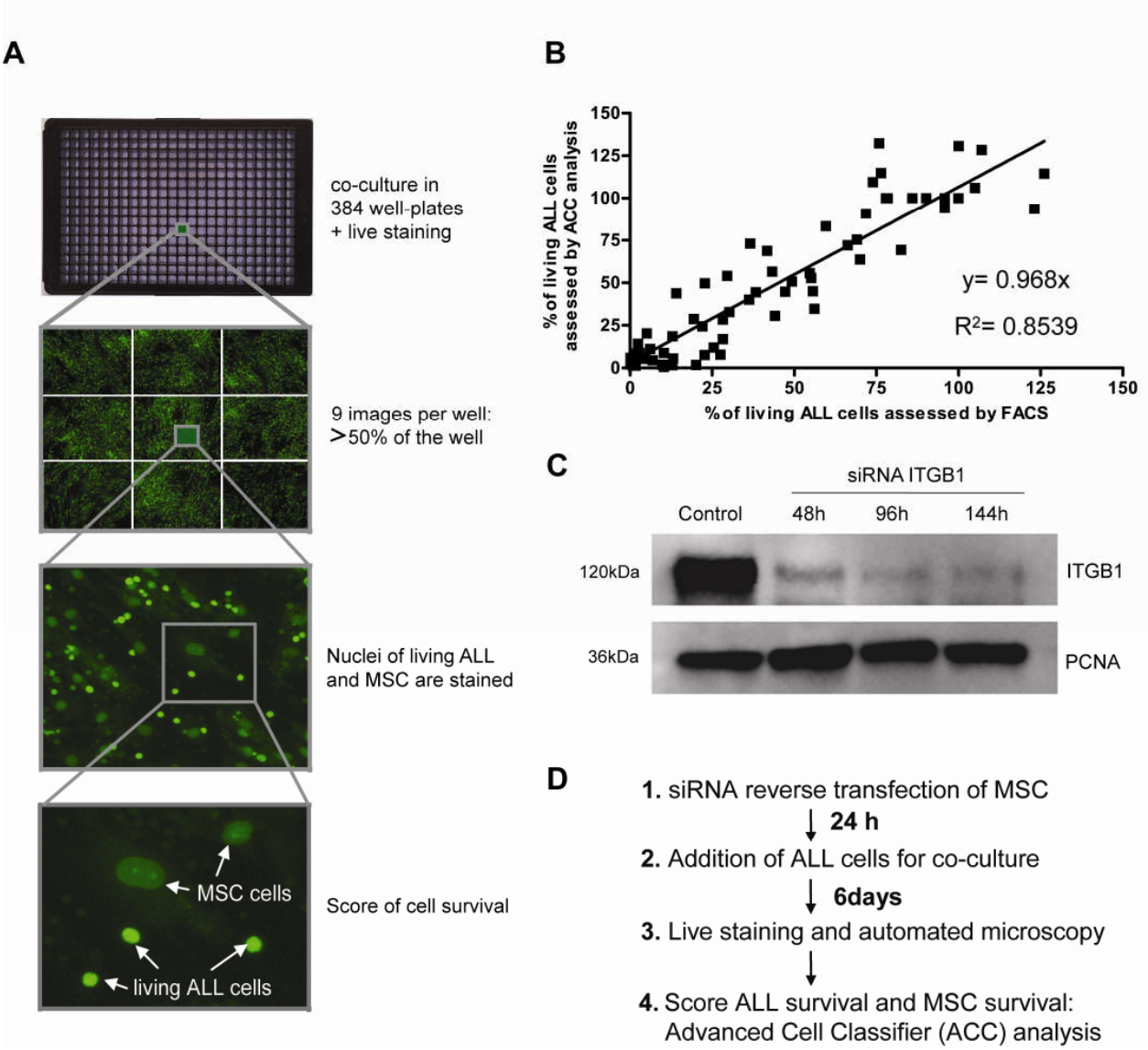

Fig. 16. Automated live cell imaging facilitates large-scale cell viability analysis of leukemia co-cultures on MSCs. (A) Workflow of the image-based assessment of ALL cell viability using the live cell dye Cyquant in the co-cultures in the 384 well-plate format. After automated microscopy which generates 9 images per well covering more than 50% and image segmentation using CellProfiler, the number of living ALL cells per well was assessed with the machine learning program Advanced Cell Classifier (ACC). (B) Correlation of living ALL cells assessed by ACC and by flow cytometry. In total, 5 experiments were run in parallel for both methods. To get the full range of possible ALL cell viabilities, conditions with negative control siRNAs and positive control siRNAs (killing the MSCs) as well as incubation with chemotherapeutic agents (dexamethasone, daunorubicin and vincristine) in different concentrations and seeding different numbers of cells were used. (C) Western blot showing the downregulation of Integrin beta 1 over a time period of 6 days. (D) Work flow for RNA interference screening: 24h after reverse transfection of MSC cells, ALL cells were added for 6 days in co-culture before live staining and automated microscopy was performed.

Intercellular interactions are case-specific

To identify critical determinants of stromal support in our model, we established a workflow for RNA interference in MSC cells (Fig. 16B, C). We then customized a small RNAi library for 110 selected candidate genes based functional annotation that were indicative of a role in cell adhesion, signalling, interactions with the extracellular matrix or a role in a hematopoietic stem cell niche function, and evidence from own gene expression profiling data and cell surface proteome data in MSC that these genes were expressed and that putative interaction partners were present on ALL cells (Suppl. Table 2). Because we expected to detect distinct patterns for different patients, we proceeded in two steps. We first performed a screen in triplicates with three cases (VHR-01, VHR-03 and VHR-04) and detected reproducible patterns in each case (suppl. Table 3). Interestingly, we did not detect any candidate gene in MSCs that supported all three cases but selected 20 genes with strong activity based on RNA interference in two out of the three cases and extended our analysis on BCP-ALL samples from 10 different patients (Fig. 17A). Interference with these genes did not affect MSC viability or morphology (data not shown). Only 3 out of the 20 selected genes did not reach significant effects on leukemia cell viability decrease (suppl. table 3). The contribution of the individual candidate stromal genes varied for each leukemia sample that we tested. Some of the hits included genes that have been reported to contribute to the normal hematopoietic niche function, such as components of the WNT/beta-catenin pathway and the NOTCH pathway. For others, direct or indirect evidence for interactions with ALL cells have been reported. VCAM1 was reported to mediate stroma-ALL interactions through the binding of VLA-4 [102, 188]. The cytokine TSLP stimulates a pathway that is also frequently mutated in BCP-ALL [22, 189], suggesting that stromal TSLP could be relevant in this context. VEGFA was shown to be expressed by stromal cells and to support leukemia cell viability in stromal co-cultures [72, 190]. We found VEGFA and VEGFC to be expressed in MSCs and tested both cytokines. Validation experiments confirmed that down-regulation of VEGFC affected survival strongly in two of 10 ALL samples (Fig. 17B). As a proof of concept, the sensitivity of samples to VEGFC RNA interference correlated with the sensitivity to two different small molecule inhibitors of the VEGF receptor (Fig. 17C), suggesting that this approach may identify targets for tailored therapeutic intervention.

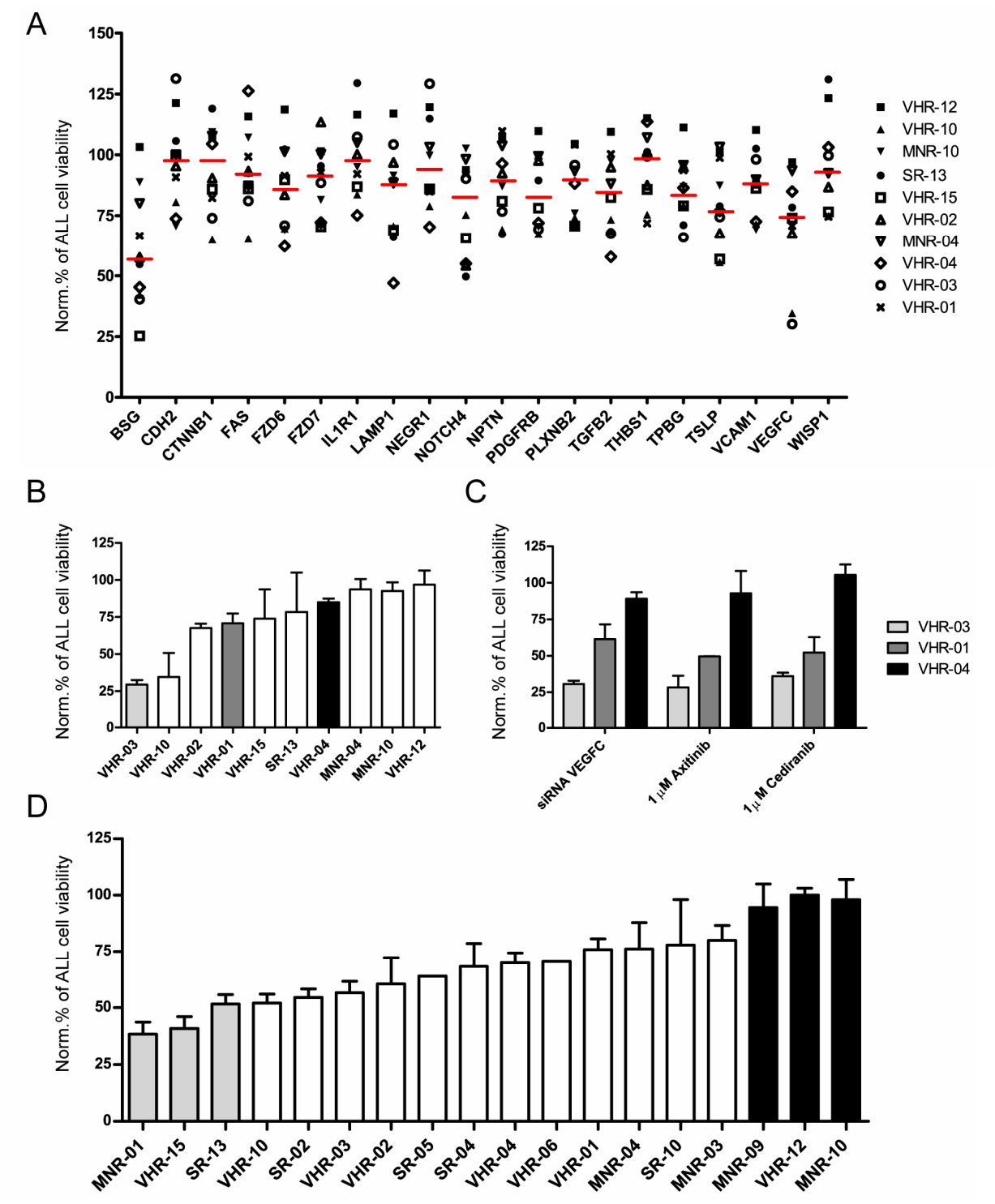

Fig. 17. Identification of patient specific signals from MSCs supporting for ALL cell viability by RNA Interference. (A) The siRNA screen for downregulation of 20 genes on stromal level was performed with 10 ALL patient samples in duplicates. Depicted is the mean survival for each patient compared to the mean survival of each patient assessed in the negative controls wells. The red bar indicates the median effect on normalized ALL cell viability for the 10 patient samples tested for one gene. (B) The down-regulation of VEGFC on MSC level differentially affects the 10 ALL patient samples. The results of the siRNA screen presented in panel A are depicted as histograms showing the mean ± SEM. (C) VEGFR inhibitors (Axitinib and Cediranib, shown for 1μM) were used to block VEGFR signalling in the co-culture with the 3 patient samples indicated. Both inhibitors decreased cell survival in the samples that were sensitive to VEGFC downregulation in MSCs, but not in those that did not respond to the downregulation, n=2. (D) ALL cell viability assessed by flow cytometry for 18 patient samples tested in co-culture after down-regulation of BSG on MSC level. The co-cultures with negative siRNA controls were used to normalize the numbers of living ALL cells. The histograms show the mean ± SEM, n=1 (samples w/o error bars) to n ≥ 3.

The multifunctional stromal cell membrane protein Basigin (BSG/CD147) contributes most prominently to ALL support

The strongest loss in ALL viability was observed after down-regulation of Basigin (CD147/BSG) in MSCs. This membrane glycoprotein has been directly implicated in cancer biology. BSG was shown to modulate matrix metalloproteinase activity [191] and S100A9 [192] on the surface of cancer cells, which is important for cell invasion and migration. BSG also interacts with different membrane transporters, including monocarboxylate transporters to support glycolysis in cancer cells [193]. Here we identified a critical function of BSG from the tumor microenvironment. We next evaluated the importance of stromal BSG expression for 18 leukemia samples that we had identified to be dependent on stromal support (Fig. 17D). Interestingly, most of the ALL samples that we tested depended on stromal BSG expression, one third of them very strongly, but three samples remained completely unaffected. Dependence or independence on BSG contact was not associated with known clinical characteristics, such as resistance to therapy (Fig. 17D and suppl. Table 1).
Taken together, our approach identified several stromal genes to interact functionally with leukemia cells in a specific way, because these cues were required for a subset of leukemia samples, each of which would show different patterns of dependence. The prominent identification of BSG suggested its possible role in stabilisation of critical intercellular interactions such solute carriers to support the metabolism of ALL cells.

The stromal amino acid transporter subunit SLC3A2 is required for the support of BSG dependent leukemia.

To identify the mechanisms of BSG-mediated prosurvival activity in our model, we evaluated the contribution of 16 proteins that were previously described to interact with BSG to the support of ALL by MSC. The gene that clustered most closely with BSG with respect to survival support in our assay was SLC3A2 (Fig. 18A). SLC3A2 is a member of the solute carrier family and corresponds to the large subunit of a heterodimeric membrane amino acid transporter (HAT), suggesting the importance of amino acid trafficking between the two cellular compartments for the pro-survival function of MSCs, at least for a subset of leukemia. Interestingly, this approach clustered the 10 patients into 2 groups, based on overall higher activity of these genes in one cluster, including metalloproteinases and integrins (Fig. 18A). In addition, we also evaluated the effect of monocarboxylate transporters, including MCT1 and MCT4, which are stabilized by BSG to exert important metabolic functions for cancer cells by modulating glucose metabolism [193]. Interference with MCT1 and MCT4 expression did not correlate with the pattern seen for BSG and did not result in a significant decrease of viability in any investigated case, nor did it influence lactate levels in the medium (data not shown). Validation studies using flow cytometry confirmed that downregulation of SLC3A2 reliably mimicked the effect of BSG downregulation (Fig. 18B). Both interventions did not result in changes in MSC morphology or MSC proliferation rates (data not shown). RNA Interference of both BSG and SCL3A2 simultaneously did not increase the effect, suggesting that the function of the HAT is limiting in this context (Fig. 18B). Given the reported evidence for an interaction between BSG and SCL3A2 [194], our data suggest that BSG is required for a critical function of the HAT on stromal cells which is specifically required for the survival of a subset of leukemias in this model of the niche.

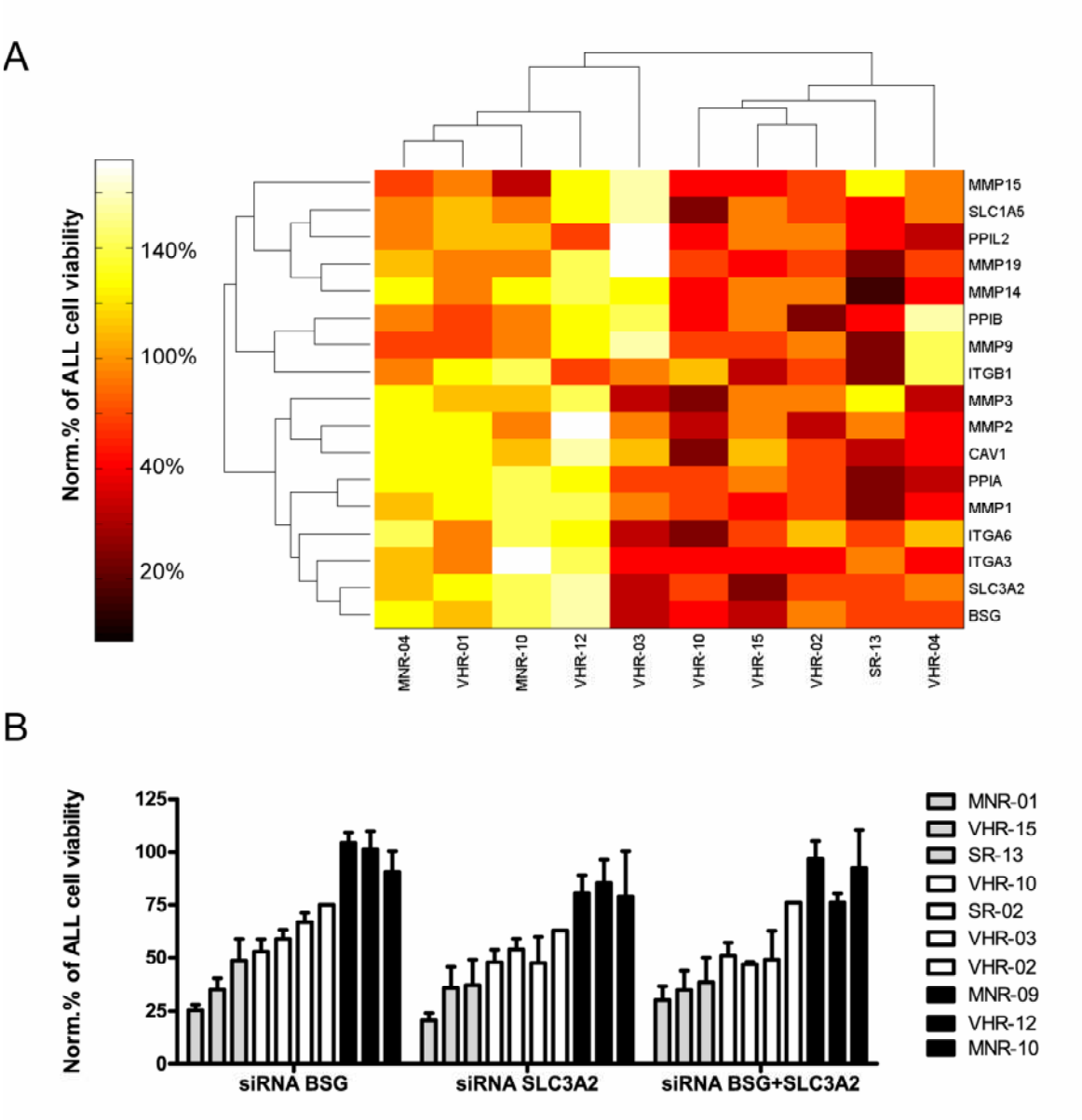

Fig. 18. Functional interaction of BSG and SLC3A2 identified by RNA interference. (A) Heatmap displaying ALL cell viability for 10 patient samples tested after the downregulation of 16 genes that are related to BSG assessed by microscopy. (B) Validation by flow cytometry of the effect of SLC3A2 downregulation, which recapitulates the BSG sensitivity pattern of samples. Histograms show the mean ± SEM of ALL cell viabilities compared to the respective negative controls, n= at least 4

BSG/SLC3A2 activity protects BSG-dependent ALL from oxidative stress

The importance of HAT activity for stromal support of ALL suggested the possibility of a metabolic interaction. Given the recent report that chronic lymphoblastic leukemia (CLL) cells depend on stromal cysteine production to maintain glutathione (GSH) synthesis for protection from oxidative stress, we next evaluated the contribution of BSG/SLC3A2 to the control of ROS levels in ALL cells. RNA interference of BSG or SLC3A2 resulted in a decrease of GSH in MSC, which did not affect their viability (data not shown). Comparing three leukemia samples that were strongly dependent on stromal BSG/SLC3A2 expression to three samples that remained unaffected by the knockdown of these genes, we detected a clear correlation

of the reduction of ALL survival with an increase of ROS and a decrease of GSH in BSG dependent ALL samples upon interference with BSG/SLC3A2 expression (Fig. 19A-C). BSG-dependent ALL thus appears to be dependent on stromal HAT function to maintain GSH levels and regulate ROS. Consistent with this hypothesis, we also found BSG-dependent ALL cells to be more sensitive to oxidative stress using hydrogen peroxide, an effect that was potentiated by interference with BSG/SLC3A2 in stromal cells (Fig. 19D). Our data support the notion that a relevant subset of ALL cases depends on stromal HAT function to cope with oxidative stress.

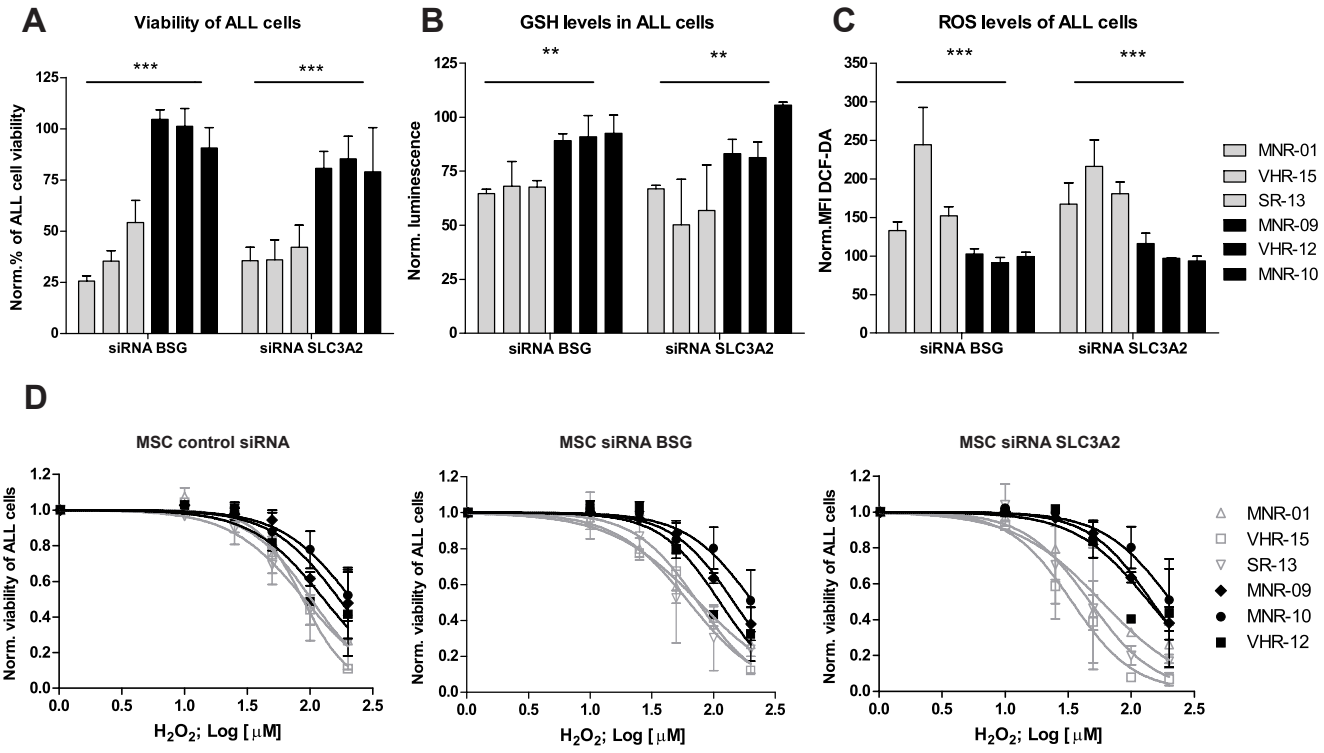

Fig. 19. BSG/SLC3A2 activity protects BSG-dependent ALL from oxidative stress. (A) Viability of patient samples sensitive (grey, n=3) and non-sensitive (black, n=3) to downregulation of BSG or SLC3A2 at MSC level measured by flow cytometry (*** P<0.001). The order of the samples is respected in every graph as depicted in the legend. (B) GSH levels measured with GSH-Glow were reduced in the 3 sensitive samples when BSG or SLC3A2 were downregulated at MSC level compared to non-sensitive samples (** P<0.01). (C) ROS levels measured by flow cytometry analyses of DCF-DA levels in the cells were increased in the 3 sensitive samples compared to non-sensitive samples (*** P<0.001). Histograms in A, B and C show the mean ± SEM of ALL cell viabilities compared to the respective negative controls, n= at least 3. (D) Sensitivity to H_2O_2 was assessed by microscopy in the 3 sensitive samples compared to the 3 non-sensitive samples and was increased in the 3 sensitive samples when BSG of SLC3A2 were downregulated, n=2.

Interference with stromal BSG/SLC3A2 can be rescued by cysteine and antioxidants

Because RNA interference of stromal SCL3A2 in the presence of sufficient amounts of cystine resulted in loss of ALL cell viability, it is possible that this perturbation interferes with stromal metabolism of cystine to cysteine to affect the GSH steady state in our model. To address this question, we performed rescue experiments in cystine depleted cell culture medium. As predicted, cystine depletion per se was detrimental to BSG/SLC3A dependent leukemia, suggesting that interference with HAT function decreases the supply of cystine for metabolism in MSC. We could detect a clear dose dependent effect of decreasing cystine

concentration in the medium with a marked effect on leukemia samples that are dependent on BSG/SLC3A (Fig. 20A). Addition of cysteine, but not cystine, fully rescued the effect of stromal BSG or SLC3A deficiency, indicating that stromal cell metabolism from cystine to cysteine is critical (Fig 20B). This effect correlated with a decrease in ROS levels after cysteine addition. The fact that cystine alone did not rescue ALL cells also confirms that leukemia cells have a limited capacity of uptake and metabolism of cystine and depend on the availability of cysteine. Importantly we could replicate these experiments using a second independent human stromal cell line, HS-5 (Fig. 21). Finally, supplementation of the medium with GSH, addition of the antioxidant N-acteylcysteine (NAC), or z-Vad, a pan-caspase inhibitor (Fig. 20C and data not shown) rescued the effect of BSG/SCL3A2 downregulation as well, confirming that GSH is a critical component of the mechanism involved and that control of oxidative stress is required to prevent apoptosis. Based on these experiments we propose that, in analogy to a recent report for CLL [115], cysteine production from the microenvironment is required for GSH synthesis and control of ROS in a relevant subset of ALL cases to prevent apoptosis.

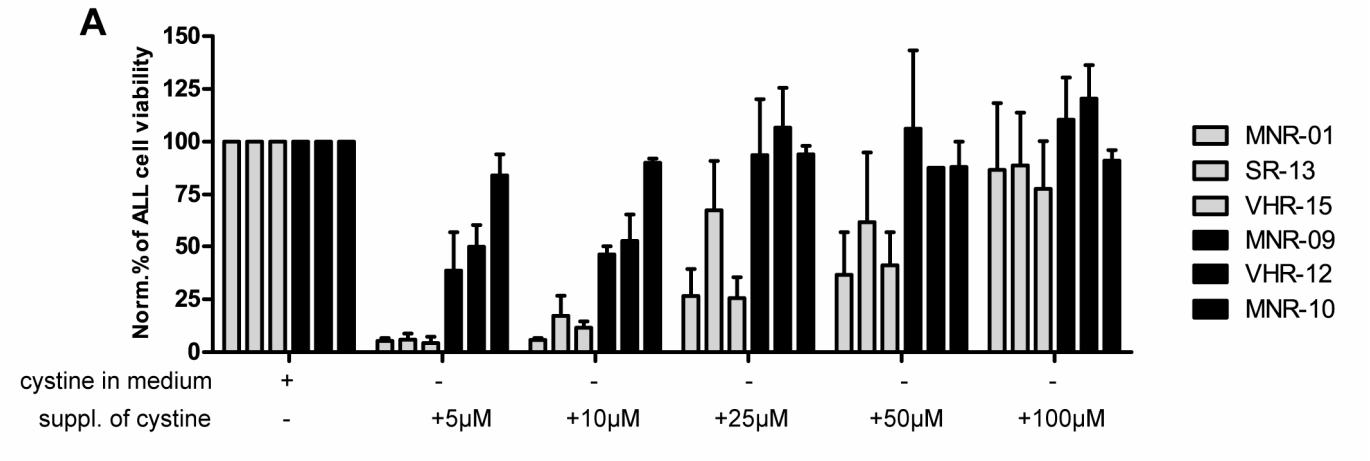

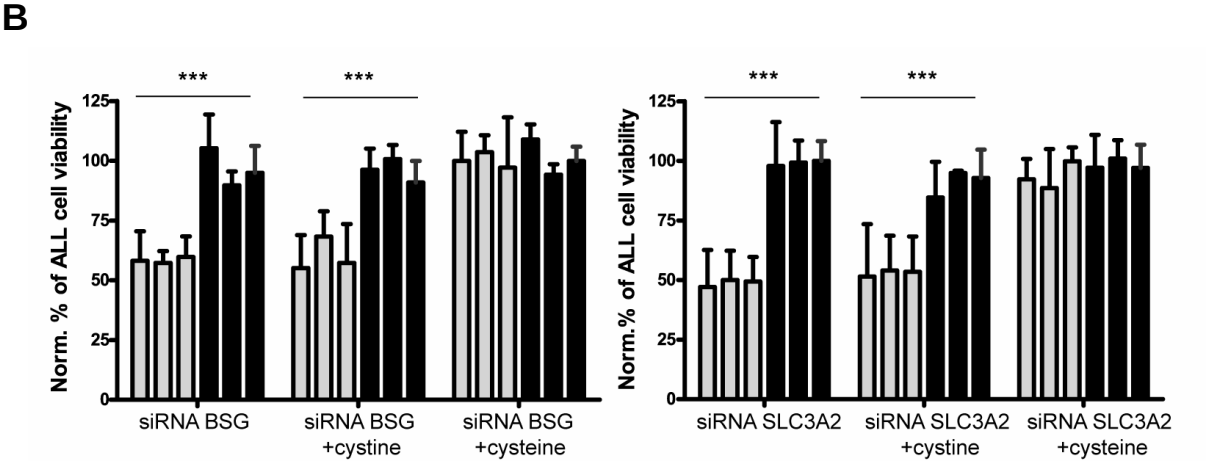

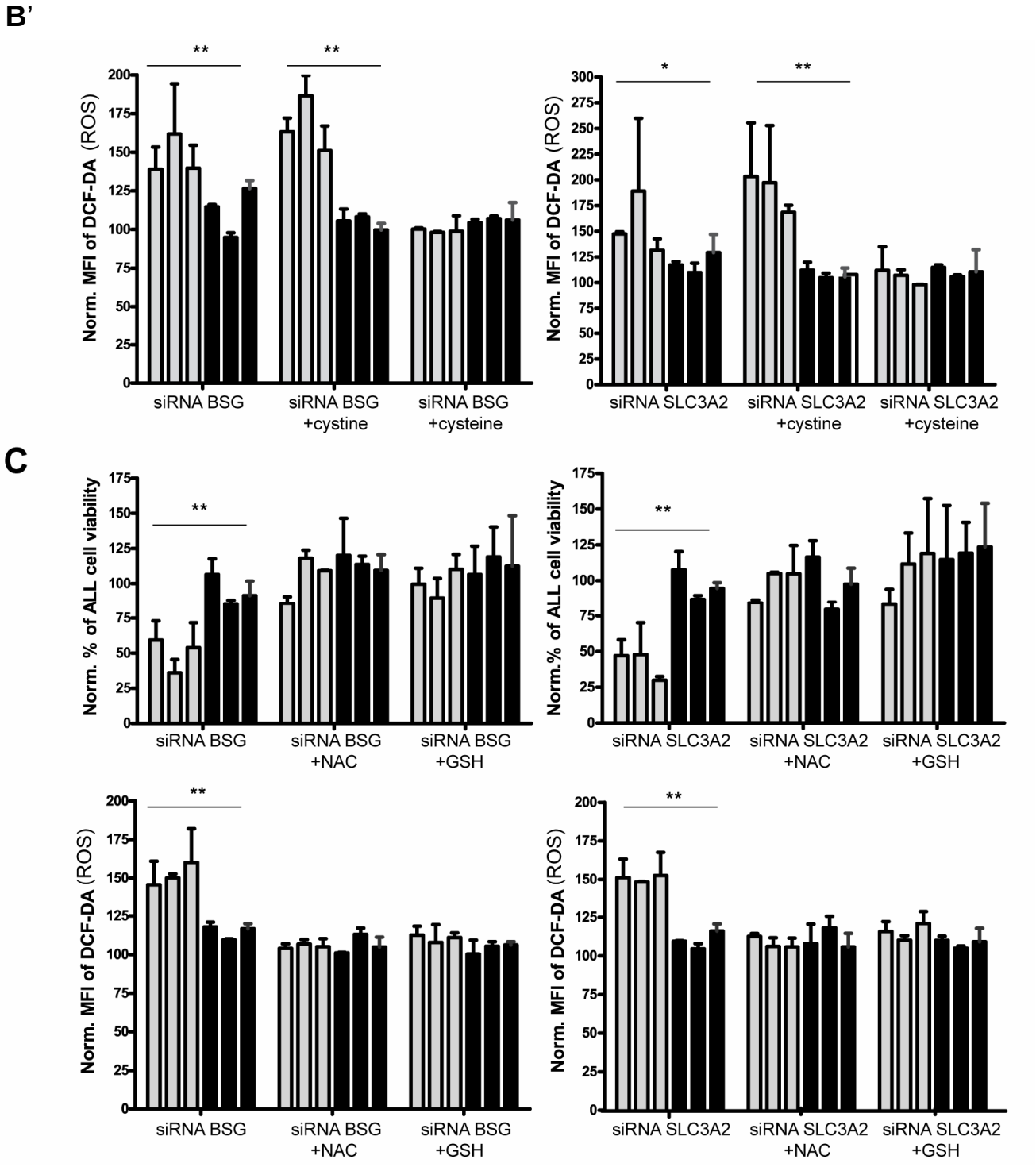

Fig. 20. Downregulation of stromal BSG/SLC3A2 is rescued by cysteine and antioxidants. (A) Viability assessed by 7-AAD stainings and flow cytometry after 6 days of co-culture with MSCs of 3 sensitive (grey) and 3 non-sensitive (black) samples in RPMI medium was decreased in cystine depleted medium in sensitive samples compared to non-sensitive samples. Supplementation of cysteine rescued cell viability in a dose dependent manner. The order of the samples is respected in every graph as depicted in the legend. (B) Viability assessed by FACS after 6 days for 3 sensitive (grey) and 3 non-sensitive (black) samples after downregulation of BSG or SLC3A2 at MSC level was restored by addition of cysteine (100µM) but not cysteine (100µM) in AIMV medium. (B') Under the same conditions, ROS levels measured by flow cytometry analysis of DCF-DA after 3 days of co-culture were decreased to control level upon addition of cysteine but not cysteine. (C) Viability of ALL cells assessed by flow cytometry after downregulation of BSG or SLC3A2 (upper panel) and ROS levels (lower panel) were rescued upon addition of NAC (5mM) or GSH (5mM). Histograms show the mean ± SEM of ALL cell viabilities or the MFI ± SEM of DCF-DA analyses normalized to the respective negative controls. Experiments assessing the viability of ALL with rescue of cystine or cysteine were performed in quadruplicates. The other experiments were performed in duplicates.

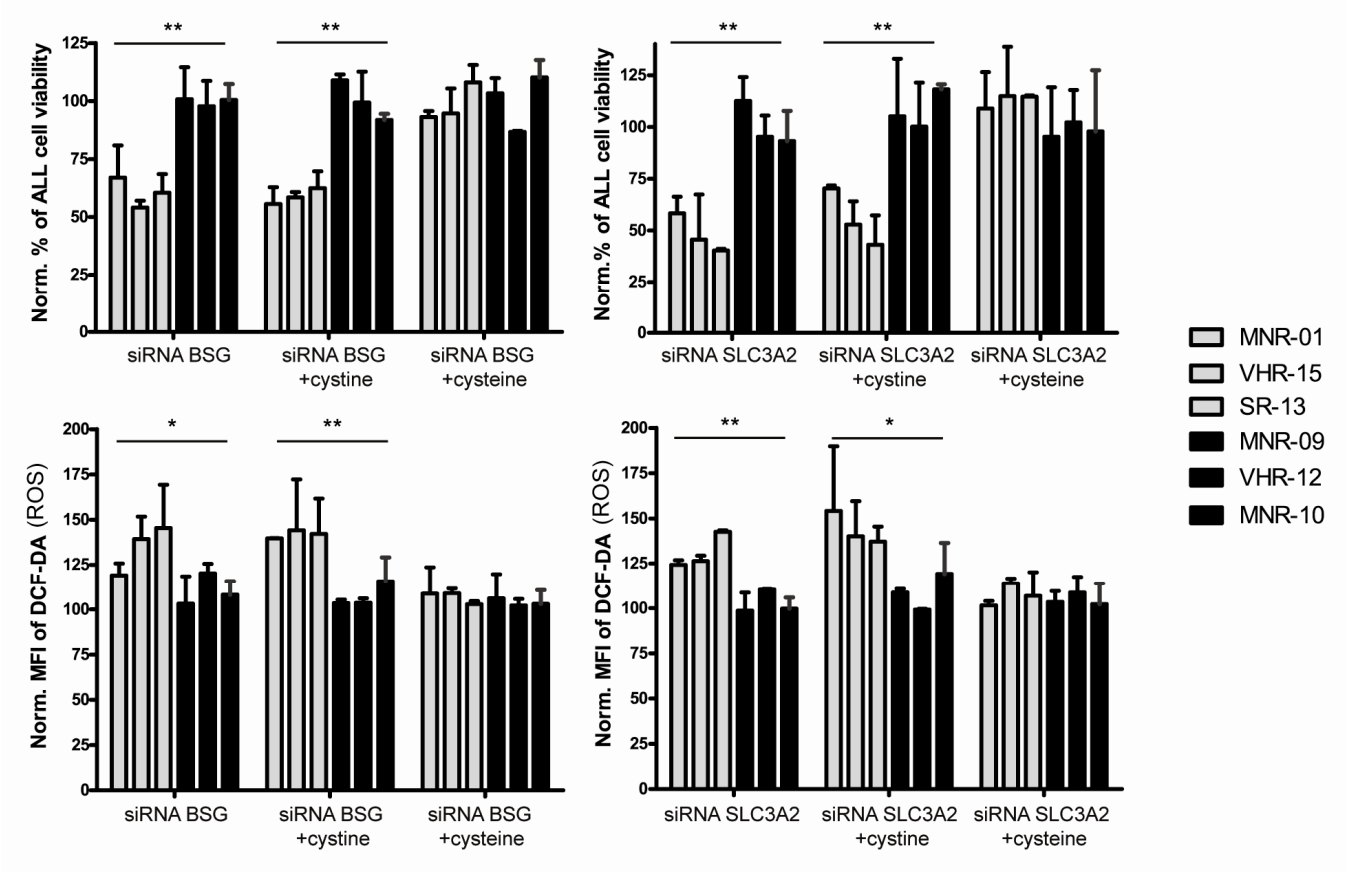

Fig. 21. Downregulation of stromal BSG/SLC3A2 is rescued by cysteine in HS-5 cells. Viability was assessed by FACS after 6 days for 3 sensitive (grey) and 3 non-sensitive (black) patients when BSG is down-regulated at HS-5 level with addition of cystine (100µM) or cysteine (100µM) to AIM-V medium. In the same conditions, ROS levels were measured by FACS assessing MFI of DCF-DA after 3 days of co-culture. The order of the patients is respected in every graph as depicted in the legend. Histograms show the mean ± SEM of ALL cell viabilities or the MFI ± SEM of DCF-DA normalized to the respective negative controls, n=2.

DISCUSSION

Interactions of leukemia cells with their microenvironment have an influence on critical cellular programs in cancer cells, with implications for resistance to currently available treatment [195]. To facilitate large-scale functional investigation in a model of the leukemia niche, we developed this imaging based platform using primary cells from patient samples on bone marrow mesenchymal stromal cells. The development of representative collections of ALL xenograft samples greatly improves our capability for systematic functional studies [135, 136, 178, 196]. The methodology reported here can be adapted for selective perturbation of one of the two cellular compartments by RNA interference and for systematic profiling with bioactive molecules or therapeutic agents. We established an open source modular image analysis pipeline with an efficient machine learning based algorithm to discriminate living cells in co-cultures upon any of these manipulations. We show that relevant patient specific information can be obtained using this platform by profiling functional interactions between MSC and leukemia cells. To a significant proportion, ALL were metabolically vulnerable to cysteine supply by MSC in order to maintain their redox state. This stromal function is mediated by the multifunctional cell surface protein CD147/Basigin and depends on heterodimeric aminocid transporters (HAT) including the SLC3A2 subunit.

Most of the BCP-ALL cases that we evaluated depended on MSC for survival in vitro, even in presence of exogenous serum factors. These observations are consistent with the difficulty to establish permanent cell lines with primary ALL cells and constituted the rationale to exploit this system for functional genetic investigations. We recognize that this *in vitro* model of the leukemia microenvironment has limitations. New approaches will be required to model our findings in the context of a humanized bone marrow structure in mice *in vivo*. Lineage mapping studies in mice identified overlapping subsets of mesenchymal progenitors based on the activity of developmental specific promoter activity (nestin and prx1 promoters) [44, 197]. These bone marrow perisinusoidal mesenchymal stem cells are an important component of the niche and contribute to the formation of this niche [31]. Explanted MSC have the capacity to generate bone [184] and to organize and reconstitute the hematopoietic niche *in vivo* [31, 32, 44]. The hTERT-immortalized MSC that were used for our study display high PRRX1 RNA levels (data not shown) and fulfill progenitor-defining criteria [129], but to which extent they correspond to these murine mesenchymal stem cells has not been characterized. Nevertheless, our platform provides stimulating insights into leukemia-specific functional interaction patterns and the basis to profile functional differences between MSC that are derived from different individuals or at different times of disease progression.

Both interactions by direct contact and soluble factors, including microvesicles [198], are important and build a unique leukemia-supporting network. For ALL cells, adhesion molecules such as VE-cadherin [199] and soluble factors such as SDF-1 or IL-7 have been implicated [72, 78]. Importantly, we detect individual patterns of stromal support using the same hTERT-MSC line with primary ALL cells from different patients. These differences could be due to the activation of MSC by leukemia cells or the specific dependence of leukemia cells from a given signal. We detected reproducible effects by interference with 16 candidate genes. A subset of ALL cases depended most strongly on paracrine signaling via VEGFC. This is consistent with a report of the activity of VEGF inhibitors on ALL cells [72]. Both autocrine and paracrine effects could be involved, as it was shown that leukemia cells can secrete VEGF [200, 201]. Our data suggest that this platform will be useful to identify leukemia-specific interaction patterns with stromal cells.

Metabolic reprogramming is a dominant feature of cancer cells [202]. Metabolite profiling of leukemia cells confirmed their increased biosynthetic activity [203]. This requires an adaptation of cancer cells to produce sufficient anti-oxidants such as NADPH [204] and reduced glutathione [202]. Here we show that stromal Basigin (BSG/CD147), a multifunctional cell surface protein, is required for specific metabolic support of leukemia samples that depend on glutathione for survival. BSG has been shown to interact functionally with different effectors, including metalloproteinases and monocarboxylate transporters. As subunit of the lactate/H+ symporters MCT1 and 4, BSG regulates the export of lactic acids [193]. As an alternative, we also considered the interaction of BSG with amino acid transporters via SLC3A2 (CD98h) [194], given a recent report showing the dependence of chronic lymphoblastic leukemia cells from stromal cystine-cysteine metabolism for glutathione synthesis [115]. Functional profiling by RNA interference with putative BSG interacting genes clustered ALL cases in two groups, one cluster corresponding to samples that depend on stromal BSG. RNA interference with SLC3A2, the heavy subunit of heteromeric aminoacid transporters HAT [205] mimicked the loss of stromal BSG most

closely. Together with SLC7A11, SLC3A2 forms a HAT that can exchange cystine for glutamate, suggesting that stromal cystine metabolism could be critical for ALL.

Our data support a model in which BSG is essential to mediate import of cystine to MSC as a first step. By quantitative PCR we confirmed very strong detection of SLC7A11 in MSC and weak detection in ALL cells (data not shown), which suggests that ALL cells may have a limited capacity to import cystine. Indeed, cystine import and metabolism to cysteine in stroma is required for ALL support, because loss of stromal BSG is not rescued by supplementation with cystine but with cysteine. Depletion of cystine affected BSG-dependent ALL in a dose dependent manner, which demonstrates that the cysteine supply by MSCs is limiting. Whether stromal BSG/SLC3A2 is required for cysteine export cannot be finally concluded based on our data. Cysteine is a rate limiting substrate for GSH synthesis together with glycine and glutamine. Because reduced cysteine is rapidly oxidized in the microenvironment, constant supply for ALL cells appears to be needed for the metabolic control of the redox state in ALL. Indeed, we show that interference with the cystine-cysteine supply is associated with a significant decrease of GSH and concomitant increase in ROS, which results in marked induction of apoptosis only in ALL samples that are dependent of this stromal function of BSG/SLC3A2. Our results suggest that major underlying differences exist in ALL with respect to the vulnerability to cysteine depletion. This phenotype is not associated with a classical clinical risk factor and does not correlate with marked differences in HAT levels on ALL cells seen on gene expression profiles (data not shown). The underlying mechanism is intriguing, and it is possible that cysteine dependent ALL have defects in alternative pathways to synthesize anti-oxidants.

Taken together, our data illustrate that distinct networks of interactions between leukemia cells and MSC exist, which has implications for the development of targeted therapies. Metabolic interactions may constitute a predominant function of the leukemia niche, as reflected by the selective dependence on stromal cysteine to control ROS in leukemia cells. This metabolic vulnerability could be targeted using inhibitors of the anti-oxidant synthesis. Similarly, the dependence of ALL on asparagine provides the basis for therapy with asparaginase, which can also be influenced by the metabolic activity of the niche [116]. As lesions in metabolic networks in leukemia are being increasingly identified, it will be essential to understand their implications in the context of the leukemia niche. Functional profiling approaches such as the one shown here will contribute to detect vulnerable leukemia specific features in an individualized manner.

MATERIAL and METHODS

Cell culture

Human hTERT-immortalized primary bone marrow MSCs were provided by D. Campana (St Jude Children's Research Hospital, Memphis, Tennessee) and maintained at 37℃ and 5% CO2 in RPMI-1640 medium supplemented with L-glutamine, penicillin/streptomycin, 10% fetal bovine serum (Hyclone) and 1µM Hydrocortisone. HS-5 cells were purchased from ATCC (CRL-11882) and maintained at 37℃ and 5% CO2 in Dulbecco's Modified Eagle's Medium supplemented with L-glutamine, penicillin/streptomycin and 10% fetal bovine serum (Hyclone). Cystine, cysteine, GSH and N-acetylcysteine (all from Sigma) and zVAD-FMK (Promega) as well as the VEGFR inhibitors axitinib and cediranib (both from Axon Medchem)

were used at indicated concentrations. MSC and ALL cells in co-culture were cultivated in AIM-V medium (Life technologies) with a ratio of 1:10, for HS-5 co-cultures a ratio of 1:20 was used. Transwells® of 0.4µ pore size (Corning) were used for the transwell assays.
For the cystine depletion experiment, cystine depleted medium (Sigma) was supplemented with L-glutamine and penicillin/streptomycin (without FCS); the control media was RPMI-1640 medium supplemented with L-glutamine, penicillin/streptomycin (without FCS).

Flow cytometry
Analyses of ALL cell viability in co-culture with MSCs were performed as described previously [129, 131] using 7-AAD (BD Pharmingen) and FITC-tagged anti-human CD45 or RPE-tagged CD19 (both AbD Serotec).

Glutathione and ROS measurements
Glutathione levels in co-culture were measured using the GSH-Glo™ Glutathione Assay from Promega according to the manufacturer's instructions. Shortly, ALL cells were cultivated with MSC cells for 3 days and separated by trypsinization. ALL cells were replated in AIMV medium to enable MSC cells to adhere to plates for one and a half hour. ALL cells were then removed, plated into 96 well plates, and GSH levels were measured on a Synergy HT (Biotek) reader. For measurements of ROS levels, cells were stained after 3 days in co-culture or 48h in suspension culture with 20µM DCF-DA (Sigma) for 2 hours at 37℃ / 5% CO2 and processed for flow cytometry analysis.

Microscopy
Co-cultures of MSC and ALL cells were stained with CyQUANT® Direct Cell Proliferation Assay (Life Technologies, C35011 and C35012) using a modified protocol. In brief, component A (diluted 1:375) and component B (diluted 1:75) were added to the cells for 45 minutes at 37℃ and 5% CO2. Staining solution was removed and AIM-V medium with compound B (diluted 1:100) was added for 1 hour at 37℃ and 5% CO2 prior imaging. Images were taken on the ImageXpress Micro microscope from Molecular Devices with a CoolSNap HQ camera from Photometrics and a 10x Plan Fluor objective from Nikon with 0.3 NA. Image acquisition was set to cover more than 50% of each well in a total of 9 images (Fig. 2A). For image analysis, images were first segmented using the CellProfiler software [180] and distinction of viable ALL cells from dead ALL cells as well as MSCs was implemented in a machine learning tool for high-content analysis (Advanced Cell Classifier-ACC) [181]. An 'a trous' wavelet transform-based spot detection algorithm [179] was implemented in the MatLab software and was built into the CellProfiler framework. For each detected spot on an image, over 50 intensity and texture-based features were extracted. The list of extracted features, CellProfiler pipelines, and the parallelization code are accessible at www.highcontentanalysis.org. For correct assignment of ALL cells, the Advanced Cell Classifier program [181] used the random forest classification method for all experiments [182].

Patient samples and xenograft model
ALL cells were recovered from cryopreserved anonymized bone marrow aspirates from patients enrolled in the ongoing ALL-BFM 2000 study of ALL-REZ-BFM 2002 who had given informed consent in accordance with the Declaration of Helsinki. Samples were anonymized with labels that refer to the clinical risk stratification. Depending on the MRD result during induction therapy (MRD1 + 2) and during consolidation therapy (MRD3), patients are defined here as standard risk (SR) if MRD1 + 2 were negative, high risk (HR) if MRD1 + 2 were positive less than or equal to 10−3, and VHR if HR patients were still positive for MRD3 (suppl. Table 1). MNR cases represent relapsed ALL cases from the ALL-REZ-BFM 2002

study. Cases are anonymized with a label according to the risk group and with a unique number. Cryopreserved ALL cells were transplanted intrafemorally to NSG mice as described (Schmitz et al, leuk lymph). Leukemia progression was monitored by flow cytometry with human CD45 and CD19 antibodies (AbD Serotec). Leukemic cells were isolated from the spleen and cryopreserved.

siRNA Screen and siRNA validation assays
The custom library (ON-TARGETplus siRNAs with a pool of 4 siRNAs per well with a final concentration of 30nM) was purchased from Thermo Fisher Scientific. For all validation experiments ON-TARGETplus pooled siRNAs (final concentration 40nM) were used. Reverse transfection was performed using the INTERFERin® reagent from Polyplus-Transfection SA according to the manufacturer's instructions. For all validation assays, RT-PCR was performed to check for the downregulation at mRNA level of the targeted genes.

Statistical analysis
Statistical significance was analyzed by the Mann-Whitney test comparing BSG/SLC3A2 sensitive patient group with the BSG/SLC3A2 non-sensitive patient group. P-values of <0.05 were considered statistically significant. Histograms and plots were generated using the Prism software (GraphPad), except the clustered Heatmap in Figure 4 which was generated using MATLAB (MathWorks).

Western blot
Whole-cell extracts were prepared from 1 x 106 cells using radioimmunoprecipitation assay (RIPA) buffer (50 mM Tris-Cl, pH 6.8, 100 mM NaCl, 1%Triton-X-100, 0.1% SDS) supplemented with complete mini protease inhibitor cocktail (Roche Applied Sciences) for 20 minutes on ice. After SDS-PAGE, proteins were blotted onto nitrocellulose membranes. Membranes were blocked in 5% non-fat dry milk and incubated with primary antibodies in 3% bovine serum albumin (Sigma). ITGB1 antibody (Abnova, clone MEM-101A) was diluted 1:1000. Horseradish peroxidase-labeled goat anti-rabbit or anti-mouse antibodies were used for signal detection with chemiluminescence substrate (Pierce) and direct scanning (Fujicolor).

ACKNOWLEDGEMENTS

We would like to thank Markus G. Manz for and Roland H Wenger for useful discussions, Blerim Marovca, Paulina Mirkowska, Maike Schmitz for support with mouse experiments, Andreas Hoffman for support with proteomic experiments.

This work was supported by funding from the Swiss Cancer League (to J.P.B), the Empiris Foundation (to J.P.B), the Mach-Gaensslen Foundation (to B.W. and J.P.B), the Novartis Research Foundation (to J.P.B.), the Swiss National Science Foundation (to J.P.B), the Hanne-Liebermann Foundation and the Foundation Kind und Krebs (to J.P.B. and to M.G.), and the clinical research focus program "human hemato-lymphatic diseases" of the University of Zurich (to J.P.B.).

Discussion

Here I describe the development of a high-content screening platform to study interactions between primary childhood acute lymphoblastic leukemia (ALL) cells and mesenchymal stromal cells derived from human bone marrow. To our knowledge this is the first report of a high throughput system using a co-culture system with primary ALL cells. The system described here has many relevant potential applications. Besides its potential for functional genetic studies, it provides an entirely new dimension for preclinical drug testing. Indeed, this platform is currently used in our laboratory to investigate synthetic lethal combinations of drugs in different ALL subtypes. Studies can be performed on stable co-cultures with viable primary ALL cells very effectively. I show here the functional importance of intercellular interactions between leukemia and stromal cells. Interestingly, patient sample specific support patterns were identified. Moreover, the system has enabled the identification of relevant combinations of new agents in resistant ALL cases, which further demonstrates the usefulness of this platform for preclinical studies.

A two dimensional model of the leukemia microenvironment constitutes a useful platform for functional studies

While most primary B-ALL cells rapidly undergo cell death in suspension cultures, hTERT immortalized primary human bone marrow stromal cells (MSC) support most B-ALL cases that we evaluated *in vitro*. This MSC cell line retains contact inhibition, has a normal karyotype, and has retained the capacity to differentiate to adipocytes or osteoblasts *in vitro* [129]. An essential component of the bone marrow niche are the skeletal stem cells, which represent single cells able to regenerate a heterotopic bone organ or an ossicle *in vivo* [31]. Mesenchymal stroma cells isolated from the bone marrow have the capacity to regenerate a functional human hematopoietic microenvironment upon xenotransplantation [184]. However, these MSCs consist of heterogeneous cell populations and controversies exist regarding the niche functions of different identified subpopulations [31]. The use of reporter systems for lineage mapping of specific subpopulations in mouse models allowed characterizing more precisely the niche functions of MSC subpopulations in mice. Subpopulations of the endosteal niche such as osteoblasts and their progenitors were compared to subpopulations from the perivascular niche (endothelial cells, CXCL12-abundant reticular (CAR) cells, and mesenchymal stem and progenitor cells (including Nestin-GFP+ cells)) in their HSC supportive functions [197]. The subpopulation of mesenchymal stem and progenitor cells expressing Prx1, which is a transcription factor expressed early during limb bud mesoderm development, proved to be essential to support HSC in mice. We observed in our gene expression analysis a high expression of the human homologue of Prx1, PRRX1, in MSCs. This indicates that at least some overlap exists between human MSC cells and the mouse HSC niche. However, models to better characterize the functions of MSCs in the human HSC niche are required. It will be important to develop models to study the pathways that we have identified *in vivo*. As a first step we will consider the development of heterotopic bone formation models [147, 148] . The advantage of this system is to use human xenografts with the possibility to genetically modify both compartments (heterotopic bone and leukemic cells).

Taken together, we use MSCs that have a phenotype that is partially overlapping with MSCs that were described to be essential in the HSC mouse niche and leukemic cells able to reflect human disease biology. With this co-culture system, we are able to model intercellular interactions between leukemic cells and cells from the bone marrow microenvironment.

The identification of individual differences in intercellular interactions between leukemia and stroma has implications for translational research

We conducted the first study by investigating the supportive functions of stromal candidate proteins for primary B-ALL cells. We could not identify a common denominator of the support of leukemia cell survival by MSCs using our candidate gene approach. Instead, we observed individual support patterns. A subset of ALL cases depended most strongly on stromal VEGFC secretion. As a proof of concept, the sensitivity of samples to VEGFC RNA interference correlated with the sensitivity to two different small molecule inhibitors of VEGF receptors, suggesting that this approach may identify targets for individually tailored therapeutic intervention. Inhibition of VEGF using the small molecule inhibitors SUI1498 or CBO-P11 inhibited the proliferation only of 3 out of 4 ALL cases that had been expanded on stroma [72], validating our observation that some patient samples do rely on VEGF signalling and some do not. A second predominant hit in this experiment was BSG, which clearly identifies a subgroup of patients that are very sensitive to interference this cell surface protein, as we will discuss below. One of the most important observations in this work is the fact that samples from different patients depend on different cues in this model. This principle has important implications on the way to approach preclinical testing in a translational perspective. Relevant studies will have to take this important heterogeneity into account. A preclinical platform that can capture such difference should therefore be an important asset to triage among different therapeutic options using directly relevant patient material.

Identification of bidirectional crosstalks between leukemic and stromal cells

Beside VEGFC and BSG, we identified other interesting pathways with a potential role for a leukemia niche function.

Although, the NOTCH pathway is very prominent for cell intrinsic transformation of T-cell ALL [95], the role of NOTCH in cell to cell interactions in the leukemia niche remains to be addressed. To assess the role of NOTCH on stromal cells, we downregulated all 4 NOTCH members, NOTCH 1, 2, 3 and 4. 4 out of 10 patient samples tested in the co-culture showed a significant decrease in ALL cell viability when stromal NOTCH4 was targeted. To our knowledge, there was only one study which investigated the role of the NOTCH pathway in co-cultures with B-ALL cells [98]. In this study, NOTCH3 and 4 were reported to play a role in B-ALL cell support. Interestingly, NOTCH1, 2 and 3 were found to be expressed on bone marrow derived MSCs before co-culture. After co-culture with B-ALL cells, expression of NOTCH2 was found to be downregulated and expression of NOTCH 3 and 4 was upregulated on MSCs. The addition of NOTCH 4 antibodies to co-cultures showed the most dramatic effect manifested by the loss of support for B-ALL cells. Based on these preliminary results, the role of NOTCH should be further investigated in this context.

Similarly, we were interested in assessing the role of the Wnt pathway in B-ALL, because of its very prominent role in the HSC niche [59, 206]. We detected some reproducible effects when interfering with several genes of this pathway in MSC. We selected 5 genes for further validation, namely *CDH2, FZD6, FZD7, CTNNB1* and *WISP1*. CDH2, FZD6 and 7 are receptors known to activate the pathway. CTNNB1 is a central key player of the canonical Wnt pathway and WISP1 (WNT1 inducible signalling protein 1) is another downstream regulator of the pathway. In addition, we included proteins that, although not directly connected to Wnt signaling, were reported to be associated with some key proteins in the investigated pathway, namely PDGFRB, TGFB2 and THBS1 (see Fig.22). Five out of 10 patient samples tested show a significant decrease in ALL cell viability when these genes are targeted. Therefore this pathway will be included in follow-up projects as well.

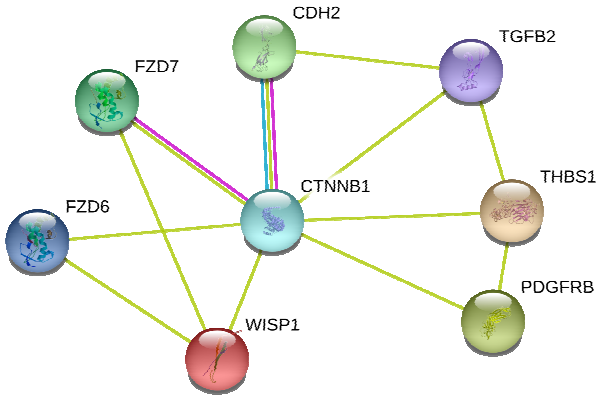

Figure 22. WNT pathway related proteins-Network generated by the STRING database

The candidate mediator of stroma interactions BSG has several functional roles that could be of relevance in this context

In leukemia, BSG expression on malignant cells was reported to correlate with patient outcome and increased risk of relapse [207, 208]. Expression of BSG on other cancer cells is associated with drug resistances [209-211]. It is therefore likely that this protein drives important pathways in cancer. In the RNA interference screen, I identified a strong dependence phenotype of ALL subsets on the function of stromal Basigin. This protein could have different mode of actions. A recent report linked BSG to the function of monocarboxylate transporters [193, 212]. These transporters, which are formed by MCT1 or MCT4, are important to modulate the flux of substrates such as lactate and pyruvate. We first explored this possibility in several ways. We did not see detectable changes in intracellular and extracellular lactate concentration upon modulation of stromal BSG nor did lactate supplementation affect ALL survival in our in vitro assay. Furthermore downregulation of stromal MCT1 or of MCT4 did not affect the same ALL samples in terms of their survival. In addition an inhibitor of MCT1 did show activity in co-cultures. Therefore, 16 genes that were implicated in other experimental models were tested using our platform. Interestingly, the 10 ALL cases that we tested on this platform clustered in two distinct subgroups based on the functional interference data with these 16 genes, separating the patients based on

dependence from stromal BSG (Manuscript 2 Figure 18). Among the genes showing activity in the BSG cluster, we found several Matrix metalloproteinases (MMP). BSG functionally interacts and triggers MMP, and is therefore also termed EMMPRIN [213-216]. Matrix metalloproteinases (MMP) are involved in cancer progression and metastasis, through degradation of the extracellular matrix [217]. Moreover, BSG is involved in adhesion processes through homotypic interactions (for example in platelets [218]) or through interaction with LFA-1 [219] and controls the formation of invadipodia [220]. Moreover, BSG is favouring anchorage independent growth due to stimulation of hyaluronan production [221]. BSG knockout mice are not fertile as BSG is important in spermatogenesis and implantation of embryos in the endometrium due to its invasion and adhesion controlling properties [222, 223]. For instance, invasion of immune cells into the CNS is mediated by BSG [224, 225].

However, we first focused on the potential functional interaction with SLC3A2 and a role for a metabolic crosstalk with leukemia. BSG was shown to interact with the solute carrier, SLC3A2 in mass spectrometry experiments in MCF7 (breast adenocarcinoma cells) and in HT1080 (fibrosarcoma cells) [194]. RNA interference with SLC3A2 mimicked the effect of BSG knockdown most closely. This became the focus of validations that are described in the manuscript 2. We could demonstrate that this was essential for cystine import by MSC and metabolism to cysteine, an important substrate for ALL cells. Whether BSG interacts moleculary directly with SLC3A2 is the focus of current investigation. BSG was describe to engender homotypic interactions [216, 218, 226]. However using the same antibodies that were reported in these publications to inhibit such interactions, we did not detect a decrease of ALL viability in our co-culture system. Alternatively, BSG could trigger signalling pathways through interaction with other ligands, such as interactions with integrins, downstream kinases (MAPK, AKT, ERK) or cyclophilins [213, 221, 227, 228].

Some but not all ALL cases require metabolic support via BSG/SLC3A2

By the time we identified SLC3A2 as a candidate to explain the selective sensitivity of ALL to BSG mediated stromal function, the importance of stromal metabolism of cystine was reported in a model of chronic lymphoblastic leukemia [115]. Here we independently showed that some ALL samples are strongly dependent on cysteine supply by stromal cells and that this required SLC3A2 import of cystine in MSC. Cysteine is used to synthesize glutathione (GSH), an important cellular anti-oxidant (the GSH pathway is depicted in Fig. 23) composed of the three amino acids glutamine, cysteine and glycine [229]. Because of the instability of cysteine, cystine, the stable dimeric form of cysteine, is routinely added to cell culture medium formulations used for *in vitro* cultures. Our data suggest that ALL cells have a restricted capacity to import cystine due to low expression levels of the co-transporter SLC7A11 (data not shown) and thus require constant supply of the unstable amino acid cysteine for their GSH synthesis. Indeed, stromal supply of cysteine restored the GSH and ROS levels detected in ALL cells (highlighted in red in Fig.23). GSH is synthesized by γ-glutamylcysteine synthetase (γ-GCS), the rate-limiting enzyme of the synthesis, and glutamyl synthase (GS) [230]. Detoxification of a variety of electrophilic compounds and peroxides occurs via catalysis of GSH by glutathione S-transferases (GST) and glutathione peroxidases (GSH-PX) [229]. GSH is oxidized to generate GSSG, which is recycled back to

GSH by the action of glutathione reductase (GSSG-RD) at the expense of reduced nicotinamide ($NADPH/H^+$) [230].

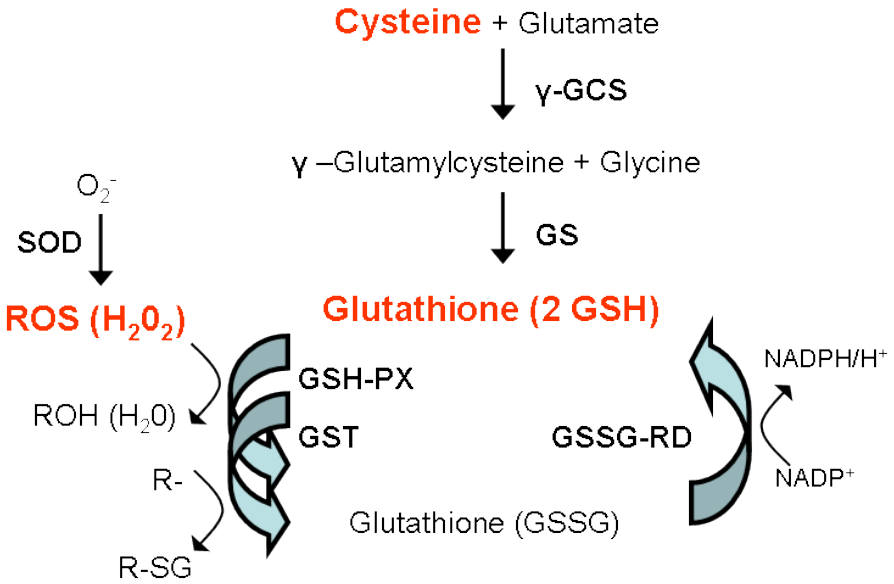

Figure 23. Model of the GSH pathway. Adapted from [230].A major source of H_2O_2 is the biochemical conversion of superoxide anion (O_2^-•) by the action of superoxide dismutase (SOD).

The molecular mechanisms underlying the differences between different ALL samples with respect to their dependence on stromal BSG will be an interesting new avenue for future exploration. One possibility would be differences in the expression of limiting enzymes in the GSH pathway. Our gene expression profiles did not show a correlation of GST or GSH-PX levels to the sensitivity pattern to cysteine depletion. However, there is a trend towards lower mRNA levels of the catalytic subunit of γ-glutamylcysteine synthetase in sensitive cases (data not shown), which requires further confirmation. Mutations or differential activities in metabolic enzymes involved in the GSH pathway could be responsible for the differential metabolic activities. Metabolomic studies will be conducted to identify suggestive differences in the metabolism of these patients. Despite the fact that high GSH levels in ALL cells were suggested to be related to poor outcome [231] and to be associated with an increased risk of relapse [232], we could not detect a direct association this in vitro phenotype with classical clinical risk stratification in these 10 patients. This may however be due to the small sample size for such comparisons.

Collectively, the experiments presented here establish our high-content platform as we could identify and validate different modalities of intercellular interactions. The data supports the use of this model for a large scale study, including more patients and testing a much larger number of genes. However, already the pathways that we identified here will constitute a solid basis for more investigations. The fact that we identify clear subsets in ALL with a pronounced dependence on signalling by VEGF is of immediate clinical relevance. Furthermore, the identification of a phenotype of metabolic interdependence for protection from oxidative stress could also be amenable to specific therapeutic targeting. Finally the development of this platform opens new dimension for combinatorial testing of primary ALL cells with new agents, which is of outmost importance in this field.

Bibliography

1. Tubergen, D.G., et al., *Improved outcome with delayed intensification for children with acute lymphoblastic leukemia and intermediate presenting features: a Childrens Cancer Group phase III trial.* J Clin Oncol, 1993. **11**(3): p. 527-37.
2. Pui, C.H., *Central nervous system disease in acute lymphoblastic leukemia: prophylaxis and treatment.* Hematology Am Soc Hematol Educ Program, 2006: p. 142-6.
3. Mann, G., et al., *Improved outcome with hematopoietic stem cell transplantation in a poor prognostic subgroup of infants with mixed-lineage-leukemia (MLL)-rearranged acute lymphoblastic leukemia: results from the Interfant-99 Study.* Blood. **116**(15): p. 2644-50.
4. Munoz, A., et al., *Allogeneic hemopoietic stem cell transplantation for childhood acute lymphoblastic leukemia in second complete remission-similar outcomes after matched related and unrelated donor transplant: a study of the Spanish Working Party for Blood and Marrow Transplantation in Children (Getmon).* Pediatr Hematol Oncol, 2008. **25**(4): p. 245-59.
5. Schrappe, M., et al., *Outcomes after induction failure in childhood acute lymphoblastic leukemia.* N Engl J Med. **366**(15): p. 1371-81.
6. Moricke, A., et al., *Long-term results of five consecutive trials in childhood acute lymphoblastic leukemia performed by the ALL-BFM study group from 1981 to 2000.* Leukemia. **24**(2): p. 265-84.
7. Pui, C.H., *Recent advances in acute lymphoblastic leukemia.* Oncology (Williston Park). **25**(4): p. 341, 346-7.
8. Moricke, A., et al., *Risk-adjusted therapy of acute lymphoblastic leukemia can decrease treatment burden and improve survival: treatment results of 2169 unselected pediatric and adolescent patients enrolled in the trial ALL-BFM 95.* Blood, 2008. **111**(9): p. 4477-89.
9. Pui, C.H., *Recent research advances in childhood acute lymphoblastic leukemia.* J Formos Med Assoc. **109**(11): p. 777-87.
10. Hunger, S.P., *Chromosomal translocations involving the E2A gene in acute lymphoblastic leukemia: clinical features and molecular pathogenesis.* Blood, 1996. **87**(4): p. 1211-24.
11. McLean, T.W., et al., *TEL/AML-1 dimerizes and is associated with a favorable outcome in childhood acute lymphoblastic leukemia.* Blood, 1996. **88**(11): p. 4252-8.
12. Armstrong, S.A. and A.T. Look, *Molecular genetics of acute lymphoblastic leukemia.* Journal of Clinical Oncology, 2005. **23**(26): p. 6306-15.
13. Pui, C.H., et al., *Outcome of treatment in childhood acute lymphoblastic leukaemia with rearrangements of the 11q23 chromosomal region.[see comment].* Lancet, 2002. **359**(9321): p. 1909-15.
14. Gleissner, B., et al., *Leading prognostic relevance of the BCR-ABL translocation in adult acute B-lineage lymphoblastic leukemia: a prospective study of the German Multicenter Trial Group and confirmed polymerase chain reaction analysis.* Blood, 2002. **99**(5): p. 1536-43.
15. Mullighan, C.G., *Molecular genetics of B-precursor acute lymphoblastic leukemia.* J Clin Invest. **122**(10): p. 3407-15.
16. Mullighan, C.G., et al., *Genome-wide analysis of genetic alterations in acute lymphoblastic leukaemia.* Nature, 2007. **446**(7137): p. 758-64.
17. Mullighan, C.G., et al., *Failure of CDKN2A/B (INK4A/B-ARF)-mediated tumor suppression and resistance to targeted therapy in acute lymphoblastic leukemia induced by BCR-ABL.* Genes Dev, 2008. **22**(11): p. 1411-5.
18. Mullighan, C.G., et al., *CREBBP mutations in relapsed acute lymphoblastic leukaemia.* Nature. **471**(7337): p. 235-9.

19. Roberts, K.G., et al., *Genetic alterations activating kinase and cytokine receptor signaling in high-risk acute lymphoblastic leukemia.* Cancer Cell. **22**(2): p. 153-66.
20. Den Boer, M.L., et al., *A subtype of childhood acute lymphoblastic leukaemia with poor treatment outcome: a genome-wide classification study.* Lancet Oncol, 2009. **10**(2): p. 125-34.
21. Mullighan, C.G., et al., *BCR-ABL1 lymphoblastic leukaemia is characterized by the deletion of Ikaros.* Nature, 2008. **453**(7191): p. 110-4.
22. Hertzberg, L., et al., *Down syndrome acute lymphoblastic leukemia, a highly heterogeneous disease in which aberrant expression of CRLF2 is associated with mutated JAK2: a report from the International BFM Study Group.* Blood, 2010. **115**(5): p. 1006-17.
23. van Dongen, J.J., et al., *Prognostic value of minimal residual disease in acute lymphoblastic leukaemia in childhood.* Lancet, 1998. **352**(9142): p. 1731-8.
24. Conter, V., et al., *Molecular response to treatment redefines all prognostic factors in children and adolescents with B-cell precursor acute lymphoblastic leukemia: results in 3184 patients of the AIEOP-BFM ALL 2000 study.* Blood, 2010. **115**(16): p. 3206-14.
25. Borowitz, M.J., et al., *Clinical significance of minimal residual disease in childhood acute lymphoblastic leukemia and its relationship to other prognostic factors: a Children's Oncology Group study.* Blood, 2008. **111**(12): p. 5477-85.
26. Parker, C., et al., *Effect of mitoxantrone on outcome of children with first relapse of acute lymphoblastic leukaemia (ALL R3): an open-label randomised trial.* Lancet, 2010. **376**(9757): p. 2009-17.
27. Hanahan, D. and R.A. Weinberg, *Hallmarks of cancer: the next generation.* Cell. **144**(5): p. 646-74.
28. Direkze, N.C., et al., *Bone marrow contribution to tumor-associated myofibroblasts and fibroblasts.* Cancer Res, 2004. **64**(23): p. 8492-5.
29. Ishii, G., et al., *Bone-marrow-derived myofibroblasts contribute to the cancer-induced stromal reaction.* Biochem Biophys Res Commun, 2003. **309**(1): p. 232-40.
30. Pittenger, M.F., et al., *Multilineage potential of adult human mesenchymal stem cells.* Science, 1999. **284**(5411): p. 143-7.
31. Bianco, P., et al., *The meaning, the sense and the significance: translating the science of mesenchymal stem cells into medicine.* Nat Med, 2013. **19**(1): p. 35-42.
32. Sacchetti, B., et al., *Self-renewing osteoprogenitors in bone marrow sinusoids can organize a hematopoietic microenvironment.* Cell, 2007. **131**(2): p. 324-36.
33. Dominici, M., et al., *Minimal criteria for defining multipotent mesenchymal stromal cells. The International Society for Cellular Therapy position statement.* Cytotherapy, 2006. **8**(4): p. 315-7.
34. Hall, B., M. Andreeff, and F. Marini, *The participation of mesenchymal stem cells in tumor stroma formation and their application as targeted-gene delivery vehicles.* Handb Exp Pharmacol, 2007(180): p. 263-83.
35. Bergfeld, S.A. and Y.A. DeClerck, *Bone marrow-derived mesenchymal stem cells and the tumor microenvironment.* Cancer Metastasis Rev. **29**(2): p. 249-61.
36. Dembinski, J.L., et al., *Tumor stroma engraftment of gene-modified mesenchymal stem cells as anti-tumor therapy against ovarian cancer.* Cytotherapy. **15**(1): p. 20-32 e2.
37. Schofield, R., *The relationship between the spleen colony-forming cell and the haemopoietic stem cell.* Blood cells, 1978. **4**: p. 7-25.
38. Park, D., D.B. Sykes, and D.T. Scadden, *The hematopoietic stem cell niche.* Front Biosci. **17**: p. 30-9.
39. Takizawa, H. and M.G. Manz, *In vivo divisional tracking of hematopoietic stem cells.* Ann N Y Acad Sci. **1266**: p. 40-6.
40. Trumpp, A., M. Essers, and A. Wilson, *Awakening dormant haematopoietic stem cells.* Nat Rev Immunol. **10**(3): p. 201-9.
41. Lo Celso, C. and D.T. Scadden, *The haematopoietic stem cell niche at a glance.* J Cell Sci, 2011. **124**(Pt 21): p. 3529-35.

42. Scadden, D.T., *The stem-cell niche as an entity of action.* Nature, 2006. **441**(7097): p. 1075-9.
43. Sugiyama, T., et al., *Maintenance of the hematopoietic stem cell pool by CXCL12-CXCR4 chemokine signaling in bone marrow stromal cell niches.* Immunity, 2006. **25**(6): p. 977-88.
44. Mendez-Ferrer, S., et al., *Mesenchymal and haematopoietic stem cells form a unique bone marrow niche.* Nature, 2010. **466**(7308): p. 829-34.
45. Mazo, I.B., S. Massberg, and U.H. von Andrian, *Hematopoietic stem and progenitor cell trafficking.* Trends Immunol. **32**(10): p. 493-503.
46. Bhattacharya, D., et al., *Niche recycling through division-independent egress of hematopoietic stem cells.* J Exp Med, 2009. **206**(12): p. 2837-50.
47. Wright, D.E., et al., *Physiological migration of hematopoietic stem and progenitor cells.* Science, 2001. **294**(5548): p. 1933-6.
48. Mendez-Ferrer, S., et al., *Haematopoietic stem cell release is regulated by circadian oscillations.* Nature, 2008. **452**(7186): p. 442-7.
49. Shen, Y., et al., *Tissue inhibitor of metalloproteinase-3 (TIMP-3) regulates hematopoiesis and bone formation in vivo.* PLoS One. **5**(9).
50. Lapidot, T. and O. Kollet, *The brain-bone-blood triad: traffic lights for stem-cell homing and mobilization.* Hematology Am Soc Hematol Educ Program. **2010**: p. 1-6.
51. Priestley, G.V., et al., *Lack of alpha4 integrin expression in stem cells restricts competitive function and self-renewal activity.* Blood, 2006. **107**(7): p. 2959-67.
52. Ulyanova, T., et al., *VCAM-1 ablation in nonhematopoietic cells in MxCre+ VCAM-1f/f mice is variable and dictates their phenotype.* Exp Hematol, 2007. **35**(4): p. 565-71.
53. Adams, G.B., et al., *Stem cell engraftment at the endosteal niche is specified by the calcium-sensing receptor.* Nature, 2006. **439**(7076): p. 599-603.
54. Arai, F., et al., *Tie2/angiopoietin-1 signaling regulates hematopoietic stem cell quiescence in the bone marrow niche.* Cell, 2004. **118**(2): p. 149-61.
55. Barker, J.E., *Early transplantation to a normal microenvironment prevents the development of Steel hematopoietic stem cell defects.* Exp Hematol, 1997. **25**(6): p. 542-7.
56. Yoshihara, H., et al., *Thrombopoietin/MPL signaling regulates hematopoietic stem cell quiescence and interaction with the osteoblastic niche.* Cell Stem Cell, 2007. **1**(6): p. 685-97.
57. Zheng, J., et al., *Angiopoietin-like protein 3 supports the activity of hematopoietic stem cells in the bone marrow niche.* Blood. **117**(2): p. 470-9.
58. Malhotra, S. and P.W. Kincade, *Wnt-related molecules and signaling pathway equilibrium in hematopoiesis.* Cell Stem Cell, 2009. **4**(1): p. 27-36.
59. Willert, K., et al., *Wnt proteins are lipid-modified and can act as stem cell growth factors.* Nature, 2003. **423**(6938): p. 448-52.
60. Murdoch, B., et al., *Wnt-5A augments repopulating capacity and primitive hematopoietic development of human blood stem cells in vivo.* Proc Natl Acad Sci U S A, 2003. **100**(6): p. 3422-7.
61. Reya, T., et al., *A role for Wnt signalling in self-renewal of haematopoietic stem cells.* Nature, 2003. **423**(6938): p. 409-14.
62. Malhotra, S. and P.W. Kincade, *Canonical Wnt pathway signaling suppresses VCAM-1 expression by marrow stromal and hematopoietic cells.* Exp Hematol, 2009. **37**(1): p. 19-30.
63. Butler, J.M., et al., *Endothelial cells are essential for the self-renewal and repopulation of Notch-dependent hematopoietic stem cells.* Cell Stem Cell. **6**(3): p. 251-64.
64. Calvi, L.M., et al., *Osteoblastic cells regulate the haematopoietic stem cell niche.* Nature, 2003. **425**(6960): p. 841-6.
65. Colmone, A., et al., *Leukemic cells create bone marrow niches that disrupt the behavior of normal hematopoietic progenitor cells.* Science, 2008. **322**(5909): p. 1861-5.

66. Shen, W., et al., *The chemokine receptor CXCR4 enhances integrin-mediated in vitro adhesion and facilitates engraftment of leukemic precursor-B cells in the bone marrow.* Exp Hematol, 2001. **29**(12): p. 1439-47.
67. Spiegel, A., et al., *Unique SDF-1-induced activation of human precursor-B ALL cells as a result of altered CXCR4 expression and signaling.* Blood, 2004. **103**(8): p. 2900-7.
68. Muller, A., et al., *Involvement of chemokine receptors in breast cancer metastasis.* Nature, 2001. **410**(6824): p. 50-6.
69. Hinton, C.V., S. Avraham, and H.K. Avraham, *Role of the CXCR4/CXCL12 signaling axis in breast cancer metastasis to the brain.* Clin Exp Metastasis. **27**(2): p. 97-105.
70. Crazzolara, R., et al., *High expression of the chemokine receptor CXCR4 predicts extramedullary organ infiltration in childhood acute lymphoblastic leukaemia.* Br J Haematol, 2001. **115**(3): p. 545-53.
71. Konoplev, S., et al., *Phosphorylated CXCR4 is associated with poor survival in adults with B-acute lymphoblastic leukemia.* Cancer. **117**(20): p. 4689-95.
72. Gaundar, S.S., K.F. Bradstock, and L.J. Bendall, *p38MAPK inhibitors attenuate cytokine production by bone marrow stromal cells and reduce stroma-mediated proliferation of acute lymphoblastic leukemia cells.* Cell Cycle, 2009. **8**(18): p. 2975-83.
73. Juarez, J., et al., *Effects of inhibitors of the chemokine receptor CXCR4 on acute lymphoblastic leukemia cells in vitro.* Leukemia, 2003. **17**(7): p. 1294-300.
74. Juarez, J., et al., *CXCR4 antagonists mobilize childhood acute lymphoblastic leukemia cells into the peripheral blood and inhibit engraftment.* Leukemia, 2007. **21**(6): p. 1249-57.
75. Welschinger, R., et al., *Plerixafor (AMD3100) induces prolonged mobilization of acute lymphoblastic leukemia cells and increases the proportion of cycling cells in the blood in mice.* Exp Hematol.
76. Uy, G.L., et al., *A phase 1/2 study of chemosensitization with the CXCR4 antagonist plerixafor in relapsed or refractory acute myeloid leukemia.* Blood. **119**(17): p. 3917-24.
77. Gibson, L.F., *Survival of B lineage leukemic cells: signals from the bone marrow microenvironment.* Leuk Lymphoma, 2002. **43**(1): p. 19-27.
78. Juarez, J., et al., *Interaction of interleukin-7 and interleukin-3 with the CXCL12-induced proliferation of B-cell progenitor acute lymphoblastic leukemia.* Haematologica, 2007. **92**(4): p. 450-9.
79. Wellmann, S., et al., *Activation of the HIF pathway in childhood ALL, prognostic implications of VEGF.* Leukemia, 2004. **18**(5): p. 926-33.
80. Forsythe, J.A., et al., *Activation of vascular endothelial growth factor gene transcription by hypoxia-inducible factor 1.* Mol Cell Biol, 1996. **16**(9): p. 4604-13.
81. Semenza, G.L., *Defining the role of hypoxia-inducible factor 1 in cancer biology and therapeutics.* Oncogene. **29**(5): p. 625-34.
82. Perez-Atayde, A.R., et al., *Spectrum of tumor angiogenesis in the bone marrow of children with acute lymphoblastic leukemia.* Am J Pathol, 1997. **150**(3): p. 815-21.
83. Stagno, F., et al., *VLA-4 and VLA-5 integrin expression in adult acute lymphoblastic leukemia.* Exp Hematol, 1996. **24**(4): p. 493.
84. Messinger, Y., et al., *Selective homing of human leukemic B-cell precursors to specific lymphohematopoietic microenvironments in SCID mice: a role for the beta 1 integrin family surface adhesion molecules VLA-4 and VLA-5.* Leuk Lymphoma, 1996. **23**(1-2): p. 61-9.
85. Filshie, R., D. Gottlieb, and K. Bradstock, *VLA-4 is involved in the engraftment of the human pre-B acute lymphoblastic leukaemia cell line NALM-6 in SCID mice.* Br J Haematol, 1998. **102**(5): p. 1292-300.
86. Shalapour, S., et al., *High VLA-4 expression is associated with adverse outcome and distinct gene expression changes in childhood B-cell precursor acute lymphoblastic leukemia at first relapse.* Haematologica, 2011. **96**(11): p. 1627-35.

87. McWhirter, J.R., et al., *Oncogenic homeodomain transcription factor E2A-Pbx1 activates a novel WNT gene in pre-B acute lymphoblastoid leukemia.* Proc Natl Acad Sci U S A, 1999. **96**(20): p. 11464-9.
88. Nygren, M.K., et al., *Wnt3A activates canonical Wnt signalling in acute lymphoblastic leukaemia (ALL) cells and inhibits the proliferation of B-ALL cell lines.* Br J Haematol, 2007. **136**(3): p. 400-13.
89. Khan, N.I., K.F. Bradstock, and L.J. Bendall, *Activation of Wnt/beta-catenin pathway mediates growth and survival in B-cell progenitor acute lymphoblastic leukaemia.* Br J Haematol, 2007. **138**(3): p. 338-48.
90. Memarian, A., et al., *Differential WNT Gene Expression in Various Subtypes of Acute Lymphoblastic Leukemia.* Iran J Immunol. **9**(1): p. 61-71.
91. Kuhnl, A., et al., *Overexpression of LEF1 predicts unfavorable outcome in adult patients with B-precursor acute lymphoblastic leukemia.* Blood. **118**(24): p. 6362-7.
92. Hogan, L.E., et al., *Integrated genomic analysis of relapsed childhood acute lymphoblastic leukemia reveals therapeutic strategies.* Blood. **118**(19): p. 5218-26.
93. Souabni, A., et al., *Pax5 promotes B lymphopoiesis and blocks T cell development by repressing Notch1.* Immunity, 2002. **17**(6): p. 781-93.
94. Pui, J.C., et al., *Notch1 expression in early lymphopoiesis influences B versus T lineage determination.* Immunity, 1999. **11**(3): p. 299-308.
95. Weng, A.P., et al., *Activating mutations of NOTCH1 in human T cell acute lymphoblastic leukemia.* Science, 2004. **306**(5694): p. 269-71.
96. Mirandola, L., et al., *Notch-ing from T-cell to B-cell lymphoid malignancies.* Cancer Lett. **308**(1): p. 1-13.
97. Kannan, S., et al., *Notch/HES1-mediated PARP1 activation: a cell type-specific mechanism for tumor suppression.* Blood. **117**(10): p. 2891-900.
98. Nwabo Kamdje, A.H., et al., *Notch-3 and Notch-4 signaling rescue from apoptosis human B-ALL cells in contact with human bone marrow-derived mesenchymal stromal cells.* Blood, 2011. **118**(2): p. 380-9.
99. Hay, N., *The Akt-mTOR tango and its relevance to cancer.* Cancer Cell, 2005. **8**(3): p. 179-83.
100. Lee-Sherick, A.B., et al., *Targeting paediatric acute lymphoblastic leukaemia: novel therapies currently in development.* Br J Haematol. **151**(4): p. 295-311.
101. Pearson, G., et al., *Mitogen-activated protein (MAP) kinase pathways: regulation and physiological functions.* Endocr Rev, 2001. **22**(2): p. 153-83.
102. Mudry, R.E., et al., *Stromal cells regulate survival of B-lineage leukemic cells during chemotherapy.* Blood, 2000. **96**(5): p. 1926-32.
103. Tabe, Y., et al., *Activation of integrin-linked kinase is a critical prosurvival pathway induced in leukemic cells by bone marrow-derived stromal cells.* Cancer Res, 2007. **67**(2): p. 684-94.
104. Acharya, M., et al., *SDF-1 and PDGF enhance alphavbeta5-mediated ERK activation and adhesion-independent growth of human pre-B cell lines.* Leukemia, 2009. **23**(10): p. 1807-17.
105. Wang, L., et al., *VEGF-induced phosphorylation of Bcl-2 influences B lineage leukemic cell response to apoptotic stimuli.* Leukemia, 2005. **19**(3): p. 344-53.
106. Fortney, J.E., et al., *Bone marrow stromal cells regulate caspase 3 activity in leukemic cells during chemotherapy.* Leuk Res, 2001. **25**(10): p. 901-7.
107. Hanahan, D. and R.A. Weinberg, *Hallmarks of cancer: the next generation.* Cell, 2011. **144**(5): p. 646-74.
108. Samudio, I., M. Fiegl, and M. Andreeff, *Mitochondrial uncoupling and the Warburg effect: molecular basis for the reprogramming of cancer cell metabolism.* Cancer Res, 2009. **69**(6): p. 2163-6.
109. Yuneva, M.O., et al., *The metabolic profile of tumors depends on both the responsible genetic lesion and tissue type.* Cell Metab, 2012. **15**(2): p. 157-70.
110. Ying, H., et al., *Oncogenic Kras maintains pancreatic tumors through regulation of anabolic glucose metabolism.* Cell, 2012. **149**(3): p. 656-70.

111. Wise, D.R., et al., *Myc regulates a transcriptional program that stimulates mitochondrial glutaminolysis and leads to glutamine addiction.* Proc Natl Acad Sci U S A, 2008. **105**(48): p. 18782-7.
112. Qing, G., et al., *ATF4 regulates MYC-mediated neuroblastoma cell death upon glutamine deprivation.* Cancer Cell, 2012. **22**(5): p. 631-44.
113. Yan, H., et al., *IDH1 and IDH2 mutations in gliomas.* N Engl J Med, 2009. **360**(8): p. 765-73.
114. Mardis, E.R., et al., *Recurring mutations found by sequencing an acute myeloid leukemia genome.* N Engl J Med, 2009. **361**(11): p. 1058-66.
115. Zhang, W., et al., *Stromal control of cystine metabolism promotes cancer cell survival in chronic lymphocytic leukaemia.* Nat Cell Biol, 2012. **14**(3): p. 276-86.
116. Iwamoto, S., et al., *Mesenchymal cells regulate the response of acute lymphoblastic leukemia cells to asparaginase.* J Clin Invest, 2007. **117**(4): p. 1049-57.
117. Rosenfeld, C., et al., *Phenotypic characterisation of a unique non-T, non-B acute lymphoblastic leukaemia cell line.* Nature, 1977. **267**(5614): p. 841-3.
118. John Masters and B. Palsson, *Human cell culture: Volume III*
Cancer lines part 3: leukemia and lymphomas. 2000.
119. Cox, C.V., et al., *Characterization of acute lymphoblastic leukemia progenitor cells.* Blood, 2004. **104**(9): p. 2919-25.
120. Campana, D., et al., *Growth requirements and immunophenotype of acute lymphoblastic leukemia progenitors.* Blood, 2005. **105**(10): p. 4150.
121. Whitlock, C.A. and O.N. Witte, *Long-term culture of B lymphocytes and their precursors from murine bone marrow.* Proc Natl Acad Sci U S A, 1982. **79**(11): p. 3608-12.
122. Gluck, U., et al., *Long-term proliferation of human leukemia cells induced by mouse stroma.* Exp Hematol, 1989. **17**(5): p. 398-404.
123. Nazarov, I., et al., *Multipotent stromal stem cells from human placenta demonstrate high therapeutic potential.* Stem Cells Transl Med. **1**(5): p. 359-72.
124. Hegyi, B., et al., *Identical, similar or different? Learning about immunomodulatory function of mesenchymal stem cells isolated from various mouse tissues: bone marrow, spleen, thymus and aorta wall.* Int Immunol. **22**(7): p. 551-9.
125. Zhu, Y.M., et al., *NOTCH1 mutations in T-cell acute lymphoblastic leukemia: prognostic significance and implication in multifactorial leukemogenesis.* Clin Cancer Res, 2006. **12**(10): p. 3043-9.
126. Li, C., et al., *Functional Hematopoietic Cells Derived From Mouse Embryonic Stem Cells* ASH abstracts 2012, 2012.
127. Itoh, K., et al., *Reproducible establishment of hemopoietic supportive stromal cell lines from murine bone marrow.* Exp Hematol, 1989. **17**(2): p. 145-53.
128. Roecklein, B.A. and B. Torok-Storb, *Functionally distinct human marrow stromal cell lines immortalized by transduction with the human papilloma virus E6/E7 genes.* Blood, 1995. **85**(4): p. 997-1005.
129. Mihara, K., et al., *Development and functional characterization of human bone marrow mesenchymal cells immortalized by enforced expression of telomerase.* Br J Haematol, 2003. **120**(5): p. 846-9.
130. Bradstock, K., et al., *Long-term survival and proliferation of precursor-B acute lymphoblastic leukemia cells on human bone marrow stroma.* Leukemia, 1996. **10**(5): p. 813-20.
131. Nishigaki, H., et al., *Prevalence and growth characteristics of malignant stem cells in B-lineage acute lymphoblastic leukemia.* Blood, 1997. **89**(10): p. 3735-44.
132. Kumagai, M., et al., *Stroma-supported culture in childhood B-lineage acute lymphoblastic leukemia cells predicts treatment outcome.* J Clin Invest, 1996. **97**(3): p. 755-60.
133. Barabe, F., et al., *Modeling the initiation and progression of human acute leukemia in mice.* Science, 2007. **316**(5824): p. 600-4.

134. Williams, R.T., W. den Besten, and C.J. Sherr, *Cytokine-dependent imatinib resistance in mouse BCR-ABL+, Arf-null lymphoblastic leukemia.* Genes Dev, 2007. **21**(18): p. 2283-7.
135. Clappier, E., et al., *Clonal selection in xenografted human T cell acute lymphoblastic leukemia recapitulates gain of malignancy at relapse.* J Exp Med, 2011. **208**(4): p. 653-61.
136. Schmitz, M., et al., *Xenografts of highly resistant leukemia recapitulate the clonal composition of the leukemogenic compartment.* Blood, 2011.
137. Meyer, L.H. and K.M. Debatin, *Diversity of human leukemia xenograft mouse models: implications for disease biology.* Cancer Res. **71**(23): p. 7141-4.
138. Mirkowska, P., *Chemoproteomic Cell Surface Mapping for the Detection of Disease Associated Features in Childhood Acute Lymphoblastic Leukemia.* Dissertation of ETH Zurich, 2012.
139. Premsrirut, P.K., et al., *A rapid and scalable system for studying gene function in mice using conditional RNA interference.* Cell. **145**(1): p. 145-58.
140. Cobas, M., et al., *Beta-catenin is dispensable for hematopoiesis and lymphopoiesis.* J Exp Med, 2004. **199**(2): p. 221-9.
141. Maillard, I., et al., *Canonical notch signaling is dispensable for the maintenance of adult hematopoietic stem cells.* Cell Stem Cell, 2008. **2**(4): p. 356-66.
142. Mancini, S.J., et al., *Jagged1-dependent Notch signaling is dispensable for hematopoietic stem cell self-renewal and differentiation.* Blood, 2005. **105**(6): p. 2340-2.
143. Satija, N.K., et al., *Mesenchymal stem cell-based therapy: a new paradigm in regenerative medicine.* J Cell Mol Med, 2009. **13**(11-12): p. 4385-402.
144. Pasha, Z., et al., *Preconditioning enhances cell survival and differentiation of stem cells during transplantation in infarcted myocardium.* Cardiovasc Res, 2008. **77**(1): p. 134-42.
145. Rosova, I., et al., *Hypoxic preconditioning results in increased motility and improved therapeutic potential of human mesenchymal stem cells.* Stem Cells, 2008. **26**(8): p. 2173-82.
146. Kumar, S. and S. Ponnazhagan, *Bone homing of mesenchymal stem cells by ectopic alpha 4 integrin expression.* Faseb J, 2007. **21**(14): p. 3917-27.
147. Chen, Y., et al., *Human extramedullary bone marrow in mice: a novel in vivo model of genetically controlled hematopoietic microenvironment.* Blood, 2012. **119**(21): p. 4971-80.
148. Vaiselbuh, S.R., et al., *Ectopic human mesenchymal stem cell-coated scaffolds in NOD/SCID mice: an in vivo model of the leukemia niche.* Tissue Eng Part C Methods. **16**(6): p. 1523-31.
149. Manz, M.G. and J.P. Di Santo, *Renaissance for mouse models of human hematopoiesis and immunobiology.* Nat Immunol, 2009. **10**(10): p. 1039-42.
150. Wunderlich, M., et al., *AML xenograft efficiency is significantly improved in NOD/SCID-IL2RG mice constitutively expressing human SCF, GM-CSF and IL-3.* Leukemia. **24**(10): p. 1785-8.
151. Willinger, T., et al., *Human IL-3/GM-CSF knock-in mice support human alveolar macrophage development and human immune responses in the lung.* Proc Natl Acad Sci U S A. **108**(6): p. 2390-5.
152. Rongvaux, A., et al., *Human thrombopoietin knockin mice efficiently support human hematopoiesis in vivo.* Proc Natl Acad Sci U S A. **108**(6): p. 2378-83.
153. Pui, C.H., et al., *Pediatric acute lymphoblastic leukemia: where are we going and how do we get there?* Blood, 2012. **120**(6): p. 1165-74.
154. Orvedahl, A., et al., *Image-based genome-wide siRNA screen identifies selective autophagy factors.* Nature. **480**(7375): p. 113-7.
155. Vassilev, L.T., et al., *Cell-based screening approach for antitumor drug leads which exploits sensitivity differences between normal and cancer cells: identification of two novel cell-cycle inhibitors.* Anticancer Drug Des, 2001. **16**(1): p. 7-17.

156. Madoux, F., et al., *An ultra-high throughput cell-based screen for wee1 degradation inhibitors.* J Biomol Screen. **15**(8): p. 907-17.
157. Snijder, B., et al., *Single-cell analysis of population context advances RNAi screening at multiple levels.* Mol Syst Biol. **8**: p. 579.
158. Lindquist, R.A., et al., *Genome-scale RNAi on living-cell microarrays identifies novel regulators of Drosophila melanogaster TORC1-S6K pathway signaling.* Genome Res. **21**(3): p. 433-46.
159. Bailey, S.N., et al., *Microarrays of lentiviruses for gene function screens in immortalized and primary cells.* Nat Methods, 2006. **3**(2): p. 117-22.
160. Wheeler, D.B., A.E. Carpenter, and D.M. Sabatini, *Cell microarrays and RNA interference chip away at gene function.* Nat Genet, 2005. **37 Suppl**: p. S25-30.
161. McMillin, D.W., et al., *Tumor cell-specific bioluminescence platform to identify stroma-induced changes to anticancer drug activity.* Nat Med, 2010. **16**(4): p. 483-9.
162. McDermott, S.P., et al., *A small molecule screening strategy with validation on human leukemia stem cells uncovers the therapeutic efficacy of kinetin riboside.* Blood. **119**(5): p. 1200-7.
163. Tibes, R., et al., *RNAi screening of the kinome with cytarabine in leukemias.* Blood. **119**(12): p. 2863-72.
164. Hartwell, K.A., et al., *Niche-Based Screening Reveals Leukemia Stem Cell Specific Therapeutics.* ASH abstracts 2011.
165. Tyner, J.W., et al., *RNAi screen for rapid therapeutic target identification in leukemia patients.* Proc Natl Acad Sci U S A, 2009. **106**(21): p. 8695-700.
166. Gullbo, J., et al., *Phenotype-based drug screening in primary ovarian carcinoma cultures identifies intracellular iron depletion as a promising strategy for cancer treatment.* Biochem Pharmacol. **82**(2): p. 139-47.
167. Krausz, E., et al., *Translation of a Tumor Microenvironment Mimicking 3D Tumor Growth Co-culture Assay Platform to High-Content Screening.* J Biomol Screen. **18**(1): p. 54-66.
168. Herrmann, R., et al., *Screening for compounds that induce apoptosis of cancer cells grown as multicellular spheroids.* J Biomol Screen, 2008. **13**(1): p. 1-8.
169. Zuber, J., et al., *RNAi screen identifies Brd4 as a therapeutic target in acute myeloid leukaemia.* Nature. **478**(7370): p. 524-8.
170. Carpenter, A.E., *Image-based chemical screening.* Nat Chem Biol, 2007. **3**(8): p. 461-5.
171. Carpenter, A.E., L. Kamentsky, and K.W. Eliceiri, *A call for bioimaging software usability.* Nat Methods. **9**(7): p. 666-70.
172. Tyson, D.R., et al., *Fractional proliferation: a method to deconvolve cell population dynamics from single-cell data.* Nat Methods. **9**(9): p. 923-8.
173. Evensen, L., W. Link, and J.B. Lorens, *Image-based high-throughput screening for inhibitors of angiogenesis.* Methods Mol Biol. **931**: p. 139-51.
174. Vogt, A., et al., *Automated image-based phenotypic analysis in zebrafish embryos.* Dev Dyn, 2009. **238**(3): p. 656-63.
175. Bailey, L.C., et al., *Bone-marrow relapse in paediatric acute lymphoblastic leukaemia.* Lancet Oncol, 2008. **9**(9): p. 873-83.
176. Dias, S., et al., *VEGF(165) promotes survival of leukemic cells by Hsp90-mediated induction of Bcl-2 expression and apoptosis inhibition.* Blood, 2002. **99**(7): p. 2532-40.
177. Nijmeijer, B.A., et al., *Monitoring of engraftment and progression of acute lymphoblastic leukemia in individual NOD/SCID mice.* Experimental Hematology, 2001. **29**(3): p. 322-9.
178. Notta, F., et al., *Evolution of human BCR-ABL1 lymphoblastic leukaemia-initiating cells.* Nature, 2011. **469**(7330): p. 362-7.
179. Olivo-Marin, J.-C., *Extraction of spots in biological images using multiscale products.* Pattern Recognition, 2002. **35**(9): p. 1989-1996.
180. Carpenter, A.E., et al., *CellProfiler: image analysis software for identifying and quantifying cell phenotypes.* Genome Biol, 2006. **7**(10): p. R100.

181. Horvath, P., et al., *Machine learning improves the precision and robustness of high-content screens: using nonlinear multiparametric methods to analyze screening results.* J Biomol Screen, 2011. **16**(9): p. 1059-67.
182. Duda R, H.P., Stork D, *Pattern Classification (2nd edition).* Wiley-Interscience, 2000.
183. Freedman, M.H., et al., *Autocrine and paracrine growth control by granulocyte-monocyte colony-stimulating factor of acute lymphoblastic leukemia cells.* Blood, 1993. **81**(11): p. 3068-75.
184. Muguruma, Y., et al., *Reconstitution of the functional human hematopoietic microenvironment derived from human mesenchymal stem cells in the murine bone marrow compartment.* Blood, 2006. **107**(5): p. 1878-87.
185. Kunisaki, Y. and P.S. Frenette, *The secrets of the bone marrow niche: Enigmatic niche brings challenge for HSC expansion.* Nat Med, 2012. **18**(6): p. 864-5.
186. Konoplev, S., et al., *Phosphorylated CXCR4 is associated with poor survival in adults with B-acute lymphoblastic leukemia.* Cancer, 2011. **117**(20): p. 4689-95.
187. Bonapace, L., et al., *Induction of autophagy-dependent necroptosis is required for childhood acute lymphoblastic leukemia cells to overcome glucocorticoid resistance.* J Clin Invest, 2010. **120**(4): p. 1310-23.
188. Bradstock, K., et al., *Analysis of the mechanism of adhesion of precursor-B acute lymphoblastic leukemia cells to bone marrow fibroblasts.* Blood, 1993. **82**(11): p. 3437-44.
189. Harvey, R.C., et al., *Identification of novel cluster groups in pediatric high-risk B-precursor acute lymphoblastic leukemia with gene expression profiling: correlation with genome-wide DNA copy number alterations, clinical characteristics, and outcome.* Blood, 2010. **116**(23): p. 4874-84.
190. Gehrke, I., et al., *Bone marrow stromal cell-derived vascular endothelial growth factor (VEGF) rather than chronic lymphocytic leukemia (CLL) cell-derived VEGF is essential for the apoptotic resistance of cultured CLL cells.* Mol Med, 2011. **17**(7-8): p. 619-27.
191. Huang, W., et al., *Modulation of CD147-induced matrix metalloproteinase activity: role of CD147 N-glycosylation.* Biochem J, 2013. **449**(2): p. 437-48.
192. Hibino, T., et al., *S100A9 Is a Novel Ligand of EMMPRIN That Promotes Melanoma Metastasis.* Cancer Res, 2013. **73**(1): p. 172-83.
193. Le Floch R, C.J., Marchiq I, Naïken T, Ilk K, Murray CM, Critchlow SE, Roux D, Simon MP, Pouysségur J., *CD147 subunit of lactate/H+ symporters MCT1 and hypoxia-inducible MCT4 is critical for energetics and growth of glycolytic tumors.* Proc Natl Acad Sci U S A, 2011. **109**(49): p. 20166.
194. Xu, D. and M.E. Hemler, *Metabolic activation-related CD147-CD98 complex.* Mol Cell Proteomics, 2005. **4**(8): p. 1061-71.
195. Meads, M.B., R.A. Gatenby, and W.S. Dalton, *Environment-mediated drug resistance: a major contributor to minimal residual disease.* Nat Rev Cancer, 2009. **9**(9): p. 665-74.
196. Lock, R.B., et al., *The nonobese diabetic/severe combined immunodeficient (NOD/SCID) mouse model of childhood acute lymphoblastic leukemia reveals intrinsic differences in biologic characteristics at diagnosis and relapse.* Blood, 2002. **99**(11): p. 4100-8.
197. Hsu Yen-Michael S., et al., *CXCL12 Production by Early Mesenchymal Progenitors Is Required for Hematopoietic Stem Cell Maintenance.* ASH abstracts, 2012.
198. Ghosh, A.K., et al., *Circulating microvesicles in B-cell chronic lymphocytic leukemia can stimulate marrow stromal cells: implications for disease progression.* Blood, 2010. **115**(9): p. 1755-64.
199. Wang, L., et al., *Ph+/VE-cadherin+ identifies a stem cell like population of acute lymphoblastic leukemia sustained by bone marrow niche cells.* Blood, 2007. **110**(9): p. 3334-44.
200. Markovic, A., K.L. MacKenzie, and R.B. Lock, *Induction of vascular endothelial growth factor secretion by childhood acute lymphoblastic leukemia cells via the FLT-3 signaling pathway.* Mol Cancer Ther, 2012. **11**(1): p. 183-93.

201. de Jonge, H.J., et al., *High VEGFC expression is associated with unique gene expression profiles and predicts adverse prognosis in pediatric and adult acute myeloid leukemia.* Blood, 2010. **116**(10): p. 1747-54.
202. Schulze, A. and A.L. Harris, *How cancer metabolism is tuned for proliferation and vulnerable to disruption.* Nature, 2012. **491**(7424): p. 364-73.
203. Jain, M., et al., *Metabolite profiling identifies a key role for glycine in rapid cancer cell proliferation.* Science, 2012. **336**(6084): p. 1040-4.
204. Vander Heiden, M.G., L.C. Cantley, and C.B. Thompson, *Understanding the Warburg effect: the metabolic requirements of cell proliferation.* Science, 2009. **324**(5930): p. 1029-33.
205. Wagner, C.A., F. Lang, and S. Broer, *Function and structure of heterodimeric amino acid transporters.* Am J Physiol Cell Physiol, 2001. **281**(4): p. C1077-93.
206. Reya, T. and H. Clevers, *Wnt signalling in stem cells and cancer.* Nature, 2005. **434**(7035): p. 843-50.
207. Beesley, A.H., et al., *The gene expression signature of relapse in paediatric acute lymphoblastic leukaemia: implications for mechanisms of therapy failure.* Br J Haematol, 2005. **131**(4): p. 447-56.
208. Beesley, A.H., R.E. Weller, and U.R. Kees, *The role of BSG (CD147) in acute lymphoblastic leukaemia and relapse.* Br J Haematol, 2008. **142**(6): p. 1000-2.
209. Chen, H., et al., *Co-expression of CD147/EMMPRIN with monocarboxylate transporters and multiple drug resistance proteins is associated with epithelial ovarian cancer progression.* Clin Exp Metastasis, 2010. **27**(8): p. 557-69.
210. Kuang, Y.H., et al., *RNA interference targeting the CD147 induces apoptosis of multi-drug resistant cancer cells related to XIAP depletion.* Cancer Lett, 2009. **276**(2): p. 189-95.
211. Wang, B., et al., *RNAi-mediated silencing of CD147 inhibits tumor cell proliferation, invasion and increases chemosensitivity to cisplatin in SGC7901 cells in vitro.* J Exp Clin Cancer Res, 2010. **29**: p. 61.
212. Slomiany, M.G., et al., *Hyaluronan, CD44, and emmprin regulate lactate efflux and membrane localization of monocarboxylate transporters in human breast carcinoma cells.* Cancer Res, 2009. **69**(4): p. 1293-301.
213. Lim, M., et al., *Tumor-derived EMMPRIN (extracellular matrix metalloproteinase inducer) stimulates collagenase transcription through MAPK p38.* FEBS Lett, 1998. **441**(1): p. 88-92.
214. Li, R., et al., *Basigin (murine EMMPRIN) stimulates matrix metalloproteinase production by fibroblasts.* J Cell Physiol, 2001. **186**(3): p. 371-9.
215. Zucker, S., et al., *Tumorigenic potential of extracellular matrix metalloproteinase inducer.* Am J Pathol, 2001. **158**(6): p. 1921-8.
216. Toole, B.P., *Emmprin (CD147), a cell surface regulator of matrix metalloproteinase production and function.* Curr Top Dev Biol, 2003. **54**: p. 371-89.
217. Kessenbrock, K., V. Plaks, and Z. Werb, *Matrix metalloproteinases: regulators of the tumor microenvironment.* Cell, 2010. **141**(1): p. 52-67.
218. Seizer, P., et al., *EMMPRIN (CD147) is a novel receptor for platelet GPVI and mediates platelet rolling via GPVI-EMMPRIN interaction.* Thromb Haemost, 2009. **101**(4): p. 682-6.
219. Khunkaewla, P., et al., *LFA-1-mediated leukocyte adhesion regulated by interaction of CD43 with LFA-1 and CD147.* Mol Immunol, 2008. **45**(6): p. 1703-11.
220. Grass, G.D., M. Bratoeva, and B.P. Toole, *Regulation of invadopodia formation and activity by CD147.* J Cell Sci, 2012. **125**(Pt 3): p. 777-88.
221. Marieb, E.A., et al., *Emmprin promotes anchorage-independent growth in human mammary carcinoma cells by stimulating hyaluronan production.* Cancer Res, 2004. **64**(4): p. 1229-32.
222. Igakura, T., et al., *A null mutation in basigin, an immunoglobulin superfamily member, indicates its important roles in peri-implantation development and spermatogenesis.* Dev Biol, 1998. **194**(2): p. 152-65.

223. Kuno, N., et al., *Female sterility in mice lacking the basigin gene, which encodes a transmembrane glycoprotein belonging to the immunoglobulin superfamily.* FEBS Lett, 1998. **425**(2): p. 191-4.
224. Agrawal, S.M., et al., *EMMPRIN: a novel regulator of leukocyte transmigration into the CNS in multiple sclerosis and experimental autoimmune encephalomyelitis.* J Neurosci, 2011. **31**(2): p. 669-77.
225. Agrawal, S.M. and V.W. Yong, *The many faces of EMMPRIN - roles in neuroinflammation.* Biochim Biophys Acta, 2011. **1812**(2): p. 213-9.
226. Sun, J. and M.E. Hemler, *Regulation of MMP-1 and MMP-2 production through CD147/extracellular matrix metalloproteinase inducer interactions.* Cancer Res, 2001. **61**(5): p. 2276-81.
227. Li, Y., et al., *Extracellular membrane-proximal domain of HAb18G/CD147 binds to metal ion-dependent adhesion site (MIDAS) motif of integrin beta1 to modulate malignant properties of hepatoma cells.* J Biol Chem, 2012. **287**(7): p. 4759-72.
228. Song, F., et al., *Cyclophilin A (CyPA) induces chemotaxis independent of its peptidylprolyl cis-trans isomerase activity: direct binding between CyPA and the ectodomain of CD147.* J Biol Chem, 2011. **286**(10): p. 8197-203.
229. Townsend, D.M., K.D. Tew, and H. Tapiero, *The importance of glutathione in human disease.* Biomed Pharmacother, 2003. **57**(3-4): p. 145-55.
230. Haddad, J.J., *Oxygen-sensing mechanisms and the regulation of redox-responsive transcription factors in development and pathophysiology.* Respir Res, 2002. **3**: p. 26.
231. Kearns, P., et al., *Glutathione in childhood acute leukaemias.* Advances in Experimental Medicine & Biology, 1999. **457**: p. 211-6.
232. Kearns, P.R., et al., *Raised blast glutathione levels are associated with an increased risk of relapse in childhood acute lymphocytic leukemia.* Blood, 2001. **97**(2): p. 393-8.

Curriculum Vitae

Jeannette Boutter

PERSONAL DETAILS

Address:
Zschokkestrasse 6
8037 Zurich
Switzerland

Born: 20.01.1984 in Völklingen, Germany

OCCUPATIONS

04. 2008 to 03.2013	**PhD Student** at the University Children's Hospital Zurich, Department of Pediatric Oncology, group of Prof. Dr. Jean-Pierre Bourquin "Profiling of Functional Intercellular Interactions in a Model of the Leukemia Microenvironment" Member of the Cancer Network Zurich Graduate School
09.2010 to 02.2012	**Business Manager** of Telejob, Academic job platform based in Switzerland, voluntary position
02.2010 to 05.2010	**Internship** at the Hospital Ramón y Cajal, Madrid, Spain Department for Neurobiology

UNIVERSITY STUDIES

01.2007 to 11.2007	**Diploma thesis** at the University of Darmstadt, group of Developmental Biology and Neurogenetics, Prof. Paul Layer Diploma passed with distinction
05.2006 to 01.2007	**Advanced studies in biology** at the University of Darmstadt, in Genetics, Physiology, Developmental Biology and Cell Biology Overall assessment of the exams: very good
09.2005 to 05.2006	**Erasmus semester** at the University of Alcalá de Henares, Spain, Courses in Genetics and Developmental Biology
10.2002 to 06.2005	**Basic studies in biology** at the University of Darmstadt Overall assessment of the exams: good
09.1995 to 06.2002	**French and German Gymnasium**, Saarbrücken, Germany Degree of Abitur and Baccalauréat, grade: 1,2

CONFERENCES

February 2011	**10th Charles Rodolphe Brupbacher Symposium Cancer Genome and DNA Repair** Poster presentation
June 2012	**European Hematology Association Annual Meeting** Oral presentation

PUBLICATIONS

Chraracterisation of cholinesterase expression during murine embryonic stem cell differentiation
Sperling LE, Steinert G, Boutter J, Langdraf D, Hescheler J, Pollet D and Layer PG
Chem Biol Interact. 2008 Sep 25; 175(1-3):156-60

Acknowledgements

I would like to acknowledge all the people that contributed to or supported this work:

I am grateful to Jean-Pierre Bourquin and Beat Bornhauser who gave me the opportunity to work in their group, although they did not look actively for a new PhD student at that time.
Thank you for the supervision of my research work, and for your valuable ideas, suggestions and numerous discussions throughout the project. The project was demanding and I am proud of the research results we achieved.

Thank you to Andreas Vonderheit and Peter Horvath for showing me all microscope and informatics related aspects and for helping me with all the unexpected issues.

Thank you to Markus Manz and Roland Wenger for participating in my committee, for their valuable help and inputs for the project, and for their interest in my work.

Thanks also go to Vaskar Saha who accepted to review my thesis. I'm sure that with his broad knowledge he will give me valuable suggestions.

I am very thankful to all current members of the leukemia group: Anna, Viktoras, Blerim and Yun and to the former leukemia group members: Laura, Maike, Paulina, Mattia, Michael, Raphael, Tali and Ithamar. The atmosphere in the lab made it a pleasure to come every day and the help given was always valuable.
Especially thanks to Laura, Maike and Paulina, in my heart, we will always stay "the leukemia girls". Special thanks to Paulina for accompanying me during the last year and for your support in the last weeks. Special thanks to Blerim, for managing the animal facility and for your good mood.

Best thanks go to each and every one in the Experimental Infectious Diseases and Cancer Research Lab of August-Forel Strasse, for their flexibility in booking schedules, their contribution to the nice atmosphere and to the job-related and job-non-related discussions.

Another valuable source of information was the PhD-Program of the Cancer Network Zurich that helped to connect to other PhD students in Zurich.

Besides the science field, I want to express my gratitude to all my friends, my family and to Moritz. Thank you for your understanding and your help.

My last thank you is dedicated to my grand father. He would have been very proud of me.

Supplementary Tables

Suppl. Table 1. ALL patient characteristics
Suppl. Table 2. Mass spectrometry identified proteins on MSCs
Suppl. Table 3. siRNA screen of 110genes-3 VHR patient samples

Suppl. Table 1. ALL patient characteristics

Patient	Immunology	Age at initial diagnosis	Sex	Prednisone response	Risk group	Relapse	Survival	Leukocye count	Blasts periph %	Additional information
HR-03	Common-ALL	16.9	f	PGR	HR	no	yes	13300	78	CNS, t(9;22), hhd
MNR-01	Pre-B-ALL	9.6	f	PGR	MNR	yes	no	2346	na	TP53 del.
MNR-03	Pre-B-ALL	4.3	f	PPR	MNR	yes	no	64410	na	
MNR-04	Pre-B-ALL	9.8	m	PPR	MNR	yes	no	5040	na	
MNR-07	Pre-B-ALL	12.6	f	PPR	MNR	yes	no	27945	na	t(4;11)
MNR-09	Pre-B-ALL	3.3	m	PPR	MNR	yes	no	250	na	
MNR-10	Pre-B-ALL	9.7	m	PPR	MNR	yes	no	4165	na	
SR-02	Pre-B-ALL	12.1	m	PGR	SR	no	yes	447000	94	Amplification AML1, t(1;19)
SR-04	Common-ALL	3.6	f	PGR	SR	no	yes	10600	42	t(1;19)
SR-09	Common-ALL	5.5	f	PGR	SR	yes	yes	317400	na	
SR-10	Common-ALL	7.3	m	PGR	SR	no	yes	17050	65	
SR-11	Common-ALL	6.1	m	PGR	SR	yes	yes	66600	87	CNS
SR-13	Common-ALL	4.1	f	PGR	SR	no	yes	21000	na	
VHR-01	Common-ALL	14.1	m	PPR	VHR	yes, 2x	no	6300	13	early relapse, t(17;19)
VHR-02	Common-ALL	12.8	f	PPR	VHR	yes	yes	79600	68	
VHR-03	Common-ALL	17.1	m	PPR	VHR	no	no	20100	78	TRM
VHR-04	Common-ALL	5.7	f	PGR	VHR	no	yes	45700	97	
VHR-06	Pre-B-ALL	17.6	m	PGR	VHR	yes	no	8000	73	complex karyotype, t(1;19), t(12;2)
VHR-07	Pro-B-ALL	11.6	m	PPR	VHR	no	yes	100000	99	t(4;11)
VHR-10	Common-ALL	14.4	f	PPR	VHR	no	yes	150000	89	
VHR-11	Pre-B-ALL	3.1	m	PGR	VHR	yes	no	16000	na	DS
VHR-12	Pre-B-ALL	15.3	f	PPR	VHR	no	yes	7412	92	
VHR-15	Pre-B-ALL	13.2	m	PGR	VHR	yes	yes	2900	60	deletion 9p
VHR-23	Common B-ALL	na	na	PGR	VHR	yes	na	na	na	t(17;19)
VHR-28	Common-B-ALL	na	f	na	VHR	yes	na	na	na	

Risk group assessed accordingly on the MRD result:

patients are defined as standard risk (SR) if MRD1 + 2 were negative, high risk (HR) if MRD1 + 2 were positive less than or equal to 10−3, and VHR if HR patients were still positive for MRD3

MNR stand for morphological non-responder, patients with relapse ALL

CNS:disease spread into central nervous system
hhd: hyperdiploid
TRM: treatment-related mortality
na: not available

Suppl. Table 2. Mass spectrometry identified proteins

Entrez gene symbol	Entrez Gene ID	CD annotation	Description	Number of distinct peptides	Assignment to membrane	UniProtKB/Swiss-Prot ID	UniProtKB/Swiss-Prot AC2
ABCA8	10351	na	180 kDa protein,Isoform 1	1	1	ABCA8_HUMAN	O94911
ACE	1636	CD143	Angiotensin-converting en	1	1	ACE_HUMAN	P12821
ACTA2	59	na	Actin, aortic smooth muscl	1	0	ABCC8_HUMAN	Q09428
ACTB	60	na	Actin, cytoplasmic 1,Actin,	2	0	ACTB_HUMAN	P60709
ADAM15	8751	na	ADAM 15 precursor,a disi	1	1	PCTK3_HUMAN	Q07002
ADAM17	6868	CD156b	Isoform B of ADAM 17 pre	1	1	ADA17_HUMAN	P78536
ADAM9	8754	na	Isoform 1 of ADAM 9 prec	1	1	PCY1A_HUMAN	P49585
ADCY9	115	na	Adenylate cyclase type 9	2	1	ADCY9_HUMAN	O60503
AGGF1	55109	na	Isoform 1 of Angiogenic fa	1	0	AGGF1_HUMAN	Q8N302
AHSG	197	na	Alpha-2-HS-glycoprotein p	1	0	FETUA_HUMAN	P02765
ALB	213	na	ALB protein,Isoform 2 of S	2	0	ALBU_HUMAN	P02768
ALCAM	214	CD166	Isoform 1 of CD166 antige	22	1	ADAM7_HUMAN	Q9H2U9
ALDOA	226	na	Fructose-bisphosphate alc	1	1	RED1_HUMAN	P78563
ALPL	249	na	Alkaline phosphatase, tiss	11	0	PPBT_HUMAN	P05186
ALS2CL	259173	na	CDNA FLJ44541 fis, clone	1	0	AL2CL_HUMAN	Q60I27
ANKFY1	51479	na	ankyrin repeat and FYVE d	1	0	ANFY1_HUMAN	Q9P2R3
ANPEP	290	CD13	Aminopeptidase N	8	1	AMPN_HUMAN	P15144
ANTXR1	84168	na	Isoform 1 of Anthrax toxin	1	1	ANTR1_HUMAN	Q9H6X2
ASAM	79827	na	adipocyte-specific adhesio	2	1	ASAM_HUMAN	Q9H6B4
ATP1B3	483	CD298	Sodium/potassium-transpo	3	1	AT1B3_HUMAN	P54709
AUTS2	26053	na	Isoform Long of Autism su	1	0	AUTS2_HUMAN	Q8WXX7
AXUD1	64651	na	Axin-1 up-regulated gene 1	1	0	AXUD1_HUMAN	Q96S65
BAT2D1	23215	na	BAT2-iso,HBxAg transacti	1	0	PIGO_HUMAN	Q8TEQ8
BRDG1	26228	na	Signal-transducing adapto	1	0	STAP1_HUMAN	Q9ULZ2
BSG	682	CD147	Isoform 2 of Basigin precu	4	1	BASI_HUMAN	P35613
BTN3A3	10384	na	Butyrophilin subfamily 3 m	1	1	RS11_HUMAN	P62280
C14orf78	113146	na	similar to AHNAK nucleop	2	1	AHNK2_HUMAN	Q8IVF2
C19orf31	404664	na	Uncharacterized protein C	1	0	na	na
C5	727	na	Complement C5 precursor	1	0	ARTN_HUMAN	Q5T4W7
CACNA1C	775	na	Isoform 1 of Voltage-depe	1	1	CAC1C_HUMAN	Q13936
CACNA2D1	781	na	Dihydropyridine receptor a	3	1	CAC2D_HUMAN	P54289
CASQ2	845	na	Calsequestrin-2 precursor	1	0	CASQ2_HUMAN	O14958
CD109	135228	CD109	Isoform 1 of CD109 antige	4	1	CD109_HUMAN	Q6YHK3
CD151	977	CD151	CD151 antigen	4	1	CD151_HUMAN	P48509
CD248	57124	CD248	Isoform 1 of Endosialin pre	2	1	CD248_HUMAN	Q9HCU0
CD276	80381	CD276	Isoform 2 of CD276 antige	2	1	CD276_HUMAN	Q5ZPR3
CD44	960	CD44	Isoform 12 of CD44 antige	6	1	CD44_HUMAN	P16070
CD55	1604	CD55	Decay-accelerating factor	3	1	DAF_HUMAN	P08174
CD59	966	CD59	CD59 glycoprotein precurs	23	1	CD59_HUMAN	P13987
CD63	967	CD63	CD63 antigen,Lysosome-a	2	1	CD63_HUMAN	P08962
CDC42	998	na	Isoform 2 of Cell division c	2	0	BCL3_HUMAN	P20749
CDH2	1000	CD325	Cadherin-2 precursor,97 k	2	1	CADH2_HUMAN	P19022
CDSN	1041	na	Corneodesmosin precurso	1	0	BFSP2_HUMAN	Q13515
CFP	5199	na	Properdin precursor,50 kD	1	0	PROP_HUMAN	P27918
CHD9	80205	na	Isoform 1 of Chromodoma	1	1	CHD9_HUMAN	Q3L8U1
CLIC4	25932	na	Chloride intracellular chan	1	0	CLIC4_HUMAN	Q9Y696
CORIN	10699	na	Atrial natriuteric peptide-co	1	1	CORIN_HUMAN	Q9Y5Q5
CPM	1368	na	Carboxypeptidase M precu	3	0	CAH1_HUMAN	P00915
CRELD1	78987	na	Isoform 2 of Cysteine-rich	1	1	CREL1_HUMAN	Q96HD1
CSHL1	1444	na	23 kDa protein,26 kDa pro	1	1	CSHL_HUMAN	Q14406
CSRP1	1465	na	Cysteine and glycine-rich p	1	0	CSRP1_HUMAN	P21291
CTGLF1	119016	na	Centaurin gamma-like fam	1	0	CTLF1_HUMAN	Q96P64
CTSB	1508	na	Cathepsin B precursor	1	0	CATB_HUMAN	P07858
CYB5R3	1727	na	Isoform 1 of NADH-cytoch	1	0	NB5R3_HUMAN	P00387
DAG1	1605	na	Dystroglycan precursor	1	1	CCR4_HUMAN	P51679
DCD	117159	na	Dermcidin precursor	4	0	DCD_HUMAN	P81605
DENND1B	163486	na	DENND1B protein,DENN/	1	1	DEN1B_HUMAN	Q6P3S1
DNA2L	1763	na	DNA2 DNA replication hel	1	0	DNA2L_HUMAN	P51530
DTNBP1	84062	na	Isoform 1 of Dysbindin,dys	1	0	DTBP1_HUMAN	Q96EV8
DVL1	1855	na	Dishevelled, dsh homolog	1	0	DVL1_HUMAN	O14640
DYX1C1	161582	na	93 kDa protein,49 kDa pro	1	1	DYXC1_HUMAN	Q8WXU2
EGFR	1956	na	Isoform 1 of Epidermal gro	5	1	EGFR_HUMAN	P00533
EMP3	2014	na	Epithelial membrane prote	2	1	EMP3_HUMAN	P54852
EMR2	30817	CD312	egf-like module containing	1	1	EMR2_HUMAN	Q9UHX3
ERBB2	2064	CD340	Receptor tyrosine-protein k	1	1	ERBB2_HUMAN	P04626
ERLIN1	10613	na	SPFH domain-containing p	1	0	ERLN1_HUMAN	O75477
FARP1	10160	na	Isoform 1 of FERM, RhoG	1	0	FARP1_HUMAN	Q9Y4F1
FAS	355	CD95	Tumor necrosis factor rece	2	1	TNR6_HUMAN	P25445
FAT	2195	na	Cadherin-related tumor su	1	1	COIA1_HUMAN	P39060
FBXL20	84961	na	F-box and leucine-rich rep	1	0	FXL20_HUMAN	Q96IG2
FHL2	2274	na	Hypothetical protein FHL2	1	0	FHL2_HUMAN	Q14192
FLJ21963	79611	na	hypothetical protein LOC7	1	0	ACSS3_HUMAN	Q9H6R
FLJ34931	388939	na	hypothetical protein LOC3	1	0	CB071_HUMAN	A6NGG8

Entrez gene symbol	Entrez Gene ID	CD annotation	Description	Number of distinct peptides	Assignment to membrane	UniProtKB/Swiss-Prot ID	UniProtKB/Swiss-Prot AC2
FLNA	2316	na	filamin A, alpha,Filamin-A,	4	0	FLNA_HUMAN	P21333
FN1	2335	na	Isoform 1 of Fibronectin pr	23	1	FINC_HUMAN	P02751
GAK	2580	na	Cyclin G-associated kinas	1	0	GAK_HUMAN	O14976
GAS2L3	283431	na	GAS2-like protein 3,64 kD	1	0	GA2L3_HUMAN	Q86XJ1
GCC2	9648	na	Isoform 1 of GRIP and coi	1	0	GCC2_HUMAN	Q8IWJ2
GGA2	23062	na	ADP-ribosylation factor bir	1	0	GGA2_HUMAN	Q9UJY4
GGTLA1	2687	na	Gamma-glutamyltransfera	4	0	GGT5_HUMAN	P36269
GJA1	2697	na	Gap junction alpha-1 prote	1	1	DBP_HUMAN	Q10586
GNAI2	2771	na	Isoform 2 of Guanine nucl	2	1	GNAI2_HUMAN	P04899
GNB1	2782	na	Guanine nucleotide-bindin	1	0	GBB1_HUMAN	P62873
GPRIN3	285513	na	G protein-regulated induce	1	0	GRIN3_HUMAN	Q6ZVF9
GTF2IRD1	9569	na	Isoform 1 of General trans	1	0	GT2D1_HUMAN	Q9UHL9
hCG_1988300	728638	na	similar to Keratin, type II c	3	0	K2C8_HUMAN	P05787
HLA-A	3105	na	HLA class I histocompatibi	3	1	multiple	multiple
HLA-B	3106	na	HLA class I histocompatibi	4	1	multiple	multiple
HLA-C	3107	na	HLA class I histocompatibi	2	1	multiple	multiple
HSPG2	3339	na	Basement membrane-spe	8	0	PGBM_HUMAN	P98160
ICAM1	3383	CD54	Intercellular adhesion mole	1	1	ICAM1_HUMAN	P05362
IGF2R	3482	CD222	Cation-independent mann	1	1	MPRI_HUMAN	P11717
INSRR	3645	na	Insulin receptor-related pr	1	1	INSRR_HUMAN	P14616
ISCU	23479	na	Isoform 1 of Iron-sulfur clu	1	1	ISCU_HUMAN	Q9H1K1
ITGA11	22801	na	Integrin alpha-11 precurso	1	1	ITA11_HUMAN	Q9UKX5
ITGA3	3675	CD49c	Isoform Alpha-3A of Integr	6	1	ITA3_HUMAN	P26006
ITGA5	3678	CD49e	Integrin alpha-5 precursor	23	1	ITA5_HUMAN	P08648
ITGAV	3685	CD51	Integrin alpha-V precursor	11	1	ITAV_HUMAN	P06756
ITGB1	3688	CD29	Isoform Beta-1C of Integri	16	1	ITB1_HUMAN	P05556
ITGB5	3693	na	Integrin beta-5 precursor,s	2	1	ITB5_HUMAN	P18084
KALRN	8997	na	Huntingtin-associated prot	1	0	KALRN_HUMAN	O60229
KIAA1546	54790	na	Protein KIAA1546,Hypothe	1	0	TET2_HUMAN	Q6N021
KIF12	113220	na	Kinesin-like protein KIF12,	1	0	KIF12_HUMAN	Q96FN5
KIF1B	23095	na	Isoform 1 of Kinesin-like p	1	0	KIF1B_HUMAN	O60333
KRT1	3848	na	Keratin, type II cytoskeleta	9	0	K2C1_HUMAN	P04264
KRT10	3858	na	Keratin, type I cytoskeletal	13	0	K1C10_HUMAN	P13645
KRT2	3849	na	Keratin, type II cytoskeleta	16	0	K22E_HUMAN	P35908
KRT4	3851	na	keratin 4,33 kDa protein	3	1	K2C4_HUMAN	P19013
KRT5	3852	na	Keratin, type II cytoskeleta	2	0	K2C5_HUMAN	P13647
KRT6A	3853	na	Keratin, type II cytoskeleta	1	0	K2C6A_HUMAN	P02538
KRT6B	3854	na	Keratin, type II cytoskeleta	4	0	K2C6B_HUMAN	P04259
KRT8	3856	na	Keratin, type II cytoskeleta	4	0	K2C8_HUMAN	P05787
KRT9	3857	na	Keratin, type I cytoskeletal	12	0	K1C9_HUMAN	P35527
LAMC3	10319	na	172 kDa protein,Laminin, g	1	0	LAMC3_HUMAN	Q9Y6N6
LAMP1	3916	CD107a	lysosomal-associated mer	1	1	LAMP1_HUMAN	P11279
LEF1	51176	na	Isoform 1 of Lymphoid enh	1	0	LEF1_HUMAN	Q9UJU2
LEPR	3953	CD295	Isoform B of Leptin recept	3	1	NCS1_HUMAN	P62166
LMNA	4000	na	Isoform A of Lamin-A/C,Is	1	0	LMNA_HUMAN	P02545
LOC644196	644196	na	similar to CG10151-PA, is	1	0	na	na
LOC645745	4496	na	Metallothionein-1H,Metallo	1	0	na	na
LRP1	4035	CD91	Low-density lipoprotein rec	18	1	LRP1_HUMAN	Q07954
LRRC16	55604	na	leucine rich repeat contain	1	0	LR16A_HUMAN	Q5VZK9
LYST	1130	na	Isoform 3 of Lysosomal-tra	1	0	LYST_HUMAN	Q99698
M6PR	4074	na	Cation-dependent mannos	1	1	MPRD_HUMAN	P20645
MASP2	10747	na	Isoform 1 of Mannan-bindi	1	0	MASP2_HUMAN	O00187
MATR3	9782	na	Matrin-3,100 kDa protein	1	0	MATR3_HUMAN	P43243
MRC2	9902	CD280	Macrophage mannose rec	1	1	MRC2_HUMAN	Q9UBG0
MSN	4478	na	Moesin	1	0	MOES_HUMAN	P26038
MT1E	4493	na	Metallothionein-1E,Metallo	1	0	MT1E_HUMAN	P04732
MT1G	4495	na	Isoform 1 of Metallothionei	2	1	MT1G_HUMAN	P13640
MTE	644314	na	MTE	1	0	na	na
MTRR	4552	na	Isoform B of Methionine sy	1	1	ALAT1_HUMAN	P24298
MTSS1	9788	na	PRO1941	1	0	MTSS1_HUMAN	O43312
MYBBP1A	10514	na	Isoform 1 of Myb-binding p	1	0	MBB1A_HUMAN	Q9BQG0
MYEF2	50804	na	Isoform 1 of Myelin expres	1	0	MYEF2_HUMAN	Q9P2K5
NCDN	23154	na	neurochondrin isoform 1,n	1	0	NCDN_HUMAN	Q9UBB6
NEGR1	257194	na	Neuronal growth regulator	5	0	NEGR1_HUMAN	Q7Z3B1
NEU4	129807	na	Sialidase-4,sialidase 4	1	0	NEUR4_HUMAN	Q8WWR8
NID2	22795	na	Nidogen-2 precursor,NID2	1	0	NID2_HUMAN	Q14112
NOPE	57722	na	HDDM36	1	1	IGDC4_HUMAN	Q8TDY8
NOTCH2	4853	na	Neurogenic locus notch ho	2	1	NOTC2_HUMAN	Q04721
NOTCH3	4854	na	Neurogenic locus notch ho	1	0	NOTC3_HUMAN	Q9UM47
NPR2	4882	na	Isoform Long of Atrial natri	1	1	ANPRB_HUMAN	P20594
NPR3	4883	na	Isoform 1 of Atrial natriure	3	1	ANPRC_HUMAN	P17342
NPTN	27020	na	Isoform 1 of Neuroplastin	2	1	NPTN_HUMAN	Q9Y639
NRP1	8829	CD304	Muscle type neuropilin 1,Is	2	1	NRP1_HUMAN	O14786
NT5E	4907	CD73	5'-nucleotidase precursor	19	1	5NTD_HUMAN	P21589
OTOF	9381	na	Isoform 1 of Otoferlin	2	1	OTOF_HUMAN	Q9HC10

Entrez gene symbol	Entrez Gene ID	CD annotation	Description	Number of distinct peptides	Assignment to membrane	UniProtKB/Swiss-Prot ID	UniProtKB/Swiss-Prot AC2
P2RX4	5025	na	P2X purinoceptor 4,32 kD	1	1	P2RX4_HUMAN	Q99571
PAX2	5076	na	Paired box Protein 2 isofo	1	0	PAX2_HUMAN	Q02962
PCCB	5096	na	Propionyl-CoA carboxylas	1	0	PCCB_HUMAN	P05166
PCDHGA1	56114	na	Isoform 1 of Protocadherir	1	1	PCDG1_HUMAN)	Q9Y5H4
PCF11	51585	na	pre-mRNA cleavage comp	1	0	PCF11_HUMAN	O94913
PDGFRB	5159	CD140b	Beta platelet-derived grow	1	1	PGFRB_HUMAN	P09619
PHLPP	23239	na	PH domain leucine-rich re	1	1	ZN473_HUMAN	Q8WTR7
PKD2L1	9033	na	Isoform 2 of Polycystic kid	1	1	PK2L1_HUMAN	Q9P0L9
PKHD1L1	93035	na	fibrocystin L	1	0	PKHL1_HUMAN	Q86WI1
PLEKHH2	130271	na	Pleckstrin homology doma	2	0	PKHH2_HUMAN	Q8IVE3
PLXNB2	23654	na	similar to Plexin-B2 precur	2	1	PLXB2_HUMAN	O15031
PLXND1	23129	na	Isoform 1 of Plexin-D1 pre	1	1	PLXD1_HUMAN	Q9Y4D7
PPAP2B	8613	na	Lipid phosphate phosphoh	2	1	LPP3_HUMAN	O14495
PRNP	5621	CD230	Major prion protein precurs	3	1	PRIO_HUMAN	P04156
PSD3	23362	na	Isoform 1 of PH and SEC7	1	0	PSD3_HUMAN	Q9NYI0
PTK7	5754	na	PTK7 protein tyrosine kina	3	1	PTK7_HUMAN	Q13308
PTPRM	5797	na	Receptor-type tyrosine-pro	1	1	PTPRM_HUMAN	P28827
PVRL2	5819	CD112	Isoform Delta of Poliovirus	1	1	PVRL2_HUMAN	Q92692
PVRL3	25945	CD113	Isoform 1 of Poliovirus rec	2	1	PVRL3_HUMAN	Q9NQS3
QRICH2	84074	na	Hypothetical protein DKFZ	2	0	QRIC2_HUMAN	Q9H0J4
RAC1	5879	na	Isoform A of Ras-related C	2	1	RAC1_HUMAN	P63000
RAD17	5884	na	Isoform 2 of Cell cycle che	1	0	RAD17_HUMAN	O75943
RECK	8434	na	Reversion-inducing cystein	18	1	RECK_HUMAN	O95980
RFC1	5981	na	Isoform 1 of Replication fa	1	0	RFC1_HUMAN	P35251
RHOQ	23433	na	16 kDa protein	1	0	RHOQ_HUMAN	P17081
RNH1	6050	na	Ribonuclease inhibitor,Rib	1	0	RINI_HUMAN	P13489
RPA3	6119	na	Replication protein A 14 kI	1	0	RFA3_HUMAN	P35244
RPL34	6164	na	60S ribosomal protein L34	1	0	RL34_HUMAN	P49207
RPS12	6206	na	40S ribosomal protein S12	1	0	JUND_HUMAN	P17535
RPS3	6188	na	40S ribosomal protein S3	1	0	RS3_HUMAN	P23396
SALL1	6299	na	Sal-like protein 1	1	0	SALL1_HUMAN	Q9NSC2
SCARF2	91179	na	Scavenger receptor class	1	0	SREC2_HUMAN	Q96GP6
SCNN1B	6338	na	Isoform 1 of Amiloride-sen	1	1	SCNNB_HUMAN	P51168
SELP	6403	CD62	P-selectin precursor,Selec	1	1	LYAM3_HUMAN	P16109
SERPINB10	5273	na	Protein	1	0	SPB10_HUMAN	P48595
SFRS2IP	9169	na	SFRS2-interacting protein	1	0	SFRIP_HUMAN	Q99590
SIAH1	6477	na	Isoform 2 of E3 ubiquitin-p	1	1	SIAH1_HUMAN	Q8IUQ4
SLC1A4	6509	na	Neutral amino acid transpo	1	1	SATT_HUMAN	P43007
SLC2A1	6513	na	Solute carrier family 2, fac	1	1	GTR1_HUMAN	P11166
SLC33A1	9197	na	Acetyl-coenzyme A transp	1	1	ACATN_HUMAN	O00400
SLC39A14	23516	na	Solute carrier family 39 me	1	1	S39AE_HUMAN	Q15043
SLC3A2	6520	CD98	4F2 cell-surface antigen h	1	1	4F2_HUMAN	P08195
SLC44A1	23446	CD92	Isoform 2 of Choline transp	3	1	CTL1_HUMAN	Q8WWI5
SLC44A2	57153	na	Isoform 2 of Choline transp	3	1	CTL2_HUMAN	Q8IWA5
SMARCD2	6603	na	54 kDa protein,SWI/SNF-r	1	0	SMRD2_HUMAN	Q92925
SNED1	25992	na	SNED1 protein,similar to s	1	0	SNED1_HUMAN	Q8TER0
SORT1	6272	na	Sortilin precursor	1	1	KCNK1_HUMAN	O00180
SPTBN5	51332	na	Spectrin beta chain, brain	1	0	SPTN5_HUMAN	Q9NRC6
STOML3	161003	na	Stomatin-like protein 3	1	1	STML3_HUMAN	Q8TAV4
tcag7.350	402694	na	similar to ribosomal protein	1	0	na	na
TCEB3	6924	na	Transcription elongation fa	1	0	ELOA1_HUMAN	Q14241
TGFBR2	7048	na	Isoform 1 of TGF-beta rec	1	1	TGFR2_HUMAN	P37173
THBS1	7057	na	Thrombospondin-1 precur	1	0	CTGE5_HUMAN	O15320
THY1	7070	CD90	Thy-1 membrane glycopro	1	1	THY1_HUMAN	P04216
TNFRSF1B	7133	CD120b	Isoform 1 of Tumor necros	1	1	TNR1B_HUMAN	P20333
TOM1L2	146691	na	Target of myb1-like protein	1	0	TM1L2_HUMAN	Q6ZVM7
TPBG	7162	na	Trophoblast glycoprotein p	5	1	MMP16_HUMAN	P51512
TPM1	7168	na	Isoform 1 of Tropomyosin-	2	0	TPM1_HUMAN	P09493
TRIM25	7706	na	Tripartite motif-containing	1	0	TRI25_HUMAN	Q14258
TSPAN14	81619	na	Isoform 2 of Tetraspanin-1	1	1	TSN14_HUMAN	Q8NG11
TSPAN4	7106	na	Tetraspanin-4,tetraspanin	1	1	TSN4_HUMAN	O14817
TTC7A	57217	na	Isoform 2 of Tetratricopept	1	0	TTC7A_HUMAN	Q9ULT0
TTN	7273	na	Titin (Fragment)	1	0	TITIN_HUMAN	Q8WZ42
TUBB2C	10383	na	Tubulin beta-2C chain,Tub	1	0	TBB2C_HUMAN	P68371
TXNDC4	23071	na	Thioredoxin domain-conta	1	0	TXND4_HUMAN	Q9BS26
UGT2B15	7366	na	UDP-glucuronosyltransfera	1	1	UDB15_HUMAN	P54855
VASN	114990	na	Vasorin precursor	2	1	VASN_HUMAN	Q6EMK4
VCAM1	7412	CD106	Isoform 1 of Vascular cell	4	1	VCAM1_HUMAN	P19320
VIM	7431	na	Vimentin,Vimentin,50 kDa	2	0	VIME_HUMAN	P08670
VTI1B	10490	na	Isoform Long of Vesicle tra	1	1	VTI1B_HUMAN	Q9UEU0
ZBED5	58486	na	zinc finger, BED-type cont	1	0	ZBED5_HUMAN	Q49AG3
ZHX3	23051	na	Zinc fingers and homeobo	1	0	ZHX3_HUMAN	Q9H4I2
ZNF417	147687	na	Zinc finger protein 417	1	0	ZN417_HUMAN	Q8TAU3
ZPBP2	124626	na	Isoform 1 of Zona pellucid	1	0	ZPBP2_HUMAN	Q6X784
ZYX	7791	na	67 kDa protein,ZYX protei	1	1	ZYX_HUMAN	Q15942

na - not assigned;

assignment to the membrane based on predicted transmembrane domain and/or GPI-link and/or CD annotation;

0 - not assigned, 1- assigned

Suppl.Table 3. siRNAscreen-110genes-VHR01

	Genes	exp1	exp2	exp3	average	stdev
1	ACVR1	122.45	104.66	111.02	112.71	9.02
2	ACVR2	101.62	107.12	70.73	93.16	19.61
3	ADAM15	101.62	78.63	92.41	90.89	11.57
4	ADAM17	101.80	95.25	102.91	99.99	4.14
5	ADAM9	73.30	84.96	124.71	94.33	26.95
6	ALCAM	105.45	109.31	115.49	110.08	5.07
7	ALPL	116.49	83.10	61.75	87.11	27.59
8	ANPEP	84.76	121.65	112.25	106.22	19.17
9	ANTXR1	104.53	110.20	82.51	99.08	14.62
10	ASAM	113.72	93.30	102.54	103.18	10.23
11	BMP1	105.57	103.89	52.62	87.36	30.09
12	BMP4	101.39	72.30	66.86	80.18	18.56
13	BSG	102.91	65.81	85.51	84.74	18.56
14	CD109	138.38	96.23	109.19	114.60	21.59
15	CD151	146.47	114.53	129.54	130.18	15.98
16	CD164L1	101.57	133.15	111.32	115.34	16.17
17	CD276	80.99	119.13	85.13	95.09	20.93
18	CD44	64.90	85.29	115.35	88.51	25.38
19	CD59	70.39	108.80	97.63	92.28	19.76
20	CD63	85.31	118.25	78.34	93.97	21.32
21	CD99	108.13	104.93	70.42	94.49	20.91
22	CDC42BPA	80.14	100.84	129.80	103.59	24.94
23	CDC42BPB	73.21	104.61	135.90	104.57	31.34
24	CDGAP	102.96	106.05	132.46	113.82	16.22
25	CDH2	86.33	90.18	101.12	92.54	7.67
26	CTNNB1	78.38	65.88	87.93	77.40	11.06
27	CTSB	82.17	81.98	93.84	86.00	6.79
28	CXC12L	84.62	103.86	92.97	93.82	9.65
29	DAF	80.74	81.01	113.61	91.78	18.90
30	DKK1	99.63	86.82	85.67	90.71	7.75
31	DKK2	125.31	85.34	131.11	113.92	24.92
32	EGFR	99.03	108.10	47.05	84.73	32.94
33	EMP3	93.67	99.91	89.36	94.31	5.30
34	ENG	98.01	87.62	120.53	102.05	16.82
35	ERBB2	127.67	114.39	119.64	120.56	6.69
36	FAS	75.15	100.47	101.58	92.40	14.95
37	FAT	103.60	110.38	92.28	102.09	9.14
38	FGF2	65.06	97.81	100.37	87.75	19.69
39	FGF7	50.76	93.20	104.94	82.97	28.50
40	FGFR1	121.66	81.52	91.70	98.29	20.87
41	FN1	107.81	92.13	71.59	90.51	18.16
42	FZD6	67.48	93.02	85.11	81.87	13.07
43	FZD7	72.15	79.45	117.94	89.85	24.60
44	HSPG2	125.77	116.71	136.66	126.38	9.99
45	ICAM1	125.03	104.24	156.07	128.45	26.09
46	IGF2R	95.43	80.96	127.02	101.14	23.55
47	IL1R1	64.90	70.67	77.52	71.03	6.32
48	IL3	62.36	78.26	94.64	78.42	16.14
49	IL6	87.34	79.84	115.44	94.21	18.77
50	IL7	57.76	88.76	85.87	77.46	17.13
51	ITGA11	101.25	111.82	71.75	94.94	20.77
52	ITGA3	103.83	106.01	77.06	95.63	16.12
53	ITGA5	101.48	105.59	129.91	112.32	15.36
54	ITGAV	80.60	118.95	118.08	105.88	21.89
55	ITGB1	91.69	99.81	130.60	107.37	20.53

	Genes	exp1	exp2	exp3	average	stdev
56	ITGB5	73.72	97.16	111.47	94.12	19.06
57	JAG1	91.36	94.69	82.76	89.61	6.16
58	JAG2	55.94	95.86	83.85	78.55	20.48
59	KITLG	88.27	87.66	100.79	92.24	7.41
60	LAMP1	76.35	75.09	83.85	78.43	4.74
61	LEPR	128.22	114.76	80.85	107.94	24.41
62	LO11C4990	107.25	134.45	103.32	115.01	16.95
63	LRP1	120.69	89.99	78.14	96.27	21.96
64	MAML1	84.02	105.17	131.84	107.01	23.96
65	MAML2	88.64	120.39	111.29	106.77	16.35
66	MAML3	87.02	110.24	128.95	108.74	21.01
67	MSN	89.79	66.71	115.16	90.55	24.23
68	NEGR1	86.37	77.98	63.23	75.86	11.72
69	NF2	98.38	93.02	98.14	96.51	3.03
70	NOTCH1	157.37	91.53	146.76	131.88	35.35
71	NOTCH2	87.71	106.05	102.83	98.86	9.79
72	NOTCH3	101.76	112.38	73.29	95.81	20.21
73	NOTCH4	74.36	88.97	78.53	80.62	7.52
74	NRP1	79.01	95.16	116.57	96.91	18.84
75	NT5E	85.13	103.21	115.25	101.20	15.16
76	P2RX4	69.12	116.81	109.29	98.41	25.64
77	PDGFRB	43.51	97.11	57.13	65.92	27.86
78	PLXNB2	72.89	70.53	84.16	75.86	7.29
79	PLXND1	63.60	78.40	103.00	81.67	19.90
80	PRNP	69.93	63.97	73.22	69.04	4.69
81	PTPRM	72.75	125.65	93.38	97.26	26.66
82	PVRL2	114.18	105.31	70.22	96.57	23.25
83	PVRL3	75.98	66.85	109.02	83.95	22.19
84	RAC1	57.83	95.34	102.73	85.30	24.08
85	RAC2	68.68	122.91	93.64	95.08	27.14
86	RAC3	72.15	92.46	84.15	82.92	10.21
87	RDX	67.85	83.52	55.05	68.81	14.26
88	RECK	70.25	106.98	76.14	84.46	19.73
89	RHOA	71.18	68.95	110.83	83.65	23.56
90	RHOB	80.65	111.69	74.72	89.02	19.85
91	RHOC	96.77	89.66	74.35	86.93	11.46
92	RHOG	114.13	86.86	59.34	86.78	27.40
93	RHOQ	65.54	106.01	68.37	79.97	22.59
94	SDFR1/NPTN	57.92	68.06	76.64	67.54	9.37
95	SMAD4	87.39	82.77	90.16	86.77	3.73
96	TGFB1	89.10	85.10	98.99	91.06	7.15
97	TGFB2	61.15	83.89	80.43	75.16	12.25
98	TGFBR1	159.77	89.80	74.89	108.15	45.32
99	TGFBR2	114.73	104.84	72.60	97.39	22.03
100	THBS1	35.52	92.18	82.72	70.14	30.35
101	THY1	132.42	137.85	75.71	115.33	34.42
102	TM4SF7	91.09	103.49	76.64	90.41	13.44
103	TPBG	51.92	83.43	75.81	70.39	16.44
104	TSLP	68.13	111.55	59.20	79.62	28.00
105	VCAM1	68.94	87.42	86.63	81.00	10.45
106	VEGF	79.31	83.10	86.13	82.85	3.42
107	VEGFC	77.92	78.58	60.18	72.23	10.44
108	VIM	98.80	85.01	65.94	83.25	16.50
109	WISP1	54.13	80.07	80.37	71.52	15.06
110	ZYX	68.73	90.50	115.18	91.47	23.24

genes selected for further validation

Suppl.Table 3. siRNAscreen-110genes-VHR01

Controls	exp1		exp2		exp3	
	average	stdev	average	stdev	average	stdev
negative controls	100	18.2455843	100	16.5077302	100	20.5954884
Positive controls	41.1188093	17.1600805	48.6809435	14.5802183	40.5695444	18.8824445
						average z-factor
z-factor	-0.80392063		-0.8173336		-0.99281323	-0.87135582

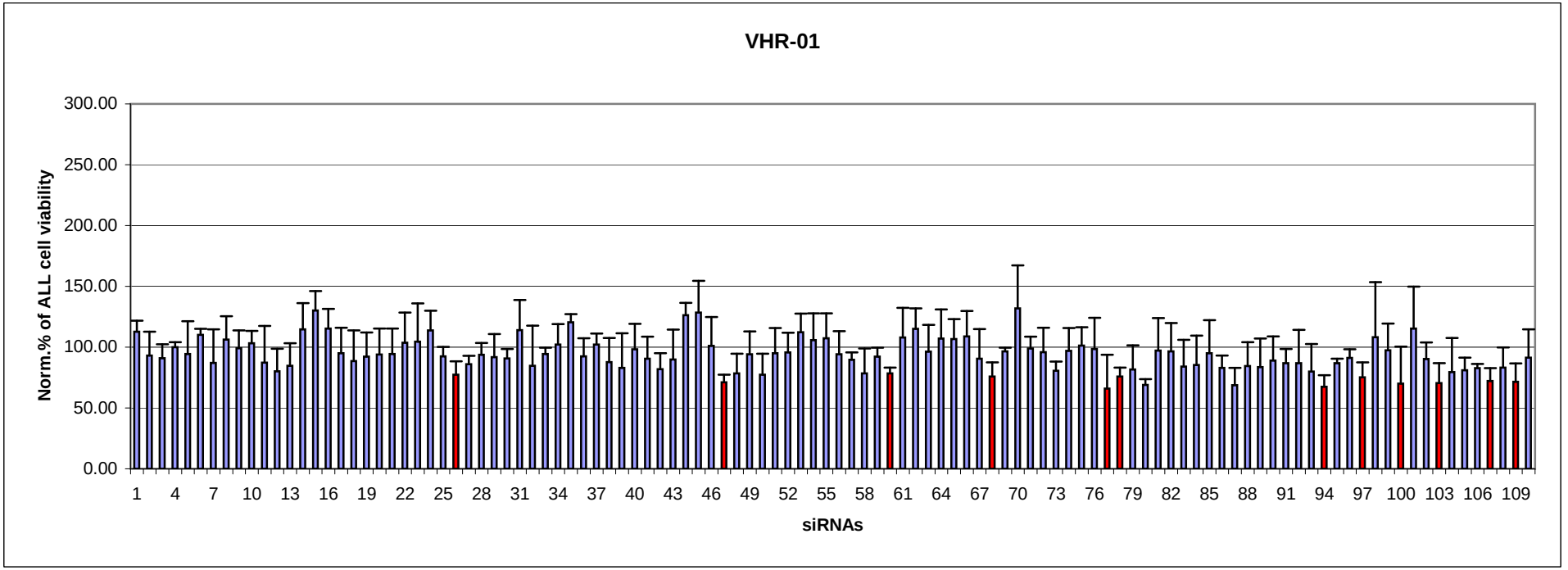

genes selected for further validation

Suppl.Table 3. siRNAscreen-110genes-VHR03

	Genes	exp1	exp2	exp3	average	stdev
1	ACVR1	166.05	76.02	136.35	126.14	45.87
2	ACVR2	69.99	85.51	91.18	82.22	10.97
3	ADAM15	35.63	12.92	61.12	36.56	24.11
4	ADAM17	148.47	91.23	121.53	120.41	28.64
5	ADAM9	142.76	74.27	76.03	97.68	39.04
6	ALCAM	121.95	74.57	95.06	97.19	23.76
7	ALPL	87.22	73.01	55.14	71.79	16.07
8	ANPEP	137.91	93.25	103.23	111.46	23.44
9	ANTXR1	87.10	71.78	63.53	74.14	11.96
10	ASAM	42.65	58.63	65.88	55.72	11.89
11	BMP1	108.78	39.31	72.08	73.39	34.76
12	BMP4	86.71	56.23	56.94	66.63	17.40
13	BSG	43.15	75.69	50.23	56.36	17.11
14	CD109	149.77	80.29	95.35	108.47	36.55
15	CD151	139.33	145.75	142.96	142.68	3.22
16	CD164L1	92.50	97.33	80.51	90.11	8.66
17	CD276	95.30	88.18	94.31	92.60	3.86
18	CD44	101.37	99.77	87.19	96.11	7.77
19	CD59	63.74	55.70	73.06	64.16	8.69
20	CD63	110.95	69.16	61.15	80.42	26.74
21	CD99	189.26	88.14	118.46	131.95	51.89
22	CDC42BPA	85.57	128.67	62.84	92.36	33.44
23	CDC42BPB	203.57	126.61	136.61	155.60	41.85
24	CDGAP	132.23	45.75	80.08	86.02	43.55
25	CDH2	100.62	24.32	68.15	64.36	38.29
26	CTNNB1	83.43	51.42	61.09	65.31	16.42
27	CTSB	91.01	54.44	68.36	71.27	18.46
28	CXC12L	108.62	85.44	72.81	88.96	18.17
29	DAF	75.71	83.11	71.50	76.77	5.88
30	DKK1	73.47	87.48	52.52	71.15	17.59
31	DKK2	54.00	101.83	56.47	70.77	26.93
32	EGFR	73.15	65.54	82.36	73.68	8.43
33	EMP3	43.10	70.87	58.05	57.34	13.90
34	ENG	99.32	61.39	64.99	75.23	20.94
35	ERBB2	93.09	116.62	68.81	92.84	23.91
36	FAS	78.55	62.52	54.53	65.20	12.23
37	FAT	78.39	94.17	89.28	87.28	8.07
38	FGF2	97.71	133.82	67.05	99.52	33.42
39	FGF7	109.21	81.93	72.66	87.93	19.00
40	FGFR1	123.29	68.05	92.30	94.55	27.69
41	FN1	47.09	38.59	66.83	50.84	14.48
42	FZD6	38.11	56.21	69.98	54.77	15.98
43	FZD7	48.96	74.00	51.78	58.25	13.72
44	HSPG2	128.96	137.32	79.82	115.37	31.07
45	ICAM1	107.48	141.94	78.33	109.25	31.84
46	IGF2R	102.59	96.61	77.58	92.26	13.06
47	IL1R1	67.08	80.79	64.35	70.74	8.81
48	IL3	98.49	125.20	76.06	99.92	24.60
49	IL6	93.57	137.36	64.13	98.35	36.85
50	IL7	79.33	93.56	38.16	70.35	28.77
51	ITGA11	79.06	130.92	64.12	91.37	35.06
52	ITGA3	45.56	124.13	33.72	67.81	49.14
53	ITGA5	39.69	129.78	32.16	67.21	54.32
54	ITGAV	97.19	101.83	61.84	86.96	21.87
55	ITGB1	91.12	175.10	62.47	109.57	58.54

	Genes	exp1	exp2	exp3	average	stdev
56	ITGB5	44.50	124.48	36.89	68.62	48.52
57	JAG1	43.10	136.94	58.21	79.42	50.39
58	JAG2	90.49	121.73	56.78	89.67	32.48
59	KITLG	121.95	141.36	80.50	114.60	31.09
60	LAMP1	81.86	90.51	73.90	82.09	8.31
61	LEPR	110.55	30.46	75.95	72.32	40.17
62	LO11C4990	96.29	72.63	57.28	75.40	19.65
63	LRP1	45.46	70.68	57.86	58.00	12.61
64	MAML1	132.35	128.97	85.58	115.63	26.08
65	MAML2	164.71	106.10	116.15	128.99	31.34
66	MAML3	105.75	114.64	74.88	98.42	20.87
67	MSN	89.88	114.83	60.88	88.53	27.00
68	NEGR1	63.26	118.41	60.43	80.70	32.69
69	NF2	115.48	64.24	69.25	82.99	28.25
70	NOTCH1	132.39	56.35	81.24	89.99	38.77
71	NOTCH2	73.15	89.86	53.57	72.19	18.17
72	NOTCH3	65.54	74.95	46.23	62.24	14.64
73	NOTCH4	33.05	70.75	54.23	52.67	18.90
74	NRP1	99.91	73.85	80.51	84.76	13.54
75	NT5E	82.18	91.27	61.00	78.15	15.53
76	P2RX4	63.10	89.55	75.08	75.91	13.25
77	PDGFRB	52.67	82.58	78.40	71.22	16.19
78	PLXNB2	81.98	72.52	64.43	72.98	8.78
79	PLXND1	101.33	44.87	71.61	72.61	28.24
80	PRNP	107.60	44.53	95.53	82.55	33.48
81	PTPRM	64.32	60.98	79.72	68.34	9.99
82	PVRL2	68.22	70.07	54.91	64.40	8.27
83	PVRL3	69.84	58.19	46.17	58.07	11.83
84	RAC1	43.75	92.64	89.50	75.30	27.37
85	RAC2	66.25	117.69	59.05	81.00	31.98
86	RAC3	91.48	97.98	96.48	95.31	3.40
87	RDX	75.67	99.39	92.45	89.17	12.19
88	RECK	68.86	133.78	51.63	84.75	43.32
89	RHOA	77.88	133.66	55.89	89.14	40.09
90	RHOB	66.73	65.61	85.14	72.49	10.96
91	RHOC	70.08	64.22	93.17	75.82	15.31
92	RHOG	84.60	54.78	84.57	74.65	17.21
93	RHOQ	67.75	63.36	72.22	67.78	4.43
94	SDFR1/NPTN	81.99	110.26	43.88	78.71	33.31
95	SMAD4	97.08	44.13	75.43	72.21	26.62
96	TGFB1	114.38	52.80	87.62	84.93	30.88
97	TGFB2	87.81	43.92	67.61	66.45	21.97
98	TGFBR1	24.50	38.70	68.99	44.06	22.72
99	TGFBR2	107.13	102.21	85.85	98.40	11.14
100	THBS1	81.98	46.88	60.26	63.04	17.71
101	THY1	72.48	58.56	87.13	72.72	14.29
102	TM4SF7	53.21	72.61	77.03	67.62	12.67
103	TPBG	39.13	49.60	62.56	50.43	11.74
104	TSLP	54.11	48.08	63.51	55.23	7.77
105	VCAM1	53.33	75.49	60.57	63.13	11.30
106	VEGF	57.74	64.75	83.30	68.60	13.21
107	VEGFC	44.71	55.10	27.73	42.51	13.82
108	VIM	91.37	63.76	74.53	76.56	13.92
109	WISP1	63.61	72.38	51.88	62.62	10.29
110	ZYX	53.80	85.23	93.15	77.39	20.81

genes selected for further validation

Suppl.Table 3. siRNAscreen-110genes-VHR03

Controls	exp1		exp2		exp3	
	average	stdev	average	stdev	average	stdev
negative controls	100	18.9088129	100	18.0694055	100	19.2847865
Positive controls	3.44430431	5.56674795	4.30169018	7.19665348	13.6904196	7.8478652
						average z-factor
z-factor	0.23954064		0.20794655		0.05690707	0.16813142

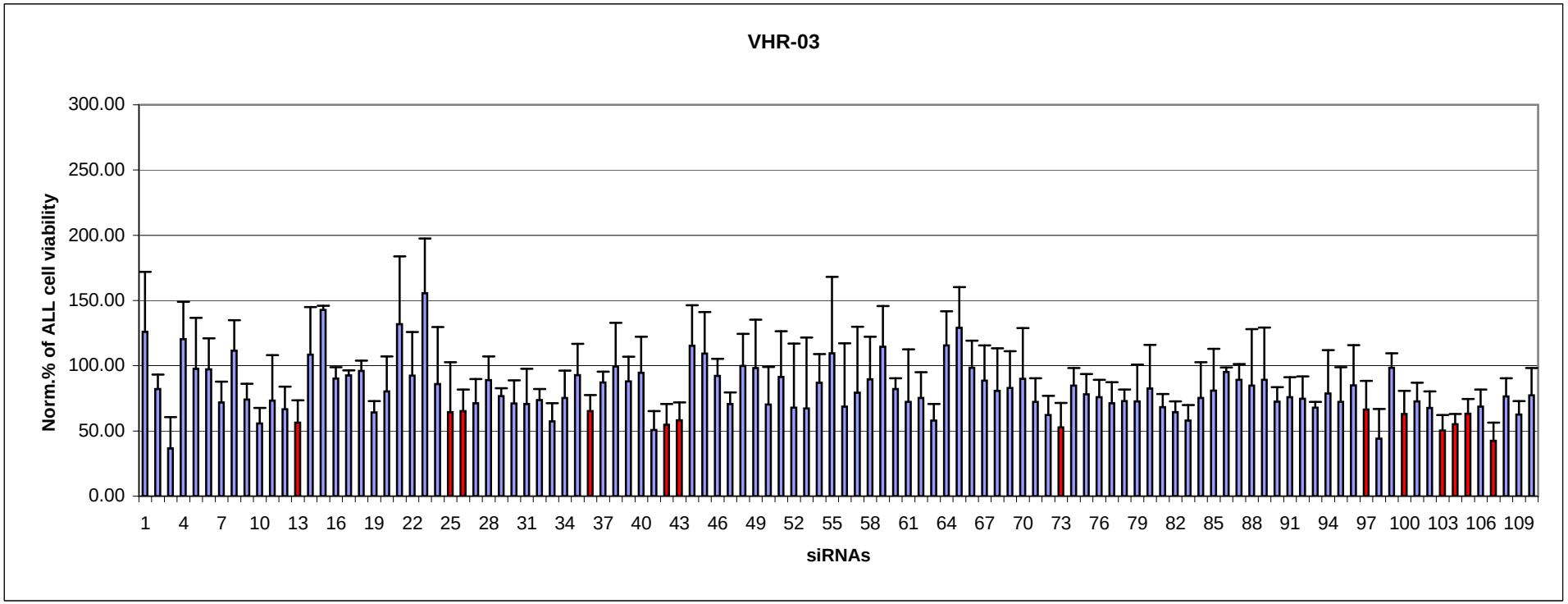

genes selected for further validation

Suppl.Table 3. siRNAscreen-110genes-VHR04

	Genes	exp1	exp2	exp3	average	stdev
1	ACVR1	156.92	185.84	143.21	161.99	21.77
2	ACVR2	85.64	87.85	118.04	97.17	18.10
3	ADAM15	85.77	90.04	117.41	97.74	17.17
4	ADAM17	134.37	125.93	94.10	118.13	21.24
5	ADAM9	108.95	79.03	116.79	101.59	19.93
6	ALCAM	108.33	103.19	142.19	117.91	21.19
7	ALPL	81.35	120.21	112.31	104.62	20.54
8	ANPEP	108.10	71.35	122.43	100.63	26.34
9	ANTXR1	97.49	72.12	110.76	93.45	19.63
10	ASAM	93.32	137.13	106.31	112.26	22.50
11	BMP1	117.45	131.12	128.07	125.55	7.18
12	BMP4	93.58	131.32	135.32	120.07	23.03
13	BSG	43.50	72.81	74.42	63.58	17.41
14	CD109	132.69	114.20	72.39	106.43	30.89
15	CD151	135.03	129.41	89.02	117.82	25.10
16	CD164L1	111.33	114.49	78.01	101.27	20.21
17	CD276	107.19	113.92	114.28	111.80	3.99
18	CD44	122.10	78.74	58.30	86.38	32.58
19	CD59	122.27	117.06	141.32	126.89	12.77
20	CD63	115.59	130.98	139.94	128.84	12.32
21	CD99	95.34	149.48	130.85	125.22	27.50
22	CDC42BPA	87.34	100.14	115.62	101.04	14.16
23	CDC42BPB	47.22	62.19	79.17	62.86	15.98
24	CDGAP	107.97	114.87	47.56	90.13	37.03
25	CDH2	80.13	92.72	59.29	77.38	16.88
26	CTNNB1	82.87	101.81	73.56	86.08	14.40
27	CTSB	82.84	90.12	71.35	81.44	9.47
28	CXC12L	103.61	91.66	99.05	98.11	6.03
29	DAF	121.13	61.82	56.96	79.97	35.73
30	DKK1	87.33	57.82	109.98	85.04	26.16
31	DKK2	111.23	134.80	101.29	115.78	17.21
32	EGFR	111.49	124.93	123.95	120.12	7.49
33	EMP3	88.76	117.59	90.45	98.94	16.18
34	ENG	99.57	94.52	87.26	93.78	6.19
35	ERBB2	123.11	111.34	71.83	102.09	26.87
36	FAS	55.61	70.02	43.91	56.52	13.08
37	FAT	70.85	124.59	108.37	101.27	27.56
38	FGF2	119.40	122.16	34.12	91.90	50.05
39	FGF7	97.00	118.59	101.92	105.84	11.32
40	FGFR1	111.36	98.24	116.61	108.73	9.46
41	FN1	76.39	129.89	63.14	89.80	35.34
42	FZD6	81.92	68.62	53.59	68.04	14.18
43	FZD7	56.98	95.28	41.14	64.47	27.84
44	HSPG2	71.65	124.21	46.84	80.90	39.51
45	ICAM1	107.06	148.38	68.51	107.98	39.94
46	IGF2R	95.08	77.96	41.14	71.39	27.56
47	IL1R1	79.71	78.32	65.74	74.59	7.70
48	IL3	116.41	133.98	82.13	110.84	26.37
49	IL6	106.45	111.44	108.01	108.63	2.55
50	IL7	87.39	74.59	112.34	91.44	19.20
51	ITGA11	129.14	164.01	147.32	146.83	17.44
52	ITGA3	133.15	112.20	41.56	95.63	47.99
53	ITGA5	82.05	112.58	48.99	81.21	31.81
54	ITGAV	85.05	89.42	64.12	79.53	13.52
55	ITGB1	94.10	123.69	86.07	101.29	19.81

	Genes	exp1	exp2	exp3	average	stdev
56	ITGB5	81.31	95.19	76.75	84.42	9.60
57	JAG1	68.35	101.67	123.68	97.90	27.86
58	JAG2	113.22	112.35	73.35	99.64	22.77
59	KITLG	140.27	114.44	67.80	107.50	36.73
60	LAMP1	64.73	99.81	43.71	69.42	28.34
61	LEPR	98.82	128.55	104.69	110.69	15.74
62	LO11C4990	90.36	78.07	85.08	84.50	6.16
63	LRP1	82.35	103.19	104.96	96.83	12.58
64	MAML1	111.59	120.02	145.18	125.59	17.47
65	MAML2	112.24	104.91	102.37	106.50	5.13
66	MAML3	115.72	125.02	72.63	104.46	27.95
67	MSN	71.02	104.39	43.26	72.89	30.61
68	NEGR1	90.00	89.18	49.17	76.12	23.34
69	NF2	108.85	134.80	61.26	101.64	37.30
70	NOTCH1	107.16	75.12	64.12	82.13	22.36
71	NOTCH2	163.82	94.04	125.11	127.66	34.96
72	NOTCH3	126.99	124.26	75.68	108.98	28.87
73	NOTCH4	73.25	92.09	49.35	71.56	21.42
74	NRP1	90.10	98.81	69.32	86.07	15.15
75	NT5E	120.61	118.21	48.27	95.70	41.09
76	P2RX4	95.40	85.89	40.30	73.87	29.45
77	PDGFRB	78.44	80.51	66.01	74.98	7.84
78	PLXNB2	98.56	56.29	63.23	72.69	22.67
79	PLXND1	97.94	75.21	67.62	80.26	15.78
80	PRNP	128.06	67.64	120.64	105.45	32.95
81	PTPRM	96.64	164.73	171.15	144.17	41.29
82	PVRL2	110.58	139.28	74.24	108.03	32.59
83	PVRL3	106.93	107.20	76.84	96.99	17.45
84	RAC1	111.88	78.36	81.86	90.70	18.43
85	RAC2	112.76	106.34	54.81	91.30	31.77
86	RAC3	64.33	80.22	44.72	63.09	17.78
87	RDX	102.11	85.65	55.44	81.07	23.67
88	RECK	108.17	74.30	83.29	88.59	17.54
89	RHOA	151.31	62.58	106.13	106.67	44.37
90	RHOB	78.44	58.58	134.52	90.51	39.38
91	RHOC	100.13	98.14	156.37	118.21	33.06
92	RHOG	111.33	147.71	130.13	129.72	18.20
93	RHOQ	79.78	137.70	86.51	101.33	31.68
94	SDFR1/NPTN	71.39	76.07	69.20	72.22	3.51
95	SMAD4	91.11	96.47	56.87	81.48	21.48
96	TGFB1	102.63	90.75	94.31	95.90	6.10
97	TGFB2	75.51	86.70	75.95	79.39	6.34
98	TGFBR1	74.37	189.47	109.35	124.40	59.00
99	TGFBR2	89.15	126.88	100.49	105.51	19.36
100	THBS1	73.95	133.65	65.92	91.17	37.01
101	THY1	73.39	239.28	204.55	172.41	87.49
102	TM4SF7	102.18	128.46	79.26	103.30	24.62
103	TPBG	87.33	117.25	93.86	99.48	15.73
104	TSLP	59.55	124.83	63.95	82.78	36.49
105	VCAM1	81.01	82.46	50.87	71.45	17.84
106	VEGF	90.27	86.56	65.11	80.65	13.58
107	VEGFC	98.99	83.08	88.57	90.22	8.08
108	VIM	76.81	143.99	81.14	100.65	37.60
109	WISP1	62.58	123.16	96.54	94.10	30.37
110	ZYX	103.90	226.17	147.50	159.19	61.96

genes selected for further validation

Suppl.Table 3. siRNAscreen-110genes-VHR04

Controls	exp1		exp2		exp3	
	average	stdev	average	stdev	average	stdev
negative controls	100	18.6370431	100	20.2749048	100	20.8932595
Positive controls	2.73695856	3.06858677	3.52981676	2.7867565	22.8077403	8.22121568
						average z-factor
z-factor	0.33050737		0.28283557		-0.13150497	0.16061266

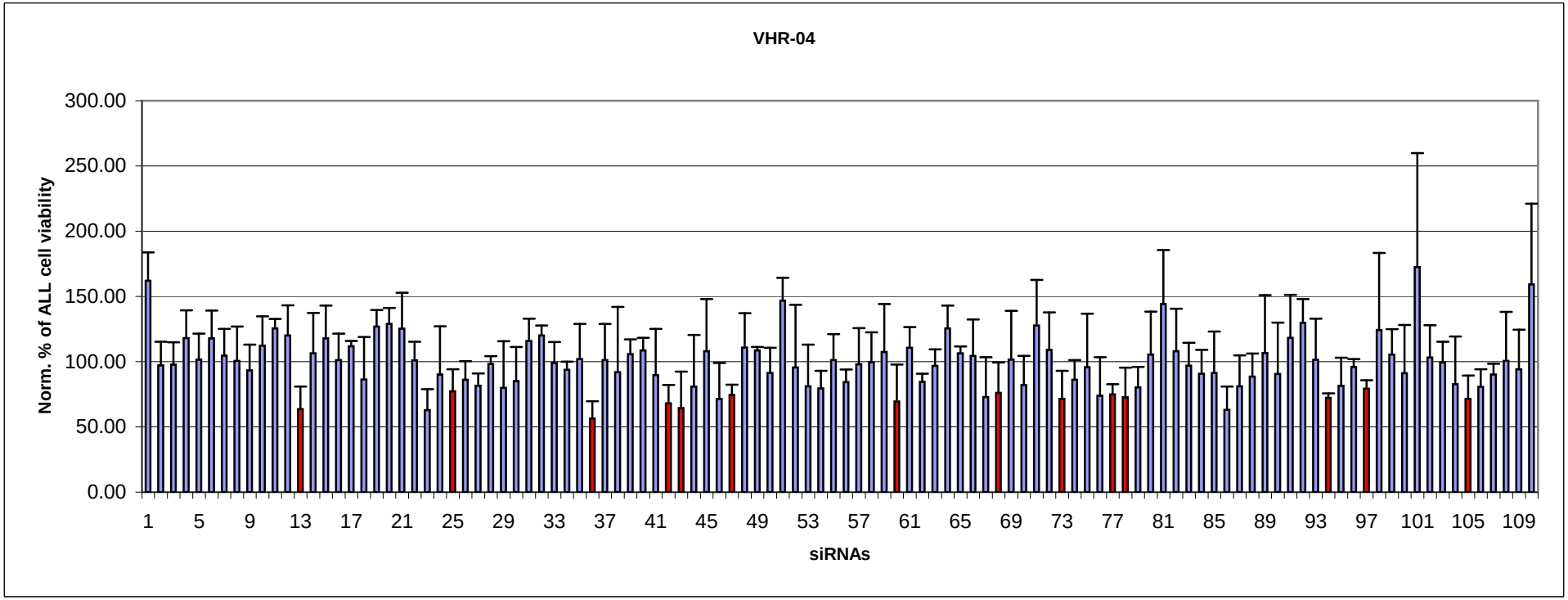

genes selected for further validation